INFORMATION TO USERS

This manuscript has been reproduced from the microfilm master. UMI films the text directly from the original or copy submitted. Thus, some thesis and dissertation copies are in typewriter face, while others may be from any type of computer printer.

The quality of this reproduction is dependent upon the quality of the copy submitted. Broken or indistinct print, colored or poor quality illustrations and photographs, print bleedthrough, substandard margins, and improper alignment can adversely affect reproduction.

In the unlikely event that the author did not send UMI a complete manuscript and there are missing pages, these will be noted. Also, if unauthorized copyright material had to be removed, a note will indicate the deletion.

Oversize materials (e.g., maps, drawings, charts) are reproduced by sectioning the original, beginning at the upper left-hand corner and continuing from left to right in equal sections with small overlaps.

Photographs included in the original manuscript have been reproduced xerographically in this copy. Higher quality 6" x 9" black and white photographic prints are available for any photographs or illustrations appearing in this copy for an additional charge. Contact UMI directly to order.

Bell & Howell Information and Learning
300 North Zeeb Road, Ann Arbor, MI 48106-1346 USA
800-521-0600

Visualization of Electron Transport Dynamics in Quantum Nanostructures

By
Jawad A. Qureshi

A dissertation submitted to the Graduate Faculty in Engineering in partial fulfillment of the requirements for the degree of Doctor of Philosophy, The City University of New York.

2001

This manuscript has been read and accepted for the Graduate Faculty in Engineering in satisfaction of the dissertation requirement for the degree of Doctor of Philosophy.

1/28/01

Date

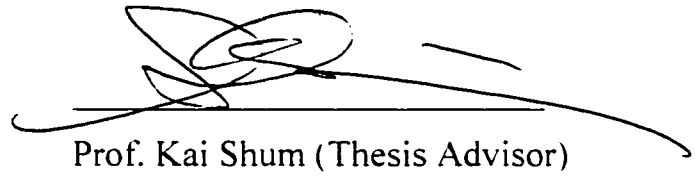

Prof. Kai Shum (Thesis Advisor)

Chair of Examining Committee

Jan. 29, 2001

Date

Mumtaz Kassir

Prof. Mumtaz Kassir

Executive Officer

Prof. Roger Dorsinville

Prof. Ping-Pei Ho

Prof. Norman Scheinberg

Dr. Cai Wei

Supervisory Committee

The City University of New York

Abstract

Visualization of Electron Transport Dynamics in Quantum Nanostructures

by

Jawad A. Qureshi

Advisor: Kai Shum, Professor of Electrical Engineering

This thesis investigates electron transport dynamics in quantum nanostructures with electron-phonon and electron-photon interactions. A real-time visualization program is designed for calculating wavepacket propagation by solving the time-dependent Schrödinger equation with electron-phonon or electron photon interaction. It is used to analyze trapping in single quantum well and also Bloch oscillations in semiconductor superlattices. The trapping in quantum well is analyzed for electron-phonon and electron-photon interaction. The decay of the center of mass of the Bloch oscillations in semiconductor superlattices under electron-phonon interaction will be calculated by the program.

The above program is written using the Crank-Nicolson algorithm. However, this method is not able to solve for complicated Hamiltonians. There are other methods of solution of the time-dependent Schrödinger equation that extend the range of Hamiltonians that can be solved. However, they cannot be used for *any* complicated Hamiltonian. A new algorithm, called recursive error method (REM), is invented (patent pending) and tested on simple structures for quantifying efficiency and accuracy. It

compares favorably to other methods in solving simple Hamiltonians and shows superb advantages for complicated multi-dimensional Hamiltonians.

The REM algorithm is used to analyze the coupling of two quantum boxes. A two-dimensional electron Hamiltonian must be used in the time-dependent Schrödinger equation resulting in massive computations. The real-benefit of the REM algorithm will only result if parallel computers are used, in which case the results for complicated Hamiltonians are obtained in real-time.

To my parents.

Mohammad and Zakia Qureshi

ACKNOWLEDGEMENTS

I would like to thank and gratefully acknowledge my thesis advisor Professor Kai Shum for his guidance and vision.

I am obliged to Professor Roger Dorsinville, Professor Ping-Pei Ho, Professor Norman Scheinberg and Dr. Cai Wei for serving on my doctoral committee.

I wish these Professors luck in their research.

TABLE OF CONTENTS

Abstract iv

Acknowledgements vii

Table of contents viii

Lists of figures xii

List of tables xix

Chapter 1 Introduction

1.1 Background 1

1.2 Thesis statement 2

1.3 Thesis organization 3

Chapter 2 Theory of electron-phonon interaction

2.1 Introduction 4

2.2 Theory 4

2.2.1 Atomic model 4

2.2.2 Dielectric model 7

2.2.3 Normal coordinates 14

2.2.4 Scattering rate in 3D 18

2.2.5 Scattering rate in 1D 24

2.3 The Schrödinger equation with electron-phonon interaction 27

2.4 References 48

Chapter 3 Theory of electron-photon interaction

3.1 Introduction 54

3.2 Theory 54

3.3 The Schrödinger equation with electron-photon interaction 61

3.4 References 64

Chapter 4 Visualization of electron transport in semiconductor nanostructures

4.1 Introduction 65

4.2 Visualization program for quantum projects 66

4.3 Semiconductor superlattice 68

Chapter 5 Electron-phonon interaction in a single quantum well

5.1 Introduction 89

5.2 Numerical model 90

5.3 Capture and escape dynamics 92

5.4 Conclusion 95

5.5 References 97

Chapter 6 Bloch oscillations in semiconductor superlattices

6.1 Introduction 108

6.2 Electron-phonon model 110

6.3 Results 113

6.4 Conclusion 115

6.5 References 116

Chapter 7 Electron-photon interaction in a single quantum well

7.1 Introduction 125

7.2 Ultrafast electronic switching via a photon pulse 128

7.3 Conclusion 130

7.4 References 131

Chapter 8 Recursive error method for solving arbitrary Hamiltonian

8.1 Introduction 139

8.2 Recursive error method for solving the TDSE 142

8.3 Algorithm to implement REM 144

8.4 Accuracy of REM 146

8.5 Computation speed of REM using 1D and 2D Hamiltonians 147

8.5.1 One-dimensional Hamiltonian 147

8.5.2 Two-dimensional Hamiltonian 149

8.6 Conclusion 150

8.7 References 151

Chapter 9 Future work

9.1 Software for real time visualization of quantum projects 161

9.2 Electron-electron and electron-hole scattering 161

9.3 2D simulator based on REM 161

Appendix

A.1 The project file to view Bloch oscillations in the example of Chapter 4 162

Bibliography 166

LIST OF FIGURES

Chapter 2

Fig. (2.1) Emission and absorption of electrons by LO Phonons for different electron energies in bulk GaAs. 49

Fig. (2.2) The electron-phonon coupling constant for different electron energies in bulk GaAs. 50

Fig. (2.3) The dispersion relation showing the four wavevectors responsible for phonon absorption from E_1 to $E_1 + \hbar\omega$ in 1D semiconductor structure. 51

Fig. (2.4) Net scattering at electron energies below LO-phonon energy in 1D semiconductor structure. 52

Fig. (2.5) The electron phonon coupling constant for low electron energies in 1D GaAs semiconductor structures. 53

Chapter 4

Fig. (4.1) A welcome dialog shows up when VQP is launched. 70

Fig. (4.2) The default settings can be changed by selecting Default Settings in the Setting menu and entering these values for a semiconductor superlattice. 71

Fig. (4.3) A 36-barrier structure can be set by selecting the N-Barrier

Square Barrier option. 72

Fig. (4.4) Enter 36 barriers for a 35-QW structure. 73

Fig. (4.5) After accepting the structure, an 'Entire Structure' window shows up. 74

Fig. (4.6) We can change the wavepacket properties by selecting these options. 75

Fig. (4.7) Set the wavepacket properties so the electron is in middle of superlattice with zero kinetic energy. 76

Fig. (4.8) The resulting quantum structure after setting the wavepacket properties. 77

Fig. (4.9) Set the applied bias across the semiconductor superlattice as 0.15 V. 78

Fig. (4.10) The resulting quantum structure after setting the bias. 79

Fig. (4.11) Set the temporal and spatial resolutions for the calculation. 80

Fig. (4.12) After setting the quantum structure, the project should be saved by selecting Save Project from the File menu. 81

Fig. (4.13) After entering the project title, the program will ask for a project note. 82

Fig. (4.14) Set up a new probability graph to zoom in on the

superlattice structure. 83

Fig. (4.15) The 'Superlattice' window pops up. Note that the 'Entire Structure' window has been manually closed. 84

Fig. (4.16) A center of mass graph for finding the charge center within the superlattice. 85

Fig. (4.17) The wavefunction and center of mass are shown in this tiled view after 3 Bloch oscillations. 86

Fig. (4.18) The center of the mass is printed by entering the print properties. 87

Fig. (4.19) Print preview window. 88

Chapter 5

Fig. (5.1) An electron at energy 24 meV resonantly emits a phonon leading to capture of electron by a SQW of depth V. 98

Fig. (5.2) The spatial variation of carrier density in a SQW for V = 25 meV and g = 0.05 at (a) t = 50 fs. (b) t = 1445 fs and (c) t = 4000 fs . 99

Fig. (5.3) The Fourier spectra of transmitted wavefunction (at t = 4000 fs) for V = 25 meV and g = 0.05. There is attenuation at a resonant energy of 23.8 meV. as compared to incident. with a small absorption component near 60 meV. 100

Fig. (5.4) The temporal dynamics of captured electron density for resonance conditions with the three states for g = 0.05, showing electron capture and escape. 101

Fig. (5.5) The temporal dynamics of charge escaping due to LO phonon absorption for different confining potentials for g = 0.05. 102

Fig. (5.6) The temporal dynamics for V = 25 meV and different interaction strengths from g = 0 to 0.1. 103

Fig. (5.7) Circles are calculated times for (a) capture and (b) escape. In (b), the solid curve is a fit using the expression of 40/g. 104

Fig. (5.8) Varying the electron energy, the resonant energy near 24 meV can be found for V = 25 meV and different interaction strengths from g = 0 to 0.1. 105

Fig. (5.9) The resonant energy is blue shifted for V = 25 meV with increasing electron-phonon interaction for small g-values. 106

Fig. (5.10) The ratio of maximum captured electron probability in the SQW is a nonlinear function of the strength of interaction. 107

Chapter 6

Fig. (6.1) The 35 eigenenergies per band are shown by the dots for the 35 quantum-well superlattice. For comparison, the Kronig-Penney calculation is shown by the solid line for the infinite superlattice. 118

Fig. (6.2) The center of mass for the case of no scattering. The electron oscillates between two extreme positions in about 0.486 ps. The first rightmost position occurs at 483 fs and then the leftmost occurs at 977 fs. 119

Fig. (6.3) The wavefunction without interaction for the two different times. (a) t = 483 fs and (b) t = 977 fs, which correspond to the center of mass at extreme right or left, respectively. 120

Fig. (6.4) The center of mass for the case of scattering with g = 9.0. The electron oscillates between two extreme positions in about 0.454 ps. The first rightmost position occurs at 546 fs and then the leftmost occurs at 1000 fs. 121

Fig. (6.5) The wavefunction with interaction for the two different times. (a) t = 456 fs and (b) t = 1000 fs, which correspond to the center of mass at extreme right or left, respectively. 122

Fig. (6.6) The scattering time of confined phonons as a function of temperature for a bias of 0.15 V. 123

Fig. (6.7) The scattering time oscillates with electric field in a semiconductor superlattice. The dashed line shows that the average scattering time is decreasing with the electric field. The effective bandwidth also increases with the applied bias as shown in inset. 124

Chapter 7

Fig. (7.1) An electrooptic switch is modulated by the delay τ induced by the voltage, V, in the transmitting chip to drive a current I_{out} in the receiving chip. 132

Fig. (7.2) Electron spatial distribution of the calculation. An electronic Gaussian pulse, with a center at z_0 and a center kinetic energy of E_1, interacts inside a SQW with a delayed optical pulse $n_p(t, t_0)$. 133

Fig. (7.3) The steady-state transmission for a constant photon flux of n photons over a SQW with a resonant energy of 24 meV. 134

Fig. (7.4) Temporal distribution of (a) incident current at z_1 and (b) three different photon pulses with temporal centers at t_{01}, t_{02} and t_{03}. 135

Fig. (7.5) Transmitted wavefunction as a function of optical pulse delay t_0 for five different power levels. The inset shows the maximum transmission differential for the various power levels. 136

Fig. (7.6) The incident, transmitted, and reflected electron currents as measured by the input and output probes for photon delays t_{01} and t_{02}. 137

Fig. (7.7) Captured charge in the quantum well (solid curve). The dashed curve is a plot of the expression $0.068(1-\exp(t/\tau_c))$, where $\tau_c = 300$ fs. 138

Chapter 8

Fig. (8.1) Implementation of the operator U_4^{-}. 152

Fig. (8.2) Accuracy of REM as a function of the number of terms for the square quantum well structure. The inset shows the structure. 153

Fig. (8.3) Stability diagram of REM for a 1D SQW Hamiltonian. The stable region is shown by the shaded region. The half-maximum time step-size line is also shown. The inset shows the structure. 154

Fig. (8.4) Calculation overhead of REM as a function of N (circles) and Jacobi as a function of time step (squares) for a 1D SQW Hamiltonian. 155

Fig. (8.5) Stability diagram of REM for a 2D QBs Hamiltonian. The stable region is shown by the shaded region The half-maximum time step-size line is also shown. The inset shows the structure. 156

Fig. (8.6) Calculation overhead of REM as a function of N (circles) and Jacobi as a function of time step (squares) for a 2D QBs Hamiltonian. 157

LIST OF TABLES

Chapter 8

Table (8.1)	The right hand side of the TDSE for different methods.	158
Table (8.2)	Analytic values of the unitary operator.	159
Table (8.3)	The REM Algorithm.	160

CHAPTER 1

INTRODUCTION

1.1 Background

The numerical solution of the time-dependent Schrödinger equation (TDSE) is computationally intensive as compared to the time-independent one. However only the steady-state behavior can be obtained by the time-independent Schrödinger equation. For electron transport dynamics in femtosecond timescale it is necessary to use the TDSE. This is especially true if there are dissipative interaction terms in the Hamiltonian.

In this thesis, the TDSE is used to study three types of semiconductor nanostructures: single quantum well, superlattice and two coupled quantum boxes. Single quantum well nanostructures will be used with both electron-phonon and electron-photon interaction. Bloch oscillations, in semiconductor superlattices, are one problem that cannot be solved by the time-independent Schrödinger equation. Even in the absence of electron-phonon where it is expected that the Bloch oscillations will exist forever, there isn't a steady state solution. Furthermore, in presence of interaction, Bloch oscillations will disappear after some time. A time-dependent approach to investigate how Bloch oscillations evolve with electron-phonon interaction will thus form an integral part of this thesis.

A new method for solution of the TDSE, called the Recursive Error Method (REM), is invented. This method is employed to solve the coupled quantum box (QB) problem where the electron goes back and forth from one QB to the other.

1.2 Thesis statement

A wavepacket approach to solve the TDSE will be used here to study different quantum structures. The various aspects studied are

(1) A quantum mechanical model is developed for including electron-phonon interaction.

(2) A quantum mechanical model is developed for including electron-photon interaction.

(3) Description of a program for visualization of quantum projects and an example project is illustrated.

(4) Trapping of charge in a single quantum well with electron-phonon interaction is investigated.

(5) Electron dynamics in the semiconductor superlattice in presence of electron-phonon interaction show damping of Bloch oscillations with time.

(6) Trapping of charge in a single quantum well with electron-photon interaction is investigated and the results are used to propose an ultrafast optoelectronic switch.

(7) A Recursive error method (REM) is outlined to solve *any* Hamiltonian on parallel computers.

1.3 Thesis organization

This thesis is organized into eight chapters including this introductory chapter and a final summary. The organization of chapters 2 through 8 parallel the tasks listed in the previous section.

In Chapter 2, the electromagnetic theory is used to derive a formula for the electron-phonon interaction based on the dielectric continuum theory. Chapters 3 derives the form of the electron-photon interaction using the dipole moment of the electron. The program to visualize the wave packets under electron-phonon and electron-photon interaction, is described in Chapter 4. The model, to include the electron-phonon interaction in the TDSE, is tested on a single quantum well in Chapter 5.

In Chapter 6, a semiconductor superlattice structure is analyzed. First the conditions under which there will be Bloch oscillations are found in the absence of interaction. Then electron-phonon interaction is turned on to investigate the decay of Bloch amplitude and compare the calculated results with experiment. A new optically controlled electronic switch, based on electron-photon interaction in a single quantum well, is proposed in Chapter 7. In Chapter 8, a new iterative method for the solution of the TDSE for arbitrary Hamiltonians, called the Recursive Error Method (REM) is presented. Several simple structures are analyzed both with REM and conventional iterative techniques. The calculation speed and accuracy of REM is compared to other methods and it is found to excel them. Furthermore, the new method REM, is capable of handing complicated Hamiltonians with ease provided all the computations can be handled by parallel computers.

CHAPTER 2

THEORY OF ELECTRON PHONON INTERACTION

2.1 Introduction

In GaAs material system, polar longitudinal-optical (LO) phonons are dominant over other kinds of phonons in terms of the scattering rate and energy loss. The dielectric continuum model[1] is derived and the assumptions are noted so confinement in quantum structure can be properly dealt with. The form of the equations used in the numerical program are found as well as reasonable values of coefficients. The role of confinement will lead to other phonons such as confinement phonons. For comparison with previous results, it should be noted that SI units are used throughout and permittivities are used rather than dielectric constants.

2.2 Theory

2.2.1 Atomic model

For a polar molecule under electric field, the dipole moments are related to displacement and localized electric field as

(2.1a) $$p_- = e_n^* u^- + \alpha_- E^{loc}.$$

(2.1b) $$p_- = -e_n^* u^- + \alpha_- E^{loc}.$$

Here the two coefficients are the effective charge and the electronic polarizabilities.

The total polarization is

(2.2) $$P = \frac{1}{v_a}(p_- - p_-) = \frac{1}{v_a}\left(e_n^*(u^- - u^-) + \alpha E^{loc}\right).$$

where v_a is the volume of the elementary cell and $\alpha = \alpha_- - \alpha_-$.

The localized electric field is

(2.3) $$E^{loc} = E + \frac{1}{3\varepsilon_0} P.$$

where the Lorenz factor for cubic lattices[2] has been used.

Substituting Eq. (2.3) into (2.2), the polarization is

(2.4) $$P = \frac{1}{v_a}\left(1 - \frac{\alpha}{3\varepsilon_0 v_a}\right)^{-1}\left(e_n^*(u^- - u^-) + \alpha E\right).$$

The polarization can be simplified by introducing

(2.5a) $$u = \sqrt{\frac{\mu_n}{v_a}}(u^- - u^-).$$

whereby

(2.5b) $$P = b_{21} u + b_{22} E.$$

(2.5c) $$b_{21} = e_n^* \sqrt{\frac{1}{v_a \mu_n}}\left(1 - \frac{\alpha}{3\varepsilon_0 v_a}\right)^{-1}, \quad b_{22} = \frac{\alpha}{v_a}\left(1 - \frac{\alpha}{3\varepsilon_0 v_a}\right)^{-1}.$$

The forces on the ions are a function of both the displacement and electric field as in the equations

(2.6a) $$m_n^- \ddot{u}^- = -f_n\left(u^+ - u^-\right) + e_n^* E^{loc}.$$

(2.6b) $$m_n^+ \ddot{u}^+ = f_n\left(u^+ - u^-\right) - e_n^* E^{loc}.$$

where the constants refer to the masses of the ions, the force constant, and the effective charge.

The above equations can be combined to give one equation for the relative displacement by introducing a reduced mass, μ_n.

(2.7a) $$\mu_n\left(\ddot{u}^+ - \ddot{u}^-\right) = -f_n\left(u^+ - u^-\right) + e_n^* E^{loc}.$$

(2.7b) $$\mu_n = \frac{m_n^- m_n^+}{m_n^- + m_n^+}.$$

Multiplying both sides by $\sqrt{\frac{\mu_n}{v_a}}$, Eq. (2.7), and using Eq. (2.5a)

(2.8) $$\mu_n \ddot{u} = -f_n u + e_n^* \sqrt{\frac{\mu_n}{v_a}}\left(E + \frac{1}{3\varepsilon_0} P\right).$$

By substituting Eq. (2.5) into (2.9), this equation results

(2.9a) $$\mu_n \ddot{u} = -f_n u + e_n^* \sqrt{\frac{\mu_n}{v_a}}\left(E + \frac{1}{3\varepsilon_0}\left(b_{21} u + b_{22} E\right)\right).$$

(2.9b) $$\mu_n \ddot{u} = \left(-f_n + e_n^* \sqrt{\frac{\mu_n}{v_a}} \frac{1}{3\varepsilon_0} b_{21}\right) u + e_n^* \sqrt{\frac{\mu_n}{v_a}}\left(1 + \frac{1}{3\varepsilon_0} b_{22}\right) E.$$

(2.9c) $$\mu_n \ddot{u} = -f_n u + e_n^* \sqrt{\frac{\mu_n}{v_a}} E + e_n^* \sqrt{\frac{\mu_n}{v_a}} \frac{1}{3\varepsilon_0} \frac{1}{v_a}\left(1 - \frac{\alpha}{3\varepsilon_0 v_a}\right)^{-1}\left(e_n^* \sqrt{\frac{v_a}{\mu_n}} u + \alpha E\right).$$

(2.9d) $$\mu_n \ddot{u} = u\left(-f_n + e_n^* \sqrt{\frac{\mu_n}{v_a}} \frac{1}{3\varepsilon_0} \frac{1}{v_a}\left(1 - \frac{\alpha}{3\varepsilon_0 v_a}\right)^{-1} e_n^* \sqrt{\frac{v_a}{\mu_n}}\right) E.$$

$$+\left(e_n^{\bullet}\sqrt{\frac{\mu_n}{v_a}}++e_n^{\bullet}\sqrt{\frac{\mu_n}{v_a}}\frac{1}{3\varepsilon_0}\frac{1}{v_a}\left(1-\frac{\alpha}{3\varepsilon_0 v_a}\right)^{-1}\alpha\right)E.$$

Now the displacement can be written as

(2.10a) $$\ddot{u} = b_{11}u + b_{12}E.$$

(2.10b) $$b_{11} = -\frac{f_n}{\mu_n} + e_n^{\bullet}\sqrt{\frac{1}{v_a\mu_n}}\frac{1}{3\varepsilon_0}\frac{1}{v_a}\left(1-\frac{\alpha}{3\varepsilon_0 v_a}\right)^{-1}\sqrt{\frac{v_a}{\mu_n}}.$$

(2.10c) $$b_{12} = e_n^{\bullet}\sqrt{\frac{1}{\mu_n v_a}}\left(1+\frac{1}{3\varepsilon_0}\frac{1}{v_a}\left(1-\frac{\alpha}{3\varepsilon_0 v_a}\right)^{-1}\alpha\right) = e_n^{\bullet}\sqrt{\frac{1}{\mu_n v_a}}\left(1-\frac{\alpha}{3\varepsilon_0 v_a}\right)^{-1}.$$

The two coupled equations (2.10a) and (2.5a) can be further simplified by noting $b_{21} = b_{12}$ and so a diatomic ion can be described by these equations

(2.11a) $$\ddot{u} = b_{11}u + b_{12}E.$$

(2.11b) $$P = b_{12}u + b_{22}E.$$

2.2.2 Dielectric model

Eq. (2.11) paves the way for a macroscopic treatment based on measurable optical constants. The b variables can be found from the description of the dielectric constant in the harmonic approximation.

(2.12a) $$E = E_0e^{-i\omega t},\ u = u_0e^{-i\omega t},\ P = P_0e^{-i\omega t}.$$

(2.12b) $$-\omega^2 u = b_{11}u + b_{12}E.$$

(2.12c) $$u\left(-\omega^2 - b_{11}\right) = b_{12}E.$$

(2.12d) $$u = \frac{b_{12}}{-\omega^2 - b_{11}} E .$$

(2.12e) $$P = b_{12} u + b_{22} E .$$

(2.12f) $$P = b_{12} \frac{b_{12}}{-b_{11} - \omega^2} E + b_{22} E .$$

(2.12g) $$P = \left(b_{22} + \frac{b_{12}^2}{-b_{11} - \omega^2} \right) E .$$

Since

(2.12h) $$D = \varepsilon_0 E + P = \varepsilon E .$$

(2.12i) $$D = \varepsilon_0 E + \left(b_{22} + \frac{b_{12}^2}{-b_{11} - \omega^2} \right) E = \varepsilon E .$$

the final equation is

(2.12j) $$\varepsilon = \left(\varepsilon_0 + b_{22} + \frac{b_{12}^2}{-b_{11} - \omega^2} \right) .$$

The permittivity can be written as

(2.13) $$\varepsilon = \varepsilon_\infty + \frac{\varepsilon_0 - \varepsilon_\infty}{1 - \left(\frac{\omega}{\omega_{T0}} \right)^2} .$$

The permittivity is ε_0 at zero frequency (it should not be confused with the free space permittivity). ε_∞ at high frequencies. and infinity at ω_{T0} which is the transverse mode where the electric field is zero.

Comparing the two equations b_{22} is simply found as

(2.14a) $$\varepsilon_0 + b_{22} = \varepsilon_\infty .$$

(2.14b) $$b_{22} = \varepsilon_\infty - \varepsilon_0 .$$

The other two constants can be determined from comparing the numerator and denominator of the following equations:

(2.15a) $$\frac{b_{12}^2}{-b_{11}-\omega^2}=\frac{\varepsilon_0-\varepsilon_\infty}{1-\left(\frac{\omega}{\omega_{TO}}\right)^2}.$$

(2.15b) $$\frac{b_{12}^2}{-b_{11}-\omega^2}=\frac{\varepsilon_0-\varepsilon_\infty}{\left(\frac{\omega_{TO}}{\omega_{TO}}\right)^2-\left(\frac{\omega}{\omega_{TO}}\right)^2}.$$

(2.15c) $$\frac{b_{12}^2}{-b_{11}-\omega^2}=\frac{\omega_{TO}^2(\varepsilon_0-\varepsilon_\infty)}{\omega_{TO}^2-\omega^2}.$$

(2.15d) $$b_{12}^2=\omega_{TO}^2(\varepsilon_0-\varepsilon_\infty).$$

(2.15e) $$b_{12}=\omega_{TO}(\varepsilon_0-\varepsilon_\infty)^{1/2}.$$

(2.15f) $$b_{11}=-\omega_{TO}^2.$$

The form of potential energy is now derived. The power flow per unit area is defined as the Poynting vector

(2.16) $$P=E\times H.$$

Using the vector identity, $\nabla\cdot(E\times H)=H\cdot(\nabla\times E)-E\cdot(\nabla\times H)$, and the Maxwell equations

(2.17a) $$\nabla\times E=-\mu\dot{H}.$$

(2.17b) $$\nabla\times H=J+\dot{D}.$$

with the definitions.

(2.18a) $$D=\varepsilon_0 E+P.$$

(2.18b) $$J = \sum_i e_i \dot{R}_i \delta(R - R_i).$$

the temporal rate of potential energy density change (J is ignored at this moment because it only contributes to kinetic energy) can be written as

(2.19) $$\mu H \cdot \dot{H} + \varepsilon_0 E \cdot \dot{E} + E \cdot \dot{P}.$$

If this potential energy density is assumed

(2.20) $$E_T = \frac{1}{2}\dot{u}^2 - \frac{1}{2}b_{11}u^2 - b_{12}u \cdot E - \frac{1}{2}b_{22}E^2 + E \cdot P + \frac{1}{2}\varepsilon_0 E^2 + \frac{1}{2}\mu H^2.$$

the time derivative of E_T is

(2.21) $$\frac{dE_T}{dt} = \dot{u}\left(\ddot{u} - b_{11}u - b_{12}E\right) + \dot{E}\left(P - b_{12}u - b_{22}E\right) + E \cdot \dot{P} + \varepsilon_0 E \cdot \dot{E} + \mu H \cdot \dot{H}.$$

The parenthesis terms are equal to zero and the two equations for potential energy density, Eqs. (2.19) and (2.21), are thus equivalent. The potential energy density can now be written as

(2.22a) $$E_T = \frac{1}{2}\dot{u}^2 - \frac{1}{2}b_{11}u^2 - b_{12}u \cdot E - \frac{1}{2}b_{22}E^2 + E \cdot P + \frac{1}{2}\varepsilon_0 E^2 + \frac{1}{2}\mu H^2.$$

(2.22b) $$E_T = \frac{1}{2}\dot{u}^2 - \frac{1}{2}b_{11}u^2 + \frac{1}{2}b_{22}E^2 + \frac{1}{2}\varepsilon_0 E^2 + \frac{1}{2}\mu H^2.$$

(2.22c) $$E_T = \frac{1}{2}\dot{u}^2 + \frac{1}{2}\omega_0^2 u^2 + \frac{1}{2}\varepsilon_r E^2 - \frac{1}{2}\varepsilon_0 E^2 + \frac{1}{2}\varepsilon_0 E^2 + \frac{1}{2}\mu H^2.$$

(2.22d) $$E_T = \frac{1}{2}\left(\dot{u}^2 + \omega_0^2 u^2\right) + \frac{1}{2}\varepsilon_r E^2 + \frac{1}{2}\mu H^2.$$

The three terms relate to the phonon, electrical and magnetic energies, respectively. Neglecting magnetic energy, the potential energy density is

(2.23) $$E_T = \frac{1}{2}\left(\dot{u}^2 + \omega_0^2 u^2\right) + \frac{1}{2}\varepsilon_r E^2.$$

The system Hamiltonian becomes, including the kinetic energy, is

$$H_{ss} = \sum \frac{1}{2} m_i \dot{R}_i^2 + \int \left\{ \frac{1}{2} \left(\dot{u}^2 + \omega_0^2 u^2 \right) + \frac{1}{2} \varepsilon_\infty E^2 \right\} dv . \tag{2.24}$$

The electric field can be found from the Maxwell equation

$$\nabla \cdot D = \nabla \cdot \left(\varepsilon_0 E + P \right) = \rho . \tag{2.25a}$$

$$\nabla \cdot \left(\varepsilon_0 E + b_{12} u + b_{22} E \right) = \rho . \tag{2.25b}$$

$$\left(\varepsilon_0 + b_{22} \right) \nabla \cdot E + b_{12} \nabla \cdot u = \rho . \tag{2.25c}$$

$$\varepsilon_\infty \nabla \cdot E + \omega_{TO} \left(\varepsilon_0 - \varepsilon_\infty \right)^{1/2} \nabla \cdot u = \rho . \tag{2.25d}$$

$$\nabla \cdot E = -\frac{\omega_{TO}}{\varepsilon_\infty} \left(\varepsilon_0 - \varepsilon_\infty \right)^{1/2} \nabla \cdot u + \frac{\rho}{\varepsilon_\infty} . \tag{2.25e}$$

The vector u can be split into transverse and longitudinal components

$$u = u_T + u_L . \tag{2.26}$$

where

$$\nabla \cdot u_T = 0 . \tag{2.27a}$$

$$\nabla \times u_L = 0 . \tag{2.27b}$$

Thus

$$\nabla \cdot u = \nabla \cdot u_T + \nabla \cdot u_L = \nabla \cdot u_L . \tag{2.28}$$

So,

$$\nabla \cdot E = -\frac{\omega_{TO}}{\varepsilon_\infty} \left(\varepsilon_0 - \varepsilon_\infty \right)^{1/2} \nabla \cdot u_L + \frac{\varepsilon_0}{\varepsilon_\infty} \frac{\rho}{\varepsilon_0} . \tag{2.29}$$

with ρ the free charge.

From (2.29) it is seen that the electric field has two terms, one dependent only on lattice and the other only on free charge.

The lattice term is simply proportional to displacement as

(2.30) $$E_L = -\frac{\omega_{TO}}{\varepsilon_r}(\varepsilon_0 - \varepsilon_r)^{1/2} u_L .$$

For the vacuum term, the relation for the electric field is

(2.31a) $$\nabla \cdot E_{vac} = \frac{\rho}{\varepsilon_0},$$

(2.31b) $$E_{vac} = -\frac{1}{4\pi\varepsilon_0}\int \frac{\rho(R')}{R - R'^2} dR'$$

The total electric field is

(2.32) $$E = -\frac{\omega_{TO}}{\varepsilon_r}(\varepsilon_0 - \varepsilon_r)^{1/2} u_L + \frac{\varepsilon_0}{\varepsilon_r} E_{vac} .$$

In the definition of energy density, the square of electric field is required

(2.33a)

$$E^2 = E \cdot E = \left(-\frac{\omega_{TO}}{\varepsilon_r}(\varepsilon_0 - \varepsilon_r)^{1/2} u_L + \frac{\varepsilon_0}{\varepsilon_r} E_{vac} \right) \cdot \left(-\frac{\omega_{TO}}{\varepsilon_r}(\varepsilon_0 - \varepsilon_r)^{1/2} u_L + \frac{\varepsilon_0}{\varepsilon_r} E_{vac} \right),$$

(2.33b) $$E^2 = \left(\frac{\omega_{TO}}{\varepsilon_r} \right)^2 (\varepsilon_0 - \varepsilon_r) u_L^2 - 2\frac{\omega_{TO}}{\varepsilon_r}\frac{\varepsilon_0}{\varepsilon_r}(\varepsilon_0 - \varepsilon_r)^{1/2} u_L \cdot E_{vac} + \frac{\varepsilon_0^2}{\varepsilon_r^2} E_{vac}^2 .$$

Now the potential energy density can be simplified

(2.34a) $$E_T = \frac{1}{2}\left((\dot{u}_T + \dot{u}_L)^2 + \omega_{TO}^2 (u_T + u_L)^2 \right)$$

$$+ \frac{1}{2}\varepsilon_\infty \left[\left(\frac{\omega_{TO}}{\varepsilon_\infty} \right)^2 (\varepsilon_0 - \varepsilon_\infty) u_L^2 - 2\frac{\omega_{TO}}{\varepsilon_\infty}\frac{\varepsilon_0}{\varepsilon_\infty}(\varepsilon_0 - \varepsilon_\infty)^{1/2} u_L \cdot E_{vac} + \frac{\varepsilon_0^2}{\varepsilon_\infty^2} E_{vac}^2 \right]$$

(2.34b) $$E_T = \frac{1}{2}\left(\dot{u}_T^{\,2} + \dot{u}_L^{\,2} + \omega_{TO}^{\,2} u_T^{\,2} + \omega_{TO}^{\,2} u_L^{\,2} \right)$$

$$+ \frac{1}{2}\left[\frac{\omega_{TO}^{\,2}}{\varepsilon_r}(\varepsilon_0 - \varepsilon_r) u_L^{\,2} - 2\omega_{TO} \frac{\varepsilon_0}{\varepsilon_r}(\varepsilon_0 - \varepsilon_r)^{1/2} u_L \cdot E_{vac} + \frac{\varepsilon_0^{\,2}}{\varepsilon_r} E_{vac}^{\,2} \right]$$

(2.34c) $$E_T = \frac{1}{2}\left(\dot{u}_T^{\,2} + \dot{u}_L^{\,2} + \omega_{TO}^{\,2} u_T^{\,2} + \omega_{TO}^{\,2} u_L^{\,2} + \omega_{TO}^{\,2}\left(\frac{\varepsilon_0}{\varepsilon_r} - 1 \right) u_L^{\,2} \right)$$

$$+ \frac{1}{2}\left[- 2\omega_{TO} \frac{\varepsilon_0}{\varepsilon_r}(\varepsilon_0 - \varepsilon_r)^{1/2} u_L \cdot E_{vac} + \frac{\varepsilon_0^{\,2}}{\varepsilon_r} E_{vac}^{\,2} \right].$$

(2.34d) $$E_T = \frac{1}{2}\left(\dot{u}_T^{\,2} + \dot{u}_L^{\,2} + \omega_{TO}^{\,2} u_T^{\,2} + \omega_{TO}^{\,2} \frac{\varepsilon_0}{\varepsilon_r} u_L^{\,2} \right)$$

$$+ \frac{1}{2}\left[- 2\omega_{TO} \frac{\varepsilon_0}{\varepsilon_r}(\varepsilon_0 \varepsilon_r)^{1/2} \frac{(\varepsilon_0 - \varepsilon_r)^{1/2}}{(\varepsilon_0 \varepsilon_r)^{1/2}} u_L \cdot E_{vac} + \frac{\varepsilon_0^{\,2}}{\varepsilon_r} E_{vac}^{\,2} \right].$$

(2.34e) $$E_T = \frac{1}{2}\left(\dot{u}_T^{\,2} + \dot{u}_L^{\,2} + \omega_{TO}^{\,2} u_T^{\,2} + \omega_{TO}^{\,2} \frac{\varepsilon_0}{\varepsilon_r} u_L^{\,2} \right)$$

$$+ \frac{1}{2}\left[- 2\omega_{TO}\varepsilon_0 \left(\frac{\varepsilon_0}{\varepsilon_r} \right)^{1/2} \left(\frac{1}{\varepsilon_r} - \frac{1}{\varepsilon_0} \right)^{1/2} u_L \cdot E_{vac} + \frac{\varepsilon_0^{\,2}}{\varepsilon_r} E_{vac}^{\,2} \right].$$

The system Hamiltonian becomes

(2.35) $$H_{sys} = \sum_i \frac{1}{2} m_i \dot{R}_i^{\,2} + \int_v \frac{\varepsilon_0^{\,2}}{2\varepsilon_r} E_{vac}^{\,2} dv + \int_v \frac{1}{2}\left\{ \left(\dot{u}_T^{\,2} + \omega_{TO}^{\,2} u_T \right) + \left(\dot{u}_L^{\,2} + \omega_{TO}^{\,2} \frac{\varepsilon_0}{\varepsilon_r} u_L \right) \right\} dv$$

$$- \omega_{TO}\varepsilon_0 \left(\frac{\varepsilon_0}{\varepsilon_r} \right)^{1/2} \left(\frac{1}{\varepsilon_r} - \frac{1}{\varepsilon_0} \right)^{1/2} \int_v u_L \cdot E_{vac} dv .$$

The four terms relate to the kinetic energy, the Columbic energy, the phonon energy and the electron-phonon interaction, respectively. The electron-phonon interaction is rewritten

$$H_{e-ph} = -\omega_{TO}\varepsilon_0\left(\frac{\varepsilon_0}{\varepsilon_r}\right)^{1/2}\left(\frac{1}{\varepsilon_r}-\frac{1}{\varepsilon_0}\right)^{1/2}\int_v u_L \cdot E_{vac}\,dv. \tag{2.36}$$

According to the Lyddane-Sachs-Teller[3] relation,

$$\frac{\varepsilon_0}{\varepsilon_r} = \frac{\omega_{LO}^2}{\omega_{TO}^2}. \tag{2.37}$$

The electron-phonon Hamiltonian can be written as

$$H_{e-ph} = -\omega_{LO}\varepsilon_0\left(\frac{1}{\varepsilon_r}-\frac{1}{\varepsilon_0}\right)^{1/2}\int_v u_L \cdot E_{vac}\,dv. \tag{2.38}$$

2.2.3 Normal coordinates

The displacement can be expressed in terms of normal operators by introducing these discrete Fourier series. For the displacement, the coefficient in (2.5a) has been taken out so results can be compared with literature.

$$(u_L)_r = \sqrt{\frac{\mu_n}{v_a}}\frac{1}{\sqrt{N}}\sum_k p_k e^{-ikra}. \tag{2.39a}$$

$$(E_{vac})_r = \frac{1}{\sqrt{N}}\sum_{k'} E_{k'} e^{-ik'ra}. \tag{2.39b}$$

The electron-phonon Hamiltonian becomes

$$H_{e-ph} = -\omega_{LO}\varepsilon_0\left(\frac{1}{\varepsilon_\infty}-\frac{1}{\varepsilon_0}\right)^{1/2}\left(\sqrt{\frac{\mu_n}{v_a}}\frac{1}{N}\right)\int_v\sum_k p_k e^{-kra}\cdot\sum_{k'} E_{k'} e^{-k'ra}dv. \tag{2.40a}$$

(2.40b) $$H_{e-ph} = -\omega_{LO}\varepsilon_0\left(\frac{1}{\varepsilon_\infty}-\frac{1}{\varepsilon_0}\right)^{1/2}\left(\sqrt{\frac{\mu_n}{v_a}}\frac{1}{N}\right)\sum_k p_k \sum_{k'} E_{k'}\int_v e^{-ikr}\cdot e^{-ik'r}dv.$$

(2.40c) $$H_{e-ph} = -\omega_{LO}\varepsilon_0\left(\frac{1}{\varepsilon_\infty}-\frac{1}{\varepsilon_0}\right)^{1/2}\left(\sqrt{\frac{\mu_n}{v_a}}\frac{1}{N}\right)\sum_k p_k \sum_{k'} E_{k'}\int_v e^{-i(k-k')r}dv.$$

The above integral equals the summation[4]

(2.41) $$\frac{1}{V}\int_v e^{-i(k-k')r}dv \equiv \sum_k e^{i(k-k')r} = N\delta(k+k').$$

Thus the electron-phonon Hamiltonian is the sum over the modes

(2.42a) $$H_{e-ph} = -\omega_{LO}\varepsilon_0\left(\frac{1}{\varepsilon_\infty}-\frac{1}{\varepsilon_0}\right)^{1/2}\left(\sqrt{\frac{\mu_n}{v_a}}\frac{NV}{N}\right)\sum_k p_k \sum_{k'} E_{k'}\,\delta(k+k').$$

(2.42b) $$H_{e-ph} = -\omega_{LO}\varepsilon_0\left(\frac{1}{\varepsilon_\infty}-\frac{1}{\varepsilon_0}\right)^{1/2}\left(\sqrt{\frac{\mu_n}{v_a}}V\right)\sum_k p_k \cdot E_{-k}.$$

The vacuum electric field will assumed due to electron at r'.

(2.43a) $$E_{vac} = \frac{e(r-r')}{4\pi\varepsilon_0|r-r'|^3}.$$

(2.43b) $$E_k = \frac{1}{\sqrt{N}}\sum\frac{e(r-r')}{4\pi\varepsilon_0|r-r'|^3}.$$

(2.43c) $$E_k = \frac{e}{4\pi\varepsilon_0}\frac{1}{\sqrt{N}}\sum\frac{e(r-r')}{|r-r'|^3}.$$

The summation can be handled by an integral[5]

(2.44a) $$I = \sum\frac{e^{ik\cdot r}(r-r')}{|r-r'|^3} \approx \frac{1}{V}\int_v\frac{e^{ik\cdot r}(r-r')}{|r-r'|^3}dv.$$

Introducing $R = r - r'$

(2.44b) $$I = \frac{1}{V} e^{-ik\cdot r'} \int_{\nu} \frac{e^{ik\cdot R}(R)}{|R|^3} dv'.$$

But[6],

(2.44c) $$\frac{R}{|R^3|} = \nabla_R \frac{1}{R}.$$

Thus,

(2.44d) $$I = e^{-ik\cdot r} \frac{1}{V} \nabla_R \int_{\nu} \frac{e^{ik\cdot R}}{|R|} dv'.$$

Using derived results[7],

(2.44d) $$\frac{1}{V} \int_{\nu} \frac{e^{ik\cdot R}}{R} = \frac{4\pi}{V} \frac{1}{k^2}.$$

(2.44e) $$I = \frac{4\pi}{V} e^{-ik\cdot r} \nabla_R \frac{1}{k^2}.$$

But since $\nabla_R = -ik$.

(2.44f) $$I = \frac{4\pi}{V} e^{-ik\cdot r} \frac{1}{k}.$$

Thus the electric field can be written as (and letting $r = r'$)

(2.45a) $$E_k = \frac{e}{4\pi\varepsilon_0} \frac{1}{\sqrt{N}} i \frac{4\pi}{V} e^{-ik\cdot r} \frac{1}{k}.$$

(2.45b) $$E_k = -i \frac{1}{\sqrt{N}} \frac{e}{\varepsilon_0} \frac{1}{V} e^{-ik\cdot r} \frac{1}{k}.$$

and using the fact that the free electric field is a real quantity

(2.45c) $$E_{-k} = E_k^* = i \frac{1}{\sqrt{N}} \frac{e}{\varepsilon_0} \frac{1}{V} e^{ik\cdot r} \frac{1}{k}.$$

The long wavelength approximation $k \cong 0$ will mean that it does not matter the origin of the electric charge and the final expression for the electric field is

$$E_{-k} = i\frac{1}{\sqrt{N}}\frac{e}{\varepsilon_0}\frac{1}{V}\frac{1}{k}. \tag{2.45d}$$

The electron-phonon Hamiltonian using this electric field can be written as

$$H_{e-ph} = -\omega_{LO}\varepsilon_0\left(\frac{1}{\varepsilon_r}-\frac{1}{\varepsilon_0}\right)^{1/2}\left(\sqrt{\frac{\mu_n}{v_a}}V\right)\sum_k p_k i\frac{1}{\sqrt{N}}\frac{e}{\varepsilon_0}\frac{1}{V}e^{-ikr}\frac{1}{k} \tag{2.46a}$$

$$H_{e-ph} = -i\omega_{LO}e\left(\frac{1}{\varepsilon_r}-\frac{1}{\varepsilon_0}\right)^{1/2}\left(\sqrt{\frac{\mu_n}{Nv_a}}\right)\sum_k p_k\frac{e^{-ikr}}{k}. \tag{2.46b}$$

We can express the displacements in terms of raising and lowering operators[8] assuming that $k \approx 0$

$$p_k = i\sqrt{\frac{\hbar}{2\mu_n\omega_{LO}}}\left(a_k e^{-i\omega_{LO}t} + a_k^{-}e^{i\omega_{LO}t}\right). \tag{2.47a}$$

The electron-phonon Hamiltonian in terms of the raising and lowering operators is

$$H_{e-ph} = -i\omega_{LO}e\left(\frac{1}{\varepsilon_r}-\frac{1}{\varepsilon_0}\right)^{1/2}\left(\sqrt{\frac{\mu_n}{Nv_a}}\right)i\sqrt{\frac{\hbar}{2\mu_n\omega_{LO}}}\sum_k\frac{1}{k}\left(a_k e^{-i\omega_{LO}t} + a_k^{-}e^{i\omega_{LO}t}\right). \tag{2.48a}$$

$$H_{e-ph} = \left(\frac{e^2\hbar\omega_{LO}}{2V}\right)^{1/2}\left(\frac{1}{\varepsilon_r}-\frac{1}{\varepsilon_0}\right)^{1/2}\sum_k\frac{1}{k}\left(a_k e^{-i\omega_{LO}t} + a_k^{-}e^{i\omega_{LO}t}\right). \tag{2.48b}$$

Finally we can write.

$$H_{e-ph} = \sum_k m(k)\left(a_k e^{-i\omega_{LO}t} + a_k^{-}e^{i\omega_{LO}t}\right). \tag{2.48c}$$

$$m(k) = \left(\frac{e^2\hbar\omega_{LO}}{2V}\right)^{1/2}\left(\frac{1}{\varepsilon_r}-\frac{1}{\varepsilon_0}\right)^{1/2}\frac{1}{k}. \tag{2.48d}$$

2.2.4 Scattering rate in 3D

The electron-phonon scattering matrix element will be derived so it can be used in the Fermi Golden Rule to calculate the scattering rate. Dropping the time dependence, the matrix element for an electron to go from k_1 to k_2 is

(2.49a) $$< k_1 | H_{e\text{-}ph} | k_2 >= \sum_k m(k) < k1 | a + a^{\dagger} | k2 >.$$

(2.49b) $$< k_1 | a + a^{\dagger} | k_2 >=< k_1 | a | k_2 > + < k_1 | a^{\dagger} | k_2 >.$$

The first term refers to phonon absorption

(2.49c) $$< k_1 | a | k_2 >=< k_1 | \sqrt{N_q} | k_2 - k >= \sqrt{N_q}\delta_{k_2,k_1-k}.$$

The Kronecker delta function is used which is zero unless $k_2 = k_1 - k$ (where k is the phonon wavevector) and the equilibrium phonon population is used with the value

(2.49d) $$N_q = \frac{1}{\exp\left(\frac{\hbar\omega_{LO}}{k_B T}\right) - 1}.$$

The second term refers to phonon emission

(2.49e) $$< k_1 | a^{\dagger} | k_2 >=< k_1 | \sqrt{N_q + 1} | k_2 + k >= \sqrt{N_q + 1}\delta_{k_2,k_1-k}.$$

(2.49f) $$< k_1 | H_{e\text{-}ph} | k_2 >= \sum_k m(k)\left(\sqrt{N_q + 1}\delta_{k_2,k_1-k} + \sqrt{N_q}\delta_{k_2,k_1-k}\right).$$

(2.49g) $$< k_1 | H_{e\text{-}ph} | k_2 >= m(k)\left(\sqrt{N_q + 1}\delta_{k_2,k_1-k} + \sqrt{N_q}\delta_{k_2,k_1-k}\right).$$

(2.49h) $$M(k_1, k) = m(k)\left(\sqrt{N_q + 1}\delta_{k_2,k_1-k} + \sqrt{N_q}\delta_{k_2,k_1-k}\right).$$

When k_1 and k_2 are fixed, so is the phonon wavevector k, and thus any two quantities are enough. The reason I kept the Kronecker delta function was because they are important in the expression for energy terms in the scattering rate.

The Fermi golden rule can be applied if the interaction is small and also in the following the dispersion relation is ignored.

$$P(k_1,k_2)=\frac{2\pi}{\hbar}|M(k_1,k)|^2\delta\left(E_{k_1}-E_{k_2}\pm\hbar\omega_{LO}\right). \tag{2.50}$$

where + is for absorption and – is for emission.

First the energies in the effective mass approximation are

$$E_{k_1}=\frac{\hbar^2k_1^2}{2m^*}. \tag{2.51a}$$

and using the Kronecker delta function (to get momentum conservation)

$$E_{k_2}=\frac{\hbar^2(k_1\pm k)\cdot(k_1\pm k)}{2m^*}=\frac{\hbar^2k_1^2}{2m^*}+\frac{\hbar^2k^2}{2m^*}\pm\frac{\hbar^2}{m^*}k_1k\cos\theta. \tag{2.51b}$$

where again the upper sign is for absorption and lower sign for emission and θ is the angle between k_1 and k.

$$E_{k_1}-E_{k_2}\pm\hbar\omega_{LO}=\frac{\hbar^2k_1^2}{2m^*}-\frac{\hbar^2k_1^2}{2m^*}-\frac{\hbar^2k^2}{2m^*}\mp\frac{\hbar^2}{m^*}k_1k\cos\theta\pm\hbar\omega_{LO}. \tag{2.51c}$$

$$E_{k_1}-E_{k_2}\pm\hbar\omega_{LO}=-\frac{\hbar^2k^2}{2m^*}\mp\frac{\hbar^2}{m^*}k_1k\cos\theta\pm\hbar\omega_{LO}. \tag{2.51d}$$

The scattering is the summation of Eq. (2.50) over all final states as

$$\Gamma(k_1)=\sum_{k_2}P(k_1,k_2)=\frac{2\pi}{\hbar}\sum_{k}|M(k_1,k)|^2\delta\left(E_{k_1}-E_{k_2}\pm\hbar\omega_{LO}\right). \tag{2.52}$$

The value inside the summation over k is just the total number of states that are available. The factor of 2 for spin is ignored, because the electron to be scattered is assumed to be scattered to a state with same spin. Further the summation is turned into an integral (over spherical coordinates) assuming that k is nearly continuous, *i.e.*, the volume is large.

(2.53a) $$\Gamma(k_1) = \frac{2\pi}{\hbar}\frac{V}{(2\pi)^3}\int_0^{2\pi} d\phi \int_k \int_0^{\pi} |M(k_1,k)|^2 \delta\left(E_{k_1} - E_{k_2} \pm \hbar\omega_{LO}\right) k^2 \sin\theta d\theta dk .$$

Since none of the values in the integral depend on azimuthal angle, a two-dimensional integral can be immediately written

(2.53b) $$\Gamma(k_1) = \frac{1}{\hbar}\frac{V}{2\pi}\int_k |M(k_1,k)|^2 k^2 dk \int_0^{\pi} \delta\left(E_{k_1} - E_{k_2} \pm \hbar\omega_{LO}\right) \sin\theta d\theta .$$

The integral over the polar angle must be evaluated first because it has dependence over both k and θ. Writing the argument as Eq. (2.51d)

(2.53c) $$I = \int_0^{\pi} \delta\left(-\frac{\hbar^2 k^2}{2m^*} \mp \frac{\hbar^2}{m^*} k_1 k\cos\theta \pm \hbar\omega_{LO}\right) \sin\theta d\theta .$$

and letting r = cos(θ). dr = -sin(θ)dθ. Now the limits are from cos(0) = 1 to cos(π) = -1

(2.53d) $$I = -\int_1^{-1} \delta\left(\left[\frac{\hbar^2}{m^*} k_1 k\right]\left[-\frac{k}{2k_1} \mp r \pm \frac{m^*\omega_{LO}}{\hbar k_1 k}\right]\right) dr .$$

(2.53e) $$I = \int_{-1}^{1} \delta\left(\left[\frac{\hbar^2}{m^*} k_1 k\right]\left[\mp r - \frac{k}{2k_1} \pm \frac{m^*\omega_{LO}}{\hbar k_1 k}\right]\right) dr .$$

Now using the shifting property of the Dirac delta function[9]

(2.53f) $$\delta(ax) = \frac{1}{|a|}\delta(x) .$$

(2.53g) $$I = \frac{m^*}{\hbar^2}\frac{1}{k_1 k}\int_{-1}^{1} \delta\left(\mp r - \frac{k}{2k_1} \pm \frac{m^*\omega_{LO}}{\hbar k_1 k}\right) dr = \frac{m^*}{\hbar^2}\frac{1}{k_1 k} .$$

This also fixes the limit of k that can take part in scattering

(2.54a) $$\mp r - \frac{k}{2k_1} \pm \frac{m^*\omega_{LO}}{\hbar k_1 k} = 0 .$$

First the general solution of the above equation will be found

(2.54b) $$\left(-\frac{1}{2k_1}\right)k^2 + (\mp r)k + \left(\pm\frac{m^*\omega_{LO}}{\hbar k_1}\right) = 0.$$

(2.54c) $$A = -\frac{1}{2k_1}. \quad B = \mp r. \quad C = \pm\frac{m^*\omega_{LO}}{\hbar k_1}.$$

(2.54d) $$k = \frac{-B \pm \sqrt{B^2 - 4AC}}{2A}.$$

(2.54e) $$k = k_1\left(\mp r \pm \sqrt{r^2 \pm \frac{2m^*\omega_{LO}}{\hbar k_1^2}}\right).$$

The dominant phonon wavevector q_0 can be derived

(2.54f) $$\hbar\omega_{LO} = \frac{\hbar^2 q_0^2}{2m^*}.$$

(2.54g) $$q_0^2 = \frac{2m^*\omega_{LO}}{\hbar}.$$

So the general relationship is

(2.54h) $$k = k_1\left(\mp r \pm \sqrt{r^2 \pm \frac{q_0^2}{k_1^2}}\right) = \mp k_1 r \pm \sqrt{k_1^2 r^2 \pm q_0^2}.$$

Consider the case of emission (lower sign)

(2.55a) $$k_{(e)} = k_1 r \pm \sqrt{k_1^2 r^2 - q_0^2}.$$

Both the maximum and minimum values occur for r = 1 (taking the + and – sign, respectively)

(2.55b) $$k_{(e)}^{+} = k_1 + \sqrt{k_1^2 - q_0^2}.$$

(2.55c) $$k_{(e)}^{-} = k_1 - \sqrt{k_1^2 - q_0^2}.$$

and the requirement $k_1^2 > q_0^2$, or the kinetic energy is greater than the phonon energy.

Consider the case of absorption (upper sign)

(2.56a) $$k_{(a)} = -k_1 r \pm \sqrt{k_1^2 r^2 + q_0^2}\,.$$

The negative sign can at once be dismissed because then k will be a negative quantity. The minimum and maximum values occur at r = -1 and r =+1 for the positive branch

(2.56b) $$k^-_{(a)} = -k_1 + \sqrt{k_1^2 + q_0^2}\,.$$

(2.56c) $$k^+_{(a)} = k_1 + \sqrt{k_1^2 + q_0^2}\,.$$

Thus the integral becomes

(2.57) $$\Gamma(k_1) = \frac{m^* V}{2\pi\hbar^3 k_1}\int_{k^-}^{k^+} |M(k_1,k)|^2 k\,dk\,.$$

From Eqs. (2.49h) and (2.48d)

(2.58a) $$M(k_1,k) = \left(\frac{e^2\hbar\omega_{LO}}{2V}\right)^{1/2}\left(\frac{1}{\varepsilon_\infty} - \frac{1}{\varepsilon_0}\right)^{1/2}\frac{1}{k}\left(\sqrt{N_q+1}\,\delta_{k_2,k_1-k} + \sqrt{N_q}\,\delta_{k_2,k_1-k}\right).$$

(2.58b) $$|M(k_1,k)|^2 = \left(\frac{e^2\hbar\omega_{LO}}{2V}\right)\left(\frac{1}{\varepsilon_\infty} - \frac{1}{\varepsilon_0}\right)\frac{1}{k^2}\left([N_q+1]\delta_{k_2,k_1-k} + N_q\delta_{k_2,k_1-k}\right).$$

The scattering rate becomes

(2.59a) $$\Gamma(k_1) = \frac{m^* V}{2\pi\hbar^3 k_1}\left(\frac{e^2\hbar\omega_{LO}}{2V}\right)\left(\frac{1}{\varepsilon_\infty} - \frac{1}{\varepsilon_0}\right)\int_{k^-}^{k^+}\frac{1}{k}\left([N_q+1]\delta_{k_2,k_1-k} + N_q\delta_{k_2,k_1-k}\right)dk\,.$$

(2.59b) $$\Gamma(k_1) = \frac{m^* e^2\omega_{LO}}{4\pi\hbar^2 k_1}\left(\frac{1}{\varepsilon_\infty} - \frac{1}{\varepsilon_0}\right)\int_{k^-}^{k^+}\frac{1}{k}\left([N_q+1]\delta_{k_2,k_1-k} + N_q\delta_{k_2,k_1-k}\right)dk\,.$$

Two scattering rates can be obtained for absorption and emission

(2.60a) $$\Gamma_{(a)}(k_1) = \frac{m^* e^2\omega_{LO}}{4\pi\hbar^2 k_1}\left(\frac{1}{\varepsilon_\infty} - \frac{1}{\varepsilon_0}\right)N_q\int_{k^-_{(a)}}^{k^+_{(a)}}\frac{dk}{k}\,.$$

(2.60b) $$\Gamma_{(e)}(k_1) = \frac{m^* e^2 \omega_{LO}}{4\pi\hbar^2 k_1}\left(\frac{1}{\varepsilon_\infty} - \frac{1}{\varepsilon_0}\right)(N_q + 1)\int_{k_{(e)}}^{k_{(e)}} \frac{dk}{k}.$$

The integrals are just natural logarithms and using the parabolic approximation.

(2.61a) $$k_1 = \frac{\sqrt{2m^* E_1}}{\hbar}.$$

the energy dependent scattering rates are

(2.61b) $$\Gamma_{(a)}(k_1) = \frac{\sqrt{m^*} e^2 \omega_{LO}}{4\sqrt{2}\pi\hbar}\left(\frac{1}{\varepsilon_\infty} - \frac{1}{\varepsilon_0}\right)\frac{N_q}{\sqrt{E_1}} \ln\left(\frac{-\sqrt{E_1} + \sqrt{E_1 + \hbar\omega_{LO}}}{\sqrt{E_1} + \sqrt{E_1 + \hbar\omega_{LO}}}\right).$$

(2.61c) $$\Gamma_{(e)}(E_1) = \frac{\sqrt{m^*} e^2 \omega_{LO}}{4\sqrt{2}\pi\hbar}\left(\frac{1}{\varepsilon_\infty} - \frac{1}{\varepsilon_0}\right)\left(\frac{N_q + 1}{\sqrt{E_1}}\right) \ln\left(\frac{\sqrt{E_1} + \sqrt{E_1 - \hbar\omega_{LO}}}{\sqrt{E_1} - \sqrt{E_1 - \hbar\omega_{LO}}}\right).$$

These two are graphed, in Fig. 2.1, for GaAs with an effective electron mass of 0.067 free-electron mass, a phonon energy $\hbar\omega = 36.2$ meV, a temperature of 300 K and for electron energies between 1 meV and 200 meV. In the computer programs, Eq. (2.62a) is used for electron-phonon Hamiltonian with g defined in (2.62b). Since the optical frequency ω_{LO} is much greater than phonon frequencies, the operators can be used with the approximation $k \cong 0$ and can be taken out of summation.

(2.62a) $$H_{e\text{-}ph} = \hbar\omega_{LO} g\left(a e^{-i\omega_{LO}t} + a^* e^{i\omega_{LO}t}\right).$$

(2.62b) $$g = \frac{\sum_k |M(k_1, k)|^2 \delta(E_{k1} - E_{k1\pm k})}{\hbar\omega_{LO}} = \frac{1}{\hbar\omega_{LO}} \frac{\hbar}{2\pi} \sum_k P(k_1, k) = \frac{\Gamma(k_1)}{2\pi\omega_{LO}}.$$

The g-value is graphed in Fig. 2.2. This shows that it reaches a maximum value of 0.025 for electron energies near 100 meV. For zero kinetic energy, the value of g is about 0.007. The effect of confinement will lead to a much greater g, as shown in the next section.

2.2.5 Scattering rate in 1D

If the initial energy of an electron is E_i, it has wavevectors $\pm k_i$ with magnitude

(2.63) $$k_i = \frac{\sqrt{2m^* E_i}}{\hbar}.$$

There are two cases to consider, absorption or emission, with the final energies

(2.64a) $$E_f^{(a)} = E_i + \hbar\omega_{LO}.$$

(2.64b) $$E_f^{(e)} = E_i - \hbar\omega_{LO}.$$

Absorption will be considered first. For $-k_i$, the final wavevectors are

(2.65a) $$\frac{\hbar^2 k_f^2}{2m^*} = \frac{\hbar^2 k_i^2}{2m^*} + \hbar\omega_{LO}.$$

(2.65b) $$k_f^2 = k_i^2 + \frac{2m^*\omega_{LO}}{\hbar} = k_i^2 + q_0^2.$$

where q_0 is dominant wavevector.

So the final wavevectors are

(2.66) $$k_f = \pm\sqrt{k_i^2 + q_0^2}.$$

Thus for this particular k_i, the two phonon wavevectors that can take place are

(2.67a) $$q = q_-^{(a)} = \sqrt{k_i^2 + q_0^2} - k_i.$$

(2.67b) $$q = q_-^{(a)} = -\sqrt{k_i^2 + q_0^2} - k_i.$$

For $-k_i$, the phonon wavevectors have same lengths. Thus at the end, the matrix element must be multiplied by 2 to account for this degeneracy. The four wavevectors taking part in absorption are shown in Fig. 2.3.

Similarly for emission, the energy conservation demands that

$$\frac{\hbar^2 k_f^2}{2m^*} = \frac{\hbar^2 k_i^2}{2m^*} - \hbar\omega_{LO}. \tag{2.68a}$$

$$k_f^2 = k_i^2 - \frac{2m^*\omega_{LO}}{\hbar} = k_i^2 - q_0^2. \tag{2.68b}$$

Thus the final wavevectors and the phonon wavevectors are

$$k_f = \pm\sqrt{k_i^2 - q_0^2}. \tag{2.69a}$$

$$q_-^{(e)} = \sqrt{k_i^2 - q_0^2} - k_i. \tag{2.69b}$$

$$q_-^{(e)} = -\sqrt{k_i^2 - q_0^2} - k_i. \tag{2.69c}$$

The emission diagram will be similar to Fig. 2.3 except that the arrows will change direction and the initial and final wavevectors are interchanged. Additionally the initial energy should be greater than $\hbar\omega_{LO}$ for emission.

The coupling is the Fröhlich relation m(q), Eq. (2.48b).

$$m(q) = \left(\frac{e^2\hbar\omega_{LO}}{2LA}\right)^{1/2}\left(\frac{1}{\varepsilon_\infty} - \frac{1}{\varepsilon_0}\right)^{1/2}\frac{1}{q}. \tag{2.70}$$

The density of states in 1D is

$$dos(E) = L\frac{\sqrt{2m^*}}{h}E^{-1/2}. \tag{2.71}$$

Here the interaction volume is LA, where L in the length and A is cross section. For an electron at energy E, where $E < \hbar\omega_{LO}$, only phonon absorption can take place. Additionally electrons with energy of $E + \hbar\omega_{LO}$ can emit a phonon to energy E.

The cross-sectional area must be small enough so the 1D density of states may be used. For a infinite box with dimensions $L_1 = A^{1/2}$, $L_2 = A^{1/2}$ and $L_3 = L$, the density

of states in the L_1 and L_2 directions can be ignored (as they are zero), if the electron energy is less than the ground-state confinement energy, e_0, in those directions[10], or

$$E < e_0 = \frac{\hbar^2\pi^2}{2m^*A}. \tag{2.72}$$

Thus for E less than $\hbar\omega_{LO}$, with $m^* = 0.067\ m_0$, an area of A = (124 Angstrom)^2 means that the 1D density-of states may be used for all E. It can be seen that area dimensions less than this number can also be used. However, the largest cross-section is used because the dielectric continuum theory has been derived for large volumes.

The Fermi Golden rule sates that the scattering from k to k' is

$$\Gamma_{kk'} = \frac{2\pi}{\hbar}|M_{kk'}|^2 dos(E_{k'}). \tag{2.73a}$$

and thus the total scattering is

$$\Gamma_k = \sum_{k'}\Gamma_{kk'} = \frac{2\pi}{\hbar}\sum_{k'}|M_{kk'}|^2 dos(E_{k'}) = \frac{2\pi}{\hbar}\sum_{k'}|m(k-k')|^2 dos(E_{k'}). \tag{2.73b}$$

The absorption scattering rate of electrons from E to $E + \hbar\omega_{LO}$ is

$$\Gamma_k^{(a)} = \frac{2\pi}{\hbar}\sum_{k'}\left(|m(q_-^{(a)})|^2 N_q dos(E+\hbar\omega_{LO}) + |m(q_+^{(a)})|^2 N_q dos(E+\hbar\omega_{LO})\right), \tag{2.74a}$$

where the factor of 2 for the degeneracy in the phonon wavevectors is crossed out with the factor of ½ for a transition to same spin state.

Likewise, for emission from $E + \hbar\omega_{LO}$ to E, the scattering rate is

$$\Gamma_k^{(e)} = \frac{2\pi}{\hbar}\sum_{k'}\left(|m(q_-^{(e)})|^2 (N_q+1) dos(E-\hbar\omega_{LO}) + |m(q_+^{(e)})|^2 (N_q+1) dos(E-\hbar\omega_{LO})\right). \tag{2.74b}$$

The net scattering from k, which has an energy E, is

$$\Gamma(E) = \Gamma_k^{(a)} - \Gamma_k^{(e)}. \tag{2.75}$$

Above $\hbar\omega_{LO}$, both emission and absorption at E can take place and we need to account for these additional processes. However, only electrons with low E are dealt with in the thesis. The total scattering rate, using Eq. (2.76), is shown in Fig. 2.4. This at once shows that scattering is two magnitudes greater than in 3D cases. The g-value is shown in Fig. 2.5, which is increasing with decreasing electron energy. Decreasing electron energy would lead to less ion displacement. Since this value is multiplied by $\hbar\omega g$ to get the actual electron-phonon interaction energy, it seen that g increases without bound so there is a constant electron-phonon interaction energy. The model presented, in Eq. (2.62a), will only be able to deal with the 1D case. In reality we must consider the quasi 1D case, where scattering to two other directions must be taken care off. In the treatment above, the motion in the L_3 was dealt with in effective mass treatment and the other two dimensions were ignored. Most treatments use a confined structure such as quantum-well in L_3 direction and effective mass treatment in the two other directions[11]. Actual 3D problems would require considerable computation time and would require parallel computers.

2.3 The Schrödinger equation with electron phonon interaction

The wavefunction for representing electron-phonon coupling must include electron and phonon terms. Here, the phonon state can be either $|n>$, $|n-1>$ or $|n+1>$, which differ by a population of one, where $|n>$ is the thermodynamic equilibrium state with a temperature-dependent population of $n = [\exp(\hbar\omega / kT) + 1]^{-1}$. This way both emission and absorption of phonons can be accounted for. There are three

electronic states, $\psi^{(0)}, \psi^{(1)}$ and $\psi^{(2)}$, associated with each of three phonon states which are separated by phonon energy $\hbar\omega$. The wavefunction is

(2.76) $$\psi = \psi^{(0)}|n> + \psi^{(1)}|n-1> + \psi^{(2)}|n+1>.$$

The time-dependent Schrödinger equation is

(2.77) $$i\hbar\frac{\partial\psi}{\partial t} = H\psi(z,t).$$

The total Hamiltonian includes a purely electronic part and a part that deals with electron-phonon interaction as

(2.78) $$H = H_e + H_{e-p}.$$

Thus we may write

(2.79) $$i\hbar\frac{\partial\psi}{\partial t} = H_e\psi(z,t) + H_{e-p}\psi(z,t).$$

When the wavefunction is substituted, the left side of Eq. (2.49) becomes

(2.80) $$i\hbar\frac{\partial\psi}{\partial t} = i\hbar\frac{\partial\psi^{(0)}|n> + \psi^{(1)}|n-1> + \psi^{(2)}|n+1>}{\partial t}$$

$$= i\hbar\frac{\partial\psi^{(0)}}{\partial t}|n> + i\hbar\frac{\partial\psi^{(1)}}{\partial t}|n-1> + i\hbar\frac{\partial\psi^{(2)}}{\partial t}|n+1>.$$

When the wavefunction is substituted into the electron Hamiltonian

(2.81) $$H_e\psi = H_e\psi^{(0)}|n> + H_e\psi^{(1)}|n-1> + H_e\psi^{(2)}|n+1>.$$

The electron-phonon Hamiltonian term is

(2.82) $$H_{e-p}\psi = \hbar\omega g\left(ae^{-i\omega t} + a^{+}e^{i\omega t}\right)\left(\psi^{(0)}|n> + \psi^{(1)}|n-1> + \psi^{(2)}|n+1>\right).$$

This equation can be expanded as

(2.83) $$H_{e-p}\psi = \hbar\omega g\left(\psi^{(0)}a|n>e^{-i\omega t} + \psi^{(1)}a|n-1>e^{-i\omega t} + \psi^{(2)}a|n+1>e^{-i\omega t}\right)$$

$$+ \hbar\omega g\left(\psi^{(0)}a^{+}|n>e^{i\omega t} + \psi^{(1)}a^{+}|n-1>e^{i\omega t} + \psi^{(2)}a^{+}|n+1>e^{i\omega t}\right).$$

Using the well-known operation of the raising and lowering operators

(2.84a) $$a|n>=\sqrt{n}|n-1>.$$

(2.84b) $$a^{\dagger}|n>=\sqrt{n+1}|n+1>.$$

as well as these restrictions due to the fact this is a three state system

(2.84c) $$a^{\dagger}|n(t,z)+1>=0.$$

(2.84d) $$a|n(t,z)-1>=0.$$

we can simplify Eq. (2.83) as

(2.85) $$H_{e-p}\psi=\hbar\omega g\sqrt{n}e^{-i\omega t}\psi^{(1)}|n-1>+\hbar\omega g\sqrt{(n+1)}\,e^{-i\omega t}\psi^{(2)}|n>$$

$$+\hbar\omega g\sqrt{(n+1)}e^{i\omega t}\psi^{(0)}|n+1>+\hbar\omega g\sqrt{n}e^{i\omega t}\psi^{(1)}|n>.$$

When Eqs. (2.80), (2.81) and (2.85) are substituted into Equation (2.79), three equations result, based on the orthogonality of the phonon states

(2.86a) $$i\hbar\frac{\partial\psi^{(0)}}{\partial t}=H_e\psi^{(0)}+\hbar\omega g\sqrt{(n+1)}e^{-i\omega t}\psi^{(2)}+\hbar\omega g\sqrt{n}e^{i\omega t}\psi^{(1)}.$$

(2.86b) $$i\hbar\frac{\partial\psi^{(1)}}{\partial t}=H_e\psi^{(1)}+\hbar\omega g\sqrt{n}e^{-i\omega t}\psi^{(0)}.$$

(2.86c) $$i\hbar\frac{\partial\psi^{(2)}}{\partial t}=H_e\psi^{(2)}+\hbar\omega g\sqrt{(n+1)}e^{i\omega t}\psi^{(0)}.$$

The following matrix equation represents the Schrödinger equation in the model

(2.87) $$i\hbar\frac{\partial}{\partial t}\begin{bmatrix}\psi^{(0)}\\ \psi^{(1)}\\ \psi^{(2)}\end{bmatrix}=\begin{bmatrix}H_e & \hbar\omega g\sqrt{n}e^{i\omega t} & \hbar\omega g\sqrt{(n+1)}e^{-i\omega t}\\ \hbar\omega g\sqrt{n}e^{-i\omega t} & H_e & 0\\ \hbar\omega g\sqrt{(n+1)}e^{i\omega t} & 0 & H_e\end{bmatrix}\begin{bmatrix}\psi^{(0)}\\ \psi^{(1)}\\ \psi^{(2)}\end{bmatrix}.$$

The discretization of the time-dependent Schrödinger equation in Crank-Nicolson formulation[12] will be given next. The time dependent Schrödinger equation is

$$\frac{\partial}{\partial t}\psi(z,t) = -\frac{iH}{\hbar}\psi(z,t). \tag{2.88}$$

From this equation a general formula for finding wavefunction at time $t + \Delta t$ from that at time t can be found. First multiply the above equation by the infinite series of the function $\exp\left(\frac{itH}{\hbar}\right)$

$$\exp\left(\frac{itH}{\hbar}\right)\frac{\partial}{\partial t}\psi(z,t) = -\exp\left(\frac{itH}{\hbar}\right)\frac{iH}{\hbar}\psi(z,t). \tag{2.89a}$$

$$\exp\left(\frac{itH}{\hbar}\right)\frac{\partial}{\partial t}\psi(z,t) + \exp\left(\frac{itH}{\hbar}\right)\frac{iH}{\hbar}\psi(z,t) = 0. \tag{2.89b}$$

But,

$$\frac{\partial}{\partial t}\left[\exp\left(\frac{itH}{\hbar}\right)\psi(z,t)\right] = \exp\left(\frac{itH}{\hbar}\right)\frac{\partial}{\partial t}\psi(z,t) + \frac{\partial}{\partial t}\exp\left(\frac{itH}{\hbar}\right)\psi(z,t). \tag{2.90a}$$

$$\frac{\partial}{\partial t}\left[\exp\left(\frac{itH}{\hbar}\right)\psi(z,t)\right] = \exp\left(\frac{itH}{\hbar}\right)\frac{\partial}{\partial t}\psi(z,t) + \frac{iH}{\hbar}\exp\left(\frac{itH}{\hbar}\right)\psi(z,t) = 0. \tag{2.90b}$$

If the derivative of a function is zero, it must be a constant

$$\exp\left(\frac{itH}{\hbar}\right)\psi(z,t) = C. \tag{2.91a}$$

and for t=0

$$\exp\left(\frac{i0H}{\hbar}\right)\psi(z,0) = C = \psi(z,0). \tag{2.91b}$$

and thus

$$\exp\left(\frac{itH}{\hbar}\right)\psi(z,t) = \psi(z,0). \tag{2.91c}$$

Now, multiply by another infinite series, $\exp\left(-\frac{itH}{\hbar}\right)$.

$$\psi(z,t) = \exp\left(-\frac{itH}{\hbar}\right)\psi(z,0). \tag{2.92}$$

Expanding the first two terms of Eq. (2.92).

$$\psi(z,t) = \left(1-\frac{itH}{\hbar}\right)\psi(z,0). \tag{2.93}$$

For large t, the above equation breaks down and more terms have to be added. However this can be remedied by going to t in steps of δ. Letting the time variable be r and using the fact that the time origin is arbitrary.

$$\psi(z,r\delta+\delta) = \left(1-\frac{i\delta H}{\hbar}\right)\psi(z,r\delta). \tag{2.94}$$

Rewriting the above equation as a discrete equation with j the spatial index.

$$\psi_j^{r+1} = \left(1-\frac{i\delta H}{\hbar}\right)\psi_j^r. \tag{2.95}$$

The above equation is unstable and not unitary. Stability can be provided by the Cayley form[12] which is true to the first order in Taylor expansion

$$1-\frac{i\delta H}{\hbar} = \frac{1-\frac{i\delta H}{2\hbar}}{1+\frac{i\delta H}{2\hbar}}. \tag{2.96}$$

Thus the equation for finding new wavefunction is

$$\psi_j^{r+1} = \frac{1-i\frac{\delta}{2\hbar}H}{1+i\frac{\delta}{2\hbar}H}\psi_j^r. \tag{2.97a}$$

$$\left[1+i\frac{\delta}{2\hbar}H\right]\psi_j^{r+1} = \left[1-i\frac{\delta}{2\hbar}H\right]\psi_j^r. \tag{2.97b}$$

$$\psi_j^{r+1} + i\frac{\delta}{2\hbar}H\psi_j^{r+1} = \psi_j^r - i\frac{\delta}{2\hbar}H\psi_j^r. \tag{2.97c}$$

Eq. (2.87) can be written in form shown below, which is useful for solving for other interactions in this approximation as well.

$$(2.98)\qquad i\hbar\frac{\partial}{\partial t}\begin{bmatrix}\psi^{(0)}\\ \psi^{(1)}\\ \psi^{(2)}\end{bmatrix}=\begin{bmatrix}H_e & a(z,t) & b(z,t)\\ c(z,t) & H_e & 0\\ d(z,t) & 0 & H_e\end{bmatrix}\begin{bmatrix}\psi^{(0)}\\ \psi^{(1)}\\ \psi^{(2)}\end{bmatrix}.$$

Eq. (2.98) can be written as three coupled equations

$$(2.99a)\qquad i\hbar\frac{\partial\psi^{(0)}}{\partial t}=H^{(0)}\psi^{(0)}.$$

$$(2.99b)\qquad i\hbar\frac{\partial\psi^{(1)}}{\partial t}=H^{(1)}\psi^{(1)}.$$

$$(2.99c)\qquad i\hbar\frac{\partial\psi^{(2)}}{\partial t}=H^{(2)}\psi^{(2)}.$$

$$(2.99d)\qquad H^{(0)}\psi^{(0)}=H_e\psi^{(0)}+a(z,t)\psi^{(1)}+b(z,t)\psi^{(2)}.$$

$$(2.99e)\qquad H^{(1)}\psi^{(1)}=H_e\psi^{(1)}+c(z,t)\psi^{(0)}.$$

$$(2.99f)\qquad H^{(2)}\psi^{(2)}=H_e\psi^{(2)}+d(z,t)\psi^{(0)}.$$

Using the discrete time-dependent Schrödinger equation, Eq. (2.97c),

$$(2.100a)\qquad \psi^{(0)r+1}_j+i\frac{\delta}{2\hbar}H^{(0)}\psi^{(0)r+1}_j=\psi^{(0)r}_i-i\frac{\delta}{2\hbar}H^{(0)}\psi^{(0)r}_j.$$

$$(2.100b)\qquad \psi^{(1)r+1}_j+i\frac{\delta}{2\hbar}H^{(1)}\psi^{(1)r+1}_i=\psi^{(1)r}_j-i\frac{\delta}{2\hbar}H^{(1)}\psi^{(1)r}_j.$$

$$(2.100c)\qquad \psi^{(2)r+1}_j+i\frac{\delta}{2\hbar}H^{(2)}\psi^{(2)r+1}_j=\psi^{(2)r}_i-i\frac{\delta}{2\hbar}H^{(2)}\psi^{(2)r}_j.$$

If all the three equations are multiplied by free electron mass, these equations result

$$(2.101a)\qquad m_e\psi^{(0)r+1}_j+i\frac{\delta}{2\hbar}m_eH^{(0)}\psi^{(0)r+1}_j=m_e\psi^{(0)r}_j-i\frac{\delta}{2\hbar}m_eH^{(0)}\psi^{(0)r}_j.$$

$$m_e\psi^{(1)r-1}_j + i\frac{\delta}{2\hbar}m_eH^{(1)}\psi^{(1)r-1}_j = m_e\psi^{(1)r}_j - i\frac{\delta}{2\hbar}m_eH^{(1)}\psi^{(1)r}_j. \quad (2.101b)$$

$$m_e\psi^{(2)r-1}_j + i\frac{\delta}{2\hbar}m_eH^{(2)}\psi^{(2)r-1}_j = m_e\psi^{(2)r}_j - i\frac{\delta}{2\hbar}m_eH^{(2)}\psi^{(2)r}_j \quad (2.101c)$$

The discrete form of the Electron Hamiltonian will be derived next. The Ben Daniel and Duke Hamiltonian[13] will be used

$$H_e = -\frac{\hbar^2}{2}\frac{\hat{c}}{\hat{c}z}\left(\frac{1}{m(z)}\frac{\hat{c}}{\hat{c}z}\right) + V(z). \quad (2.102a)$$

$$H_e = -\hbar^2\frac{\hat{c}}{\hat{c}z}\left(\frac{1}{2m(z)}\frac{\hat{c}}{\hat{c}z}\right) + V(z) \quad (2.102b)$$

The space index is j and the step is ε. Instead of using the mass at location z, the mass of two locations is used

$$2m(z) \rightarrow m(z+\varepsilon) + m(z). \quad (2.103)$$

In the limit of ε going to zero the above equation should have an equal sign instead of an arrow.

The Hamiltonian operating on the wavefunction is

$$H_e\psi = -\hbar^2\frac{\hat{c}}{\hat{c}z}\left(\frac{1}{m(z+\varepsilon)+m(z)}\frac{\hat{c}\psi}{\hat{c}z}\right) + V(z)\psi. \quad (2.104)$$

Expanding the first two terms of the wavefunction at z + ε,

$$\psi(z+\varepsilon) = \psi(z) + \varepsilon\frac{\hat{c}\psi}{\hat{c}z}. \quad (2.105a)$$

$$\frac{\hat{c}\psi}{\hat{c}z} = \frac{\psi(z+\varepsilon)-\psi(z)}{\varepsilon}. \quad (2.105b)$$

Substituting this into Eq. (2.104), the Hamiltonian operation on the wavefunction is

$$H_e\psi = -\hbar^2 \frac{\partial}{\partial z}\left(\frac{1}{m(z+\varepsilon)+m(z)} \frac{\psi(z+\varepsilon)-\psi(z)}{\varepsilon} \right) + V(z)\psi . \tag{2.106}$$

The term in the parenthesis is

$$F(z) = \frac{1}{m(z+\varepsilon)+m(z)} \frac{\psi(z+\varepsilon)-\psi(z)}{\varepsilon} . \tag{2.107}$$

But since.

$$F(z-\varepsilon) = F(z) - \varepsilon \frac{\partial F}{\partial z} . \tag{2.107a}$$

$$-\varepsilon \frac{\partial F}{\partial z} = F(z-\varepsilon) - F(z) . \tag{2.107b}$$

$$\frac{\partial F}{\partial z} = \frac{F(z-\varepsilon)-F(z)}{-\varepsilon} . \tag{2.107c}$$

$$\frac{\partial F}{\partial z} = \frac{F(z)-F(z-\varepsilon)}{\varepsilon} . \tag{2.107d}$$

The value of F at z-ε can be found is simply

$$F(z-\varepsilon) = \frac{1}{m(z)+m(z-\varepsilon)} \frac{\psi(z)-\psi(z-\varepsilon)}{\varepsilon} . \tag{2.108}$$

Thus.

(2.109a)

$$\frac{\partial F}{\partial z} = \frac{\dfrac{1}{m(z+\varepsilon)+m(z)} \dfrac{\psi(z+\varepsilon)-\psi(z)}{\varepsilon} - \dfrac{1}{m(z)+m(z-\varepsilon)} \dfrac{\psi(z)-\psi(z-\varepsilon)}{\varepsilon}}{\varepsilon}$$

(2.109b)

$$\frac{\partial F}{\partial z} = \frac{1}{m(z+\varepsilon)+m(z)} \frac{\psi(z+\varepsilon)-\psi(z)}{\varepsilon^2} - \frac{1}{m(z)+m(z-\varepsilon)} \frac{\psi(z)-\psi(z-\varepsilon)}{\varepsilon^2}$$

$$\frac{\partial F}{\partial z} = \frac{1}{\varepsilon^2}\left[\frac{\psi(z+\varepsilon)-\psi(z)}{m(z+\varepsilon)+m(z)} - \frac{\psi(z)-\psi(z-\varepsilon)}{m(z)+m(z-\varepsilon)} \right] . \tag{2.109c}$$

In discrete units, the above becomes

$$\frac{\partial F}{\partial z} = \frac{1}{\varepsilon^2}\left[\frac{\psi_{j-1} - \psi_j}{m_{j-1} + m_j} - \frac{\psi_j - \psi_{j-1}}{m_j + m_{j-1}}\right]. \tag{2.110}$$

The relation of the Electron Hamiltonian operating on the wavefunction to F is

$$H_e\psi = -\hbar^2 \frac{\partial F}{\partial z} + V_j\psi_j. \tag{2.111}$$

Thus the final result for how the Electron Hamiltonian modifies a wavefunction is

$$H_e\psi = -\frac{\hbar^2}{\varepsilon^2}\left[\frac{\psi_{j-1} - \psi_j}{m_{j-1} + m_j} - \frac{\psi_j - \psi_{j-1}}{m_j + m_{j-1}}\right] + V_j\psi_j. \tag{2.112a}$$

$$H_e\psi = -\frac{\hbar^2}{\varepsilon^2}\left[\frac{\psi_{j-1}}{m_{j-1} + m_j} + \frac{\psi_{j-1}}{m_{j-1} + m_j} - \frac{\psi_j}{m_{j-1} + m_j} - \frac{\psi_j}{m_{j-1} + m_j}\right] + V_j\psi_j. \tag{2.112b}$$

First multiply the above equation by electron mass

$$m_e H_e\psi = -\frac{\hbar^2}{\varepsilon^2}\left[\frac{m_e\psi_{j-1}}{m_{j-1} + m_j} + \frac{m_e\psi_{j-1}}{m_{j-1} + m_j} - \frac{m_e\psi_j}{m_{j-1} + m_j} - \frac{m_e\psi_j}{m_{j-1} + m_j}\right] + m_e V_j\psi_j. \tag{2.113}$$

Introduce two space-dependent vectors

$$A_j = \frac{m_e}{m_{j-1} + m_j}. \tag{2.114a}$$

$$C_j = \frac{m_e}{m_{j-1} + m_j}. \tag{2.114b}$$

Eq. (2.113) can be rewritten

$$m_e H_e\psi = -\frac{\hbar^2}{\varepsilon^2}\left[C_j\psi_{j-1} + A_j\psi_{j-1} - C_j\psi_j - A_j\psi_j\right] + m_e V_j\psi_j. \tag{2.115}$$

This equation generalized to handle the three wavefunction components at times r and r+1

(2.116a) $m_e H_e \psi^{(0)r-1}_j = -\frac{\hbar^2}{\varepsilon^2}\left[C_j \psi^{(0)r-1}_{j-1} + A_j \psi^{(0)r-1}_{j-1} - C_j \psi^{(0)r-1}_j - A_j \psi^{(0)r-1}_j\right] + m_e V_j \psi^{(0)r-1}_j$

(2.116b) $m_e H_e \psi^{(0)r}_j = -\frac{\hbar^2}{\varepsilon^2}\left[C_j \psi^{(0)r}_{j-1} + A_j \psi^{(0)r}_{j-1} - C_j \psi^{(0)r}_j - A_j \psi^{(0)r}_j\right] + m_e V_j \psi^{(0)r}_j$

(2.116c) $m_e H_e \psi^{(1)r-1}_j = -\frac{\hbar^2}{\varepsilon^2}\left[C_j \psi^{(1)r-1}_{j-1} + A_j \psi^{(1)r-1}_{j-1} - C_j \psi^{(1)r-1}_j - A_j \psi^{(1)r-1}_j\right] + m_e V_j \psi^{(1)r-1}_j.$

(2.116d) $m_e H_e \psi^{(1)r}_j = -\frac{\hbar^2}{\varepsilon^2}\left[C_j \psi^{(1)r}_{j-1} + A_j \psi^{(1)r}_{j-1} - C_j \psi^{(1)r}_j - A_j \psi^{(1)r}_j\right] + m_e V_j \psi^{(1)r}_j.$

(2.116e) $m_e H_e \psi^{(2)r-1}_j = -\frac{\hbar^2}{\varepsilon^2}\left[C_j \psi^{(2)r-1}_{j-1} + A_j \psi^{(2)r-1}_{j-1} - C_j \psi^{(2)r-1}_j - A_j \psi^{(2)r-1}_j\right] + m_e V_j \psi^{(2)r-1}_j$

(2.116f) $m_e H_e \psi^{(2)r}_j = -\frac{\hbar^2}{\varepsilon^2}\left[C_j \psi^{(2)r}_{j-1} + A_j \psi^{(2)r}_{j-1} - C_j \psi^{(2)r}_j - A_j \psi^{(2)r}_j\right] + m_e V_j \psi^{(2)r}_j.$

Eq. (2.99d-f) for total Hamiltonian for the two times is

(2.117a) $m_e H^{(0)} \psi^{(0)r-1}_j = m_e H_e \psi^{(0)r-1}_j + m_e a^{r-1}_j \psi^{(1)r-1}_j + m_e b^{r-1}_j \psi^{(2)r-1}_j.$

(2.117b) $m_e H^{(0)} \psi^{(0)r}_j = m_e H_e \psi^{(0)r}_j + m_e a^{r}_j \psi^{(1)r}_j + m_e b^{r}_j \psi^{(2)r}_j.$

(2.117c) $m_e H^{(1)} \psi^{(1)r-1}_j = m_e H_e \psi^{(1)r-1}_j + m_e c^{r-1}_j \psi^{(0)r-1}_j.$

(2.117d) $m_e H^{(1)} \psi^{(1)r}_j = m_e H_e \psi^{(1)r}_j + m_e c^{r}_j \psi^{(0)r}_j.$

(2.117e) $m_e H^{(2)} \psi^{(2)r-1}_j = m_e H_e \psi^{(2)r-1}_j + m_e d^{r-1}_j \psi^{(0)r-1}_j.$

(2.117f) $m_e H^{(2)} \psi^{(2)r}_j = m_e H_e \psi^{(2)r}_j + m_e d^{r}_j \psi^{(0)r}_j.$

The left side of Eq. (2.101a) is

(2.118) $m_e \psi^{(0)r-1}_j + i\frac{\delta}{2\hbar} m_e H^{(0)} \psi^{(0)r-1}_j = m_e \psi^{(0)r-1}_j$

$$+ i\frac{\delta}{2\hbar}\left[-\frac{\hbar^2}{\varepsilon^2}\left[C_j \psi^{(0)r-1}_{j-1} + A_j \psi^{(0)r-1}_{j-1} - C_j \psi^{(0)r-1}_j - A_j \psi^{(0)r-1}_j\right] + m_e V_j \psi^{(0)r-1}_j\right]$$

$$+ i\frac{\delta}{2\hbar} m_e \left[a_j^{r-1} \psi^{(1)r-1}_j + b_j^{r-1} \psi^{(2)r-1}_j \right].$$

The right side of Eq. (2.101a) is

(2.119)
$$m_e \psi^{(0)r}_j - i\frac{\delta}{2\hbar} m_e H^{(0)} \psi^{(0)r}_j = m_e \psi^{(0)r}_j$$

$$- i\frac{\delta}{2\hbar} \left[-\frac{\hbar^2}{\varepsilon^2} \left[C_j \psi^{(0)r}_{j-1} + A_j \psi^{(0)r}_{j-1} - C_j \psi^{(0)r}_j - A_j \psi^{(0)r}_j \right] + m_e V_j \psi^{(0)r}_j \right]$$

$$- i\frac{\delta}{2\hbar} m_e \left[a_j^r \psi^{(1)r}_j + b_j^r \psi^{(2)r}_j \right].$$

The two sides can be combined to give

(2.120a)
$$m_e \psi^{(0)r-1}_j -$$

$$i\frac{\delta}{2\hbar} \left[-\frac{\hbar^2}{\varepsilon^2} \left[C_j \psi^{(0)r-1}_{j-1} + A_j \psi^{(0)r-1}_{j-1} - C_j \psi^{(0)r-1}_j - A_j \psi^{(0)r-1}_j \right] + m_e V_j \psi^{(0)r-1}_j \right]$$

$$+ i\frac{\delta}{2\hbar} m_e \left[a_j^{r-1} \psi^{(1)r-1}_j + b_j^{r-1} \psi^{(2)r-1}_j \right]$$

$$= m_e \psi^{(0)r}_j$$
$$- i\frac{\delta}{2\hbar} \left[-\frac{\hbar^2}{\varepsilon^2} \left[C_j \psi^{(0)r}_{j-1} + A_j \psi^{(0)r}_{j-1} - C_j \psi^{(0)r}_j - A_j \psi^{(0)r}_j \right] + m_e V_j \psi^{(0)r}_j \right]$$

$$- i\frac{\delta}{2\hbar} m_e \left[a_j^r \psi^{(1)r}_j + b_j^r \psi^{(2)r}_j \right].$$

Simplifying the equation

(2.120b)
$$m_e \psi^{(0)r-1}_j - i\frac{\hbar\delta}{2\varepsilon^2} \left[C_j \psi^{(0)r-1}_{j-1} + A_j \psi^{(0)r-1}_{j-1} - C_j \psi^{(0)r-1}_j - A_j \psi^{(0)r-1}_j \right] + i\frac{\delta}{2\hbar} m_e V_j \psi^{(0)r-1}_j$$

$$+ i\frac{\delta}{2\hbar} m_e a_j^{r-1} \psi^{(1)r-1}_j + i\frac{\delta}{2\hbar} m_e b_j^{r-1} \psi^{(2)r-1}_j$$

$$= m_e \psi^{(0)r}_j + i\frac{\hbar\delta}{2\varepsilon^2} \left[C_j \psi^{(0)r}_{j-1} + A_j \psi^{(0)r}_{j-1} - C_j \psi^{(0)r}_j - A_j \psi^{(0)r}_j \right] - i\frac{\delta}{2\hbar} m_e V_j \psi^{(0)r}_j$$

$$-i\frac{\delta}{2\hbar}m_e a_j^r \psi^{(1)r}_j - i\frac{\delta}{2\hbar}m_e b_j^r \psi^{(2)r}_j .$$

Next multiply by $i\frac{2\varepsilon^2}{\hbar\delta}$.

$$(2.120c)\; i\frac{2\varepsilon^2}{\hbar\delta}m_e\psi^{(0)r-1}_j + C_j\psi^{(0)r-1}_{j-1} + A_j\psi^{(0)r-1}_{j-1} - C_j\psi^{(0)r-1}_j - A_j\psi^{(0)r-1}_j - \frac{\varepsilon^2 m_e V_j}{\hbar^2}\psi^{(0)r-1}_j$$

$$-\frac{\varepsilon^2 m_e}{\hbar^2}a_j^{r-1}\psi^{(1)r-1}_j - \frac{\varepsilon^2 m_e}{\hbar^2}b_j^{r-1}\psi^{(2)r-1}_j$$

$$= i\frac{2\varepsilon^2}{\hbar\delta}m_e\psi^{(0)r}_j - C_j\psi^{(0)r}_{j-1} - A_j\psi^{(0)r}_{j-1} + C_j\psi^{(0)r}_j + A_j\psi^{(0)r}_j + \frac{\varepsilon^2 m_e V_j}{\hbar^2}\psi^{(0)r}_j$$

$$+\frac{\varepsilon^2 m_e}{\hbar^2}a_j^r\psi^{(1)r}_j + \frac{\varepsilon^2 m_e}{\hbar^2}b_j^r\psi^{(2)r}_j .$$

Defining $p = i\frac{2\varepsilon^2}{\hbar\delta}m_e$.

$$(2.120d)\qquad A_j\psi^{(0)r-1}_{j-1} + C_j\psi^{(0)r-1}_{j-1} + \left(p - A_j - C_j - \frac{\varepsilon^2 m_e V_j}{\hbar^2}\right)\psi^{(0)r-1}_j$$

$$-\frac{\varepsilon^2 m_e}{\hbar^2}a_j^{r-1}\psi^{(1)r-1}_j - \frac{\varepsilon^2 m_e}{\hbar^2}b_j^{r-1}\psi^{(2)r-1}_j$$

$$= -A_j\psi^{(0)r}_{j-1} - C_j\psi^{(0)r}_{j-1} + \left(p + A_j + C_j + \frac{\varepsilon^2 m_e V_j}{\hbar^2}\right)\psi^{(0)r}_j$$

$$+\frac{\varepsilon^2 m_e}{\hbar^2}a_j^r\psi^{(1)r}_j + \frac{\varepsilon^2 m_e}{\hbar^2}b_j^r\psi^{(2)r}_j .$$

Defining $B_j = p - A_j - C_j - \frac{\varepsilon^2}{\hbar^2}m_e V_j$ and $BH_j = p + A_j + C_j + \frac{\varepsilon^2}{\hbar^2}m_e V_j$.

$$(2.120e)\qquad A_j\psi^{(0)r-1}_{j-1} + B_j\psi^{(0)r-1}_j + C_j\psi^{(0)r-1}_{j-1} - \frac{\varepsilon^2 m_e}{\hbar^2}a_j^{r-1}\psi^{(1)r-1}_j - \frac{\varepsilon^2 m_e}{\hbar^2}b_j^{r-1}\psi^{(2)r-1}_j$$

$$= -A_j\psi^{(0)r}_{j-1} + BH_j\psi^{(0)r}_j - C_j\psi^{(0)r}_{j-1} + \frac{\varepsilon^2 m_e}{\hbar^2}a^r_j\psi^{(1)r}_j + \frac{\varepsilon^2 m_e}{\hbar^2}b^r_j\psi^{(2)r}_j.$$

Letting

$$D^{r-1}_j = -\frac{\varepsilon^2 m_e}{\hbar^2}a^{r-1}_j. \qquad E^{r-1}_j = -\frac{\varepsilon^2 m_e}{\hbar^2}b^{r-1}_j.$$

$$DH^r_j = \frac{\varepsilon^2 m_e}{\hbar^2}a^r_j. \qquad EH^r_j = \frac{\varepsilon^2 m_e}{\hbar^2}b^r_j.$$

(2.120f) $$A_j\psi^{(0)r-1}_{j-1} + B_j\psi^{(0)r-1}_j + C_j\psi^{(0)r-1}_{j-1} + D^{r-1}_j\psi^{(1)r-1}_j + E^{r-1}_j\psi^{(2)r-1}_j$$

$$= -A_j\psi^{(0)r}_{j-1} + BH_j\psi^{(0)r}_j - C_j\psi^{(0)r}_{j-1} + DH^r_j\psi^{(1)r}_j + EH^r_j\psi^{(2)r}_j.$$

Instead of solving for $\psi^{(0)r-1}_j$ as a function of $\psi^{(0)r}_j$, I will solve for $Q^{(0)r-1}_j = \psi^{(0)r-1}_j + \psi^{(0)r}_j$ as a function of $\psi^{(0)r}_j$. After solving for Q, I can find $\psi^{(0)r-1}_j$.

Thus,

(2.120g) $$A_jQ^{(0)r-1}_{j-1} + B_j\psi^{(0)r-1}_j - BH_j\psi^{(0)r}_j + C_jQ^{(0)r-1}_{j-1}$$

$$+ D^{r-1}_j\psi^{(1)r-1}_j + E^{r-1}_j\psi^{(2)r-1}_j - DH^r_j\psi^{(1)r}_j - EH^r_j\psi^{(2)r}_j = 0.$$

But, $B_j\psi^{(0)r-1}_j - BH_j\psi^{(0)r}_j$ is simply

$$\left(p - A_j - C_j - \frac{\varepsilon^2}{\hbar^2}m_eV_j\right)\psi^{(0)r-1}_j - \left(p + A_j + C_j + \frac{\varepsilon^2}{\hbar^2}m_eV_j\right)\psi^{(0)r}_j$$

$$= \left(p - A_j - C_j - \frac{\varepsilon^2}{\hbar^2}m_eV_j\right)\psi^{(0)r-1}_j - \left(-p + A_j + C_j + \frac{\varepsilon^2}{\hbar^2}m_eV_j + 2p\right)\psi^{(0)r}_j$$

$$= \left(p - A_j - C_j - \frac{\varepsilon^2}{\hbar^2}m_eV_j\right)\psi^{(0)r-1}_j + \left(p - A_j - C_j - \frac{\varepsilon^2}{\hbar^2}m_eV_j\right)\psi^{(0)r}_j - 2p\psi^{(0)r}_j$$

$$=\left(p-A_j-C_j-\frac{\varepsilon^2}{\hbar^2}m_eV_j\right)\left(\psi^{(0)r-1}_j+\psi^{(0)r}_j\right)-2p\psi^{(0)r}_j=B_jQ^{(0)r-1}_j-2p\psi^{(0)r}_j$$

Thus,

(2.120h) $$A_jQ^{(0)r-1}_{j-1}+B_jQ^{(0)r-1}_j-2p\psi^{(0)r}_j+C_jQ^{(0)r-1}_{j-1}$$

$$+D^{r-1}_j\psi^{(1)r-1}_j+E^{r-1}_j\psi^{(2)r-1}_j-DH^r_j\psi^{(1)r}_j-EH^r_j\psi^{(2)r}_j=0.$$

(2.120i) $$A_jQ^{(0)r-1}_{j-1}+B_jQ^{(0)r-1}_j+C_jQ^{(0)r-1}_{j-1}$$

$$+D^{r-1}_j\psi^{(1)r-1}_j+E^{r-1}_j\psi^{(2)r-1}_j-DH^r_j\psi^{(1)r}_j-EH^r_j\psi^{(2)r}_j=2p\psi^{(0)r}_j.$$

Simplifying $D^{r-1}_j\psi^{(1)r-1}_j-DH^r_j\psi^{(1)r}_j$ as,

$$D^{r-1}_j\psi^{(1)r-1}_j+D^{r-1}_j\psi^{(1)r}_j-D^{r-1}_j\psi^{(1)r}_j-DH^r_j\psi^{(1)r}_j=D^{r-1}_jQ^{(1)r-1}_j-\left(D^{r-1}_j+DH^r_j\right)\psi^{(1)r}_j.$$

Simplifying $E^{r-1}_j\psi^{(2)r-1}_j-EH^r_j\psi^{(2)r}_j$ as,

$$E^{r-1}_j\psi^{(2)r-1}_j+E^{r-1}_j\psi^{(2)r}_j-E^{r-1}_j\psi^{(2)r}_j-EH^r_j\psi^{(2)r}_j=E^{r-1}_jQ^{(2)r-1}_j-\left(E^{r-1}_j+EH^r_j\right)\psi^{(2)r}_j.$$

Finally,

(2.120j) $$A_jQ^{(0)r-1}_{j-1}+B_jQ^{(0)r-1}_j+C_jQ^{(0)r-1}_{j-1}$$

$$+D^{r-1}_jQ^{(1)r-1}_j+E^{r-1}_jQ^{(2)r-1}_j-\left(D^{r-1}_j+DH^r_j\right)\psi^{(1)r}_j-\left(E^{r-1}_j+EH^r_j\right)\psi^{(2)r}_j=2p\psi^{(0)r}_j.$$

(2.120k) $$A_jQ^{(0)r-1}_{j-1}+B_jQ^{(0)r-1}_j+C_jQ^{(0)r-1}_{j-1}+D^{r-1}_jQ^{(1)r-1}_j+E^{r-1}_jQ^{(2)r-1}_j$$

$$=2p\psi^{(0)r}_j+\left(D^{r-1}_j+DH^r_j\right)\psi^{(1)r}_j+\left(E^{r-1}_j+EH^r_j\right)\psi^{(2)}.$$

The left side of Eq. (2.101b) is

(2.121)

$$m_e\psi^{(1)r-1}_j+i\frac{\delta}{2\hbar}\left[-\frac{\hbar^2}{\varepsilon^2}\left[C_j\psi^{(1)r-1}_{j-1}+A_j\psi^{(1)r-1}_{j-1}-C_j\psi^{(1)r-1}_j-A_j\psi^{(1)r-1}_j\right]+m_eV_j\psi^{(1)r-1}_j\right]$$

$$+i\frac{\delta}{2\hbar}m_e c_j^{r-1}\psi^{(0)r-1}_j .$$

The right side of Eq. (2.101b) is

(2.122) $m_e\psi^{(1)r}_j$

$$-i\frac{\delta}{2\hbar}\left[-\frac{\hbar^2}{\varepsilon^2}\left[C_j\psi^{(1)r}_{j-1}+A_j\psi^{(1)r}_{j-1}-C_j\psi^{(1)r}_j-A_j\psi^{(1)r}_j\right]+m_e V_j\psi^{(1)r}_j\right]-i\frac{\delta}{2\hbar}m_e c_j^r\psi^{(0)r}_j .$$

Combing the two.

(2.123a)

$$m_e\psi^{(1)r-1}_j+i\frac{\delta}{2\hbar}\left[-\frac{\hbar^2}{\varepsilon^2}\left[C_j\psi^{(1)r-1}_{j-1}+A_j\psi^{(1)r-1}_{j-1}-C_j\psi^{(1)r-1}_j-A_j\psi^{(1)r-1}_j\right]+m_e V_j\psi^{(1)r-1}_j\right]$$

$$+i\frac{\delta}{2\hbar}m_e c_j^{r-1}\psi^{(0)r-1}_j = m_e\psi^{(1)r}_j$$

$$-i\frac{\delta}{2\hbar}\left[-\frac{\hbar^2}{\varepsilon^2}\left[C_j\psi^{(1)r}_{j-1}+A_j\psi^{(1)r}_{j-1}-C_j\psi^{(1)r}_j-A_j\psi^{(1)r}_j\right]+m_e V_j\psi^{(1)r}_j\right]-i\frac{\delta}{2\hbar}m_e c_j^r\psi^{(0)r}_j .$$

Simplifying

(2.123b)

$$m_e\psi^{(1)r-1}_j-i\frac{\hbar\delta}{2\varepsilon^2}\left[C_j\psi^{(1)r-1}_{j-1}+A_j\psi^{(1)r-1}_{j-1}-C_j\psi^{(1)r-1}_j-A_j\psi^{(1)r-1}_j\right]+i\frac{\delta m_e V_j}{2\hbar}\psi^{(1)r-1}_j$$

$$+i\frac{\delta}{2\hbar}m_e c_j^{r-1}\psi^{(0)r-1}_j = m_e\psi^{(1)r}_j$$

$$+i\frac{\hbar\delta}{2\varepsilon^2}\left[C_j\psi^{(1)r}_{j-1}+A_j\psi^{(1)r}_{j-1}-C_j\psi^{(1)r}_j-A_j\psi^{(1)r}_j\right]-i\frac{\delta m_e V_j}{2\hbar}\psi^{(1)r}_j-i\frac{\delta}{2\hbar}m_e c_j^r\psi^{(0)r}_j .$$

Multiplying by $i\frac{2\varepsilon^2}{\hbar\delta}$.

(2.123d)

$$i\frac{2\varepsilon^2}{\hbar\delta}m_e\psi^{(1)r-1}_j + C_j\psi^{(1)r-1}_{j-1} + A_j\psi^{(1)r-1}_{j-1} - C_j\psi^{(1)r-1}_j - A_j\psi^{(1)r-1}_j - \frac{\varepsilon^2 m_e V_j}{\hbar^2}\psi^{(1)r-1}_j$$

$$-\frac{\varepsilon^2}{\hbar^2}m_e c^{r-1}_j\psi^{(0)r-1}_j = i\frac{2\varepsilon^2}{\hbar\delta}m_e\psi^{(1)r}_j$$

$$-C_j\psi^{(1)r}_{j-1} - A_j\psi^{(1)r}_{j-1} + C_j\psi^{(1)r}_j + A_j\psi^{(1)r}_j + \frac{\varepsilon^2 m_e V_j}{\hbar^2}\psi^{(1)r}_j + \frac{\varepsilon^2}{\hbar^2}m_e c^r_j\psi^{(0)r}_j.$$

Letting $p = i\frac{2\varepsilon^2}{\hbar\delta}m_e$ and grouping together common terms

(2.123e)
$$A_j\psi^{(1)r-1}_{j-1} + C_j\psi^{(1)r-1}_{j-1} + \left(p - A_j - C_j - \frac{\varepsilon^2 m_e V_j}{\hbar^2}\right)\psi^{(1)r-1}_j$$

$$-\frac{\varepsilon^2}{\hbar^2}m_e c^{r-1}_j\psi^{(0)r-1}_j = -A_j\psi^{(1)r}_{j-1} - C_j\psi^{(1)r}_{j-1}$$

$$+\left(p + A_j + C_j + \frac{\varepsilon^2 m_e V_j}{\hbar^2}\right)\psi^{(1)r}_j + \frac{\varepsilon^2}{\hbar^2}m_e c^r_j\psi^{(0)r}_j.$$

Letting,

$B_j = p - A_j - C_j - \frac{\varepsilon^2}{\hbar^2}m_e V_j$ and $BH_j = p + A_j + C_j + \frac{\varepsilon^2}{\hbar^2}m_e V_j$ as before.

(2.123f)
$$A_j\psi^{(1)r-1}_{j-1} + C_j\psi^{(1)r-1}_{j-1} + B_j\psi^{(1)r-1}_j - \frac{\varepsilon^2}{\hbar^2}m_e c^{r-1}_j\psi^{(0)r-1}_j$$

$$= -A_j\psi^{(1)r}_{j-1} - C_j\psi^{(1)r}_{j-1} + BH_j\psi^{(1)r}_j + \frac{\varepsilon^2}{\hbar^2}m_e c^r_j\psi^{(0)r}_j.$$

Introducing

$$F^{r-1}_j = -\frac{\varepsilon^2}{\hbar^2}m_e c^{r-1}_j \text{ and } FH^r_j = \frac{\varepsilon^2}{\hbar^2}m_e c^r_j.$$

(2.124g)
$$A_j\psi^{(1)r-1}_{j-1} + C_j\psi^{(1)r-1}_{j-1} + B_j\psi^{(1)r-1}_j + F^{r-1}_j\psi^{(0)r-1}_j$$

$$= -A_j\psi^{(1)r}_{j-1} - C_j\psi^{(1)r}_{j-1} + BH_j\psi^{(1)r}_j + FH^r_j\psi^{(0)r}_j.$$

Again, instead of solving for $\psi^{(1)r-1}_j$ as a function of $\psi^{(1)r}_j$, I will solved for $Q^{(1)r-1}_j = \psi^{(1)r-1}_j + \psi^{(1)r}_j$ as a function of $\psi^{(1)r}_j$. After solving to Q, I can find $\psi^{(1)r-1}_j$.

Immediately,

(2.124h) $$A_jQ^{(1)r-1}_{j-1} + C_jQ^{(1)r-1}_{j-1} + B_j\psi^{(1)r-1}_j - BH_j\psi^{(1)r}_j + F^{r-1}_j\psi^{(0)r-1}_j = FH^r_j\psi^{(0)r}_j.$$

But, $B_j\psi^{(1)r-1}_j - BH_j\psi^{(1)r}_j$ has been found as $B_jQ^{(1)r-1}_j - 2p\psi^{(1)r}_j$.

(2.124i) $$A_jQ^{(1)r-1}_{j-1} + C_jQ^{(1)r-1}_{j-1} + B_jQ^{(1)r-1}_j - 2p\psi^{(1)r}_j + F^{r-1}_j\psi^{(0)r-1}_j - FH^r_j\psi^{(0)r}_j = 0.$$

Simplifying $F^{r-1}_j\psi^{(0)r-1}_j - FH^r_j\psi^{(0)r}_j$.

$$F^{r-1}_j\psi^{(0)r-1}_j + F^{r-1}_j\psi^{(0)r}_j - F^{r-1}_j\psi^{(0)r}_j - FH^r_j\psi^{(0)r}_j = F^{r-1}_jQ^{(0)r-1}_j - \left(F^{r-1}_j + FH^r_j\right)\psi^{(0)r}_j.$$

(2.124j) $$A_jQ^{(1)r-1}_{j-1} + C_jQ^{(1)r-1}_{j-1} + B_jQ^{(1)r-1}_j - 2p\psi^{(1)r}_j + F^{r-1}_jQ^{(0)r-1}_j - \left(F^{r-1}_j + FH^r_j\right)\psi^{(0)r}_j = 0.$$

(2.125k) $$A_jQ^{(1)r-1}_{j-1} + C_jQ^{(1)r-1}_{j-1} + B_jQ^{(1)r-1}_j + F^{r-1}_jQ^{(0)r-1}_j = 2p\psi^{(1)r}_j + \left(F^{r-1}_j + FH^r_j\right)\psi^{(0)r-1}_j$$

The left side of Eq. (2.101c) is

(2.126) $$m_e\psi^{(2)r-1}_j$$

$$-i\frac{\delta}{2\hbar}\left[-\frac{\hbar^2}{\varepsilon^2}\left[C_j\psi^{(2)r-1}_{j-1} + A_j\psi^{(2)r-1}_{j-1} - C_j\psi^{(2)r-1}_j - A_j\psi^{(2)r-1}_j\right] + m_eV_j\psi^{(2)r-1}_j\right]$$

$$+i\frac{\delta}{2\hbar}m_ed^{r-1}_j\psi^{(0)r-1}_j.$$

The right side of Eq. (2.101c) is

(2.127) $$m_e\psi^{(2)r}_j$$

$$-i\frac{\delta}{2\hbar}\left[-\frac{\hbar^2}{\varepsilon^2}\left[C_j\psi^{(2)r}_{j-1} + A_j\psi^{(2)r}_{j-1} - C_j\psi^{(2)r}_j - A_j\psi^{(2)r}_j\right] + m_eV_j\psi^{(2)r}_j\right]$$

$$-i\frac{\delta}{2\hbar}m_e d_j^r \psi^{(0)r}_j.$$

Combing the two.

(2.128a) $m_e \psi^{(2)r-1}_j$

$$+i\frac{\delta}{2\hbar}\left[-\frac{\hbar^2}{\varepsilon^2}\left[C_j\psi^{(2)r-1}_{j-1}+A_j\psi^{(2)r-1}_{j-1}-C_j\psi^{(2)r-1}_{j}-A_j\psi^{(2)r-1}_{j}\right]+m_e V_j\psi^{(2)r-1}_{j}\right]$$

$$+i\frac{\delta}{2\hbar}m_e d_j^{r-1}\psi^{(0)r-1}_j = m_e\psi^{(2)r}_j - i\frac{\delta}{2\hbar}m d_j^r\psi^{(0)r}_j$$

$$-i\frac{\delta}{2\hbar}\left[-\frac{\hbar^2}{\varepsilon^2}\left[C_j\psi^{(2)r}_{j-1}+A_j\psi^{(2)r}_{j-1}-C_j\psi^{(2)r}_{j}-A_j\psi^{(2)r}_{j}\right]+m_e V_j\psi^{(2)r}_{j}\right].$$

Simplifying Equation (2.100c):

(2.128b)

$$m_e\psi^{(2)r-1}_j - i\frac{\hbar\delta}{2\varepsilon^2}\left[C_j\psi^{(2)r-1}_{j-1}+A_j\psi^{(2)r-1}_{j-1}-C_j\psi^{(2)r-1}_{j}-A_j\psi^{(2)r-1}_{j}\right]+i\frac{\delta m_e V_j}{2\hbar}\psi^{(2)r-1}_j$$

$$+i\frac{\delta}{2\hbar}m_e d_j^{r-1}\psi^{(0)r-1}_j = m_e\psi^{(2)r}_j - i\frac{\delta}{2\hbar}m_e d_j^r\psi^{(0)r}_j$$

$$i\frac{\hbar\delta}{2\varepsilon^2}\left[C_j\psi^{(2)r}_{j-1}+A_j\psi^{(2)r}_{j-1}-C_j\psi^{(2)r}_{j}-A_j\psi^{(2)r}_{j}\right]-i\frac{\delta m_e V_j}{2\hbar}\psi^{(2)r}_j.$$

Multiplying by $i\frac{2\varepsilon^2}{\hbar\delta}$.

(2.128c)

$$i\frac{2\varepsilon^2}{\hbar\delta}m_e\psi^{(2)r-1}_j - C_j\psi^{(2)r-1}_{j-1}+A_j\psi^{(2)r-1}_{j-1}-C_j\psi^{(2)r-1}_{j}-A_j\psi^{(2)r-1}_{j}-\frac{\varepsilon^2 m_e V_j}{\hbar^2}\psi^{(2)r-1}_j$$

$$-\frac{\varepsilon^2 m_e d_j^{r-1}}{\hbar^2}\psi^{(0)r-1}_j = i\frac{2\varepsilon^2}{\hbar\delta}m_e\psi^{(2)r}_j+\frac{\varepsilon^2 m_e d_j^r}{\hbar^2}\psi^{(0)r}_j$$

$$-C_j\psi^{(2)r}_{j-1} - A_j\psi^{(2)r}_{j-1} + C_j\psi^{(2)r}_{j} + A_j\psi^{(2)r}_{j} + \frac{\varepsilon^2 m_e V_j}{\hbar^2}\psi^{(2)r}_{j}.$$

Letting $p = i\frac{2\varepsilon^2}{\hbar\delta}m_e$ and grouping together common terms

(2.128d)

$$A_j\psi^{(2)r+1}_{j-1} + C_j\psi^{(2)r+1}_{j-1} + \left(p - A_j - C_j - \frac{\varepsilon^2 m_e V_j}{\hbar^2}\right)\psi^{(2)r+1}_{j} - \frac{\varepsilon^2 m_e d^{r+1}_j}{\hbar^2}\psi^{(0)r+1}_{j}$$

$$= -A_j\psi^{(2)r}_{j-1} - C_j\psi^{(2)r}_{j-1} + \left(p + A_j + +C_j + \frac{\varepsilon^2 m_e V_j}{\hbar^2}\right)\psi^{(2)r}_{j} + \frac{\varepsilon^2 m_e d^{r}_j}{\hbar^2}\psi^{(0)r}_{j}.$$

Letting $B_j = p - A_j - C_j - \frac{\varepsilon^2}{\hbar^2}m_e V_j$ and $BH_j = p + A_j + C_j + \frac{\varepsilon^2}{\hbar^2}m_e V_j$.

(2.128e) $$A_j\psi^{(2)r+1}_{j-1} + C_j\psi^{(2)r+1}_{j-1} + B_j\psi^{(2)r+1}_{j} - \frac{\varepsilon^2 m_e d^{r+1}_j}{\hbar^2}\psi^{(0)r+1}_{j}$$

$$= -A_j\psi^{(2)r}_{j-1} - C_j\psi^{(2)r}_{j-1} + BH_j\psi^{(2)r}_{j} + \frac{\varepsilon^2 m_e d^{r}_j}{\hbar^2}\psi^{(0)r}_{j}.$$

Letting $G^{r+1}_j = -\frac{\varepsilon^2 m_e d^{r+1}_j}{\hbar^2}$ and $GH^r_j = \frac{\varepsilon^2 m_e d^{r}_j}{\hbar^2}$.

(2.128f) $$A_j\psi^{(2)r+1}_{j-1} + C_j\psi^{(2)r+1}_{j-1} + B_j\psi^{(2)r+1}_{j} + G^{r+1}_j\psi^{(0)r+1}_{j}$$

$$= -A_j\psi^{(2)r}_{j-1} - C_j\psi^{(2)r}_{j-1} + BH_j\psi^{(2)r}_{j} + GH^r_j\psi^{(0)r}_{j}.$$

Again, instead of solving for $\psi^{(2)r+1}_j$ as a function of $\psi^{(2)r}_j$, I will solve for $Q^{(2)r+1}_j = \psi^{(2)r+1}_j + \psi^{(2)r}_j$ as a function of $\psi^{(2)r}_j$. After solving for Q, I can find $\psi^{(2)r+1}_j$.

Immediately,

(2.128g) $$A_jQ^{(2)r+1}_{j-1} + C_jQ^{(2)r+1}_{j-1} + B_j\psi^{(2)r+1}_{j} - BH_j\psi^{(2)r}_{j} + G^{r+1}_j\psi^{(0)r+1}_{j} = GH^r_j\psi^{(0)r}_{j}.$$

But $B_j\psi^{(1)r-1}_j - BH_j\psi^{(1)r}_j$ is equal to $B_jQ^{(2)r-1}_j - 2p\psi^{(2)r}_j$.

(2.128h) $$A_jQ^{(2)r-1}_{j-1} + C_jQ^{(2)r-1}_{j-1} + B_jQ^{(2)r-1}_j - 2p\psi^{(2)r}_j + G^{r-1}_j\psi^{(0)r-1}_j - GH^r_j\psi^{(0)r}_j = 0.$$

Simplifying $G^{r-1}_j\psi^{(0)r-1}_j - GH^r_j\psi^{(0)r}_j$.

(2.128i)

$$G^{r-1}_j\psi^{(0)r-1}_j + G^{r-1}_j\psi^{(0)r}_j - G^{r-1}_j\psi^{(0)r}_j - GH^r_j\psi^{(0)r}_j = G^{r-1}_jQ^{(0)r-1}_j - \left(G^{r-1}_j + GH^r_j\right)\psi^{(0)r}_j.$$

(2.128j)

$$A_jQ^{(2)r-1}_{j-1} + B_jQ^{(2)r-1}_j + C_jQ^{(2)r-1}_{j-1} + G^{r-1}_jQ^{(0)r-1}_j = 2p\psi^{(2)r}_j + \left(G^{r-1}_j + GH^r_j\right)\psi^{(0)r}_j.$$

Eqs. (2.121.2.124.2.126) can be combined into matrix equation

(2.130a)
$$A_j\begin{bmatrix} Q^{(0)r-1}_{j-1} \\ Q^{(1)r-1}_{j-1} \\ Q^{(2)r-1}_{j-1} \end{bmatrix} + \begin{bmatrix} B_j & D^{r-1}_j & E^{r-1}_j \\ F^{r-1}_j & B_j & 0 \\ G^{r-1}_j & 0 & B_j \end{bmatrix}\begin{bmatrix} Q^{(0)r-1}_j \\ Q^{(1)r-1}_j \\ Q^{(2)r-1}_j \end{bmatrix} + C_j\begin{bmatrix} Q^{(0)r-1}_{j-1} \\ Q^{(1)r-1}_{j-1} \\ Q^{(2)r-1}_{j-1} \end{bmatrix}$$

$$= \begin{bmatrix} 2p & D^{r-1}_j + DH^r_j & E^{r-1}_j + EH^r_j \\ F^{r-1}_j + FH^r_j & 2p & 0 \\ G^{r-1}_j + GH^r_j & 0 & 2p \end{bmatrix}\begin{bmatrix} \psi^{(0)r-1}_j \\ \psi^{(1)r-1}_j \\ \psi^{(2)r-1}_j \end{bmatrix}.$$

(2.130b) $$Q^{(1)r-1}_j = \psi^{(1)r-1}_j + \psi^{(1)r}_j.$$

(2.130c) $$p = i\frac{2\varepsilon^2}{\hbar\delta}m_e.$$

(2.130d) $$A_j = \frac{m_e}{m_{j-1} + m_j}.$$

(2.130e) $$C_j = \frac{m_e}{m_{j-1} + m_j}.$$

(2.130f) $$B_j = p - A_j - C_j - \frac{\varepsilon^2}{\hbar^2}m_eV_j.$$

(2.130g) $$D_j^{r-1} = -\frac{\varepsilon^2 m_e}{\hbar^2} a_j^{r-1}.$$

(2.130i) $$DH_j^r = \frac{\varepsilon^2 m_e}{\hbar^2} a_j^r.$$

(2.130h) $$E_j^{r-1} = -\frac{\varepsilon^2 m_e}{\hbar^2} b_j^{r-1}.$$

(2.130j) $$EH_j^r = \frac{\varepsilon^2 m_e}{\hbar^2} b_j^r.$$

(2.130k) $$F_j^{r-1} = -\frac{\varepsilon^2}{\hbar^2} m_e c_j^{r-1}.$$

(2.130l) $$FH_j^r = \frac{\varepsilon^2}{\hbar^2} m_e c_j^r.$$

(2.130m) $$G_j^{r-1} = -\frac{\varepsilon^2 m_e d_j^{r-1}}{\hbar^2}.$$

(2.130n) $$GH_j^r = \frac{\varepsilon^2 m_e d_j^r}{\hbar^2}.$$

(2.130o) $$a_j^r = \hbar\omega g\sqrt{n}\, e^{i\omega\delta r}.$$

(2.130p) $$b_j^r = \hbar\omega g\sqrt{(n+1)}\, e^{-i\omega\delta r}$$

(2.130q) $$c_j^r = \hbar\omega g\sqrt{n}\, e^{-i\omega\delta r}$$

(2.130r) $$d_j^r = \hbar\omega g\sqrt{(n+1)}\, e^{i\omega\delta r}.$$

2.4 References

1. M. Born and K. Huang. *Dynamical Theory of Crystal Lattices* (Oxford University Press, London, 1954), p. 82-100.

2. C. Kittel, *Introduction to Solid State Physics*, 6th Ed. (John Wiley & Sons, New York, 1986), p. 366.

3. D. K. Ferry, *Semiconductors* (Macmillan Publishing Company, New York, 1991), p. 94.

4. A. Yariv, *Quantum Electronics*, 2nd Ed. (John Wiley & Sons, New York, 1975), p. 71.

5. T. Wenckbach, *Essentials of Semiconductor Physics* (John Wiley & Sons, New York, 1991), p. 275.

6. D. K. Cheng, *Field and Wave Electromagnetics* (Addison Wesley Publishing Company, Reading, MA, 1983), p. 97.

7. Reference 5, p. 289.

8. G. D. Mahan, *Many-Particle Physics* (Plenum Press, New York, 1981), p. 12.

9. L. Couch II, *Digital and Analog Communication Systems*, 3rd Ed. (Macmillan Publising Company, New Yok, 1990), p. 657.

10. K. Shum, J. Appl. Phys. **69**, 6484 (1991).

11. N. S. Wingreen, K. W. Jacobsen and J. W. Wilkins, Phys. Rev. Lett. **61**, 1396 (1988).

12. A. Goldberg, H. M. Schey and J. L. Schwartz, Am. J. Phys. **35**, 177 (1967).

13. J. M. Mohaidat, K. Shum and R. R. Alfano, Phys. Rev. B **45**, 3822 (1992).

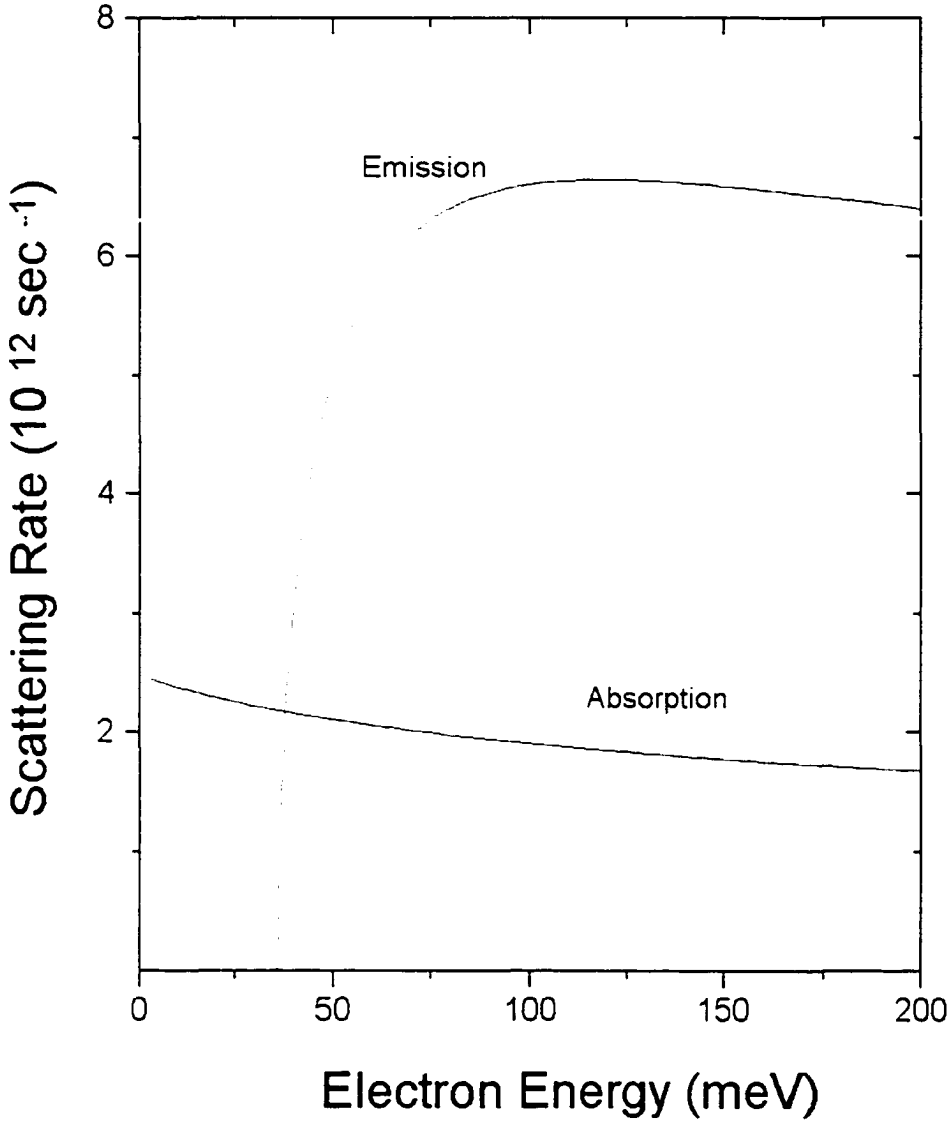

Fig. 2.1: Emission and absorption of electrons by LO phonons for different electron energies in bulk GaAs.

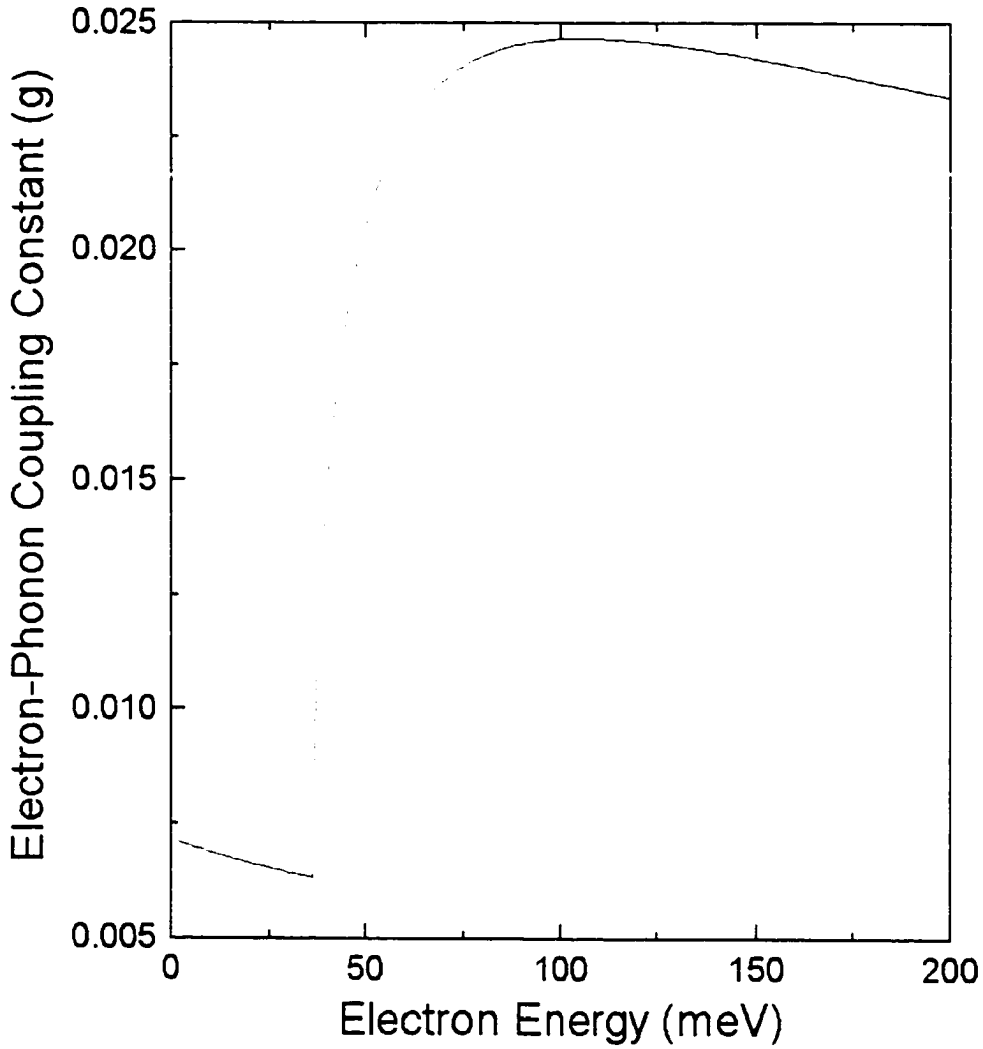

Fig. 2.2: The electron-phonon coupling constant for different electron energies in bulk GaAs.

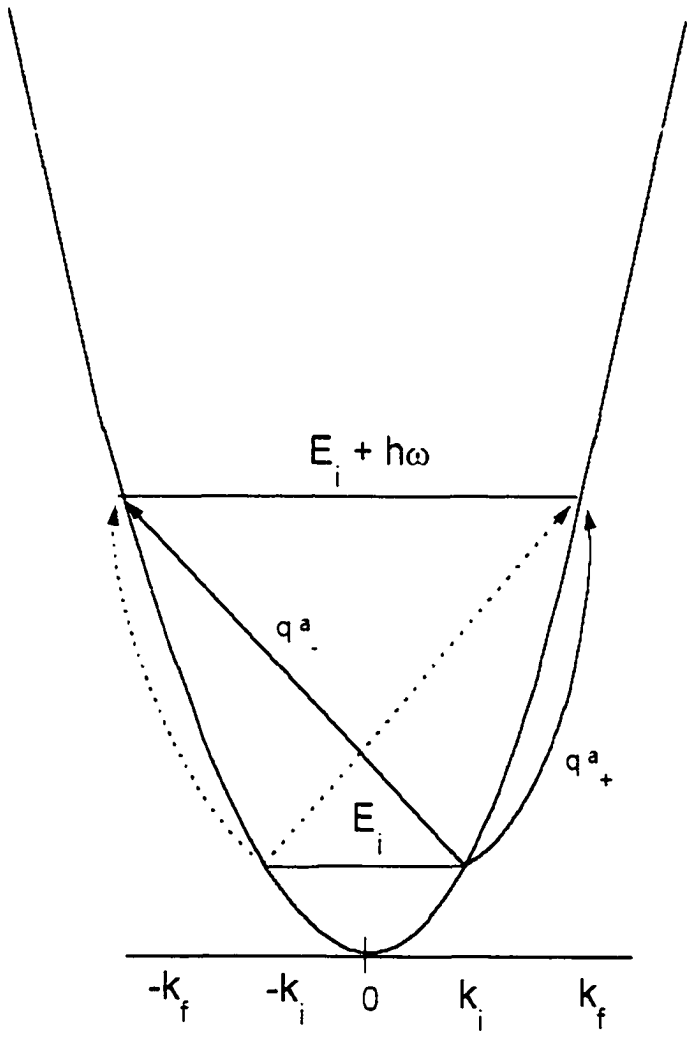

Fig. 2.3: The dispersion relation showing the four wavevectors responsible for phonon absorption from E_i to $E_i + \hbar\omega$ in 1D semiconductor structure.

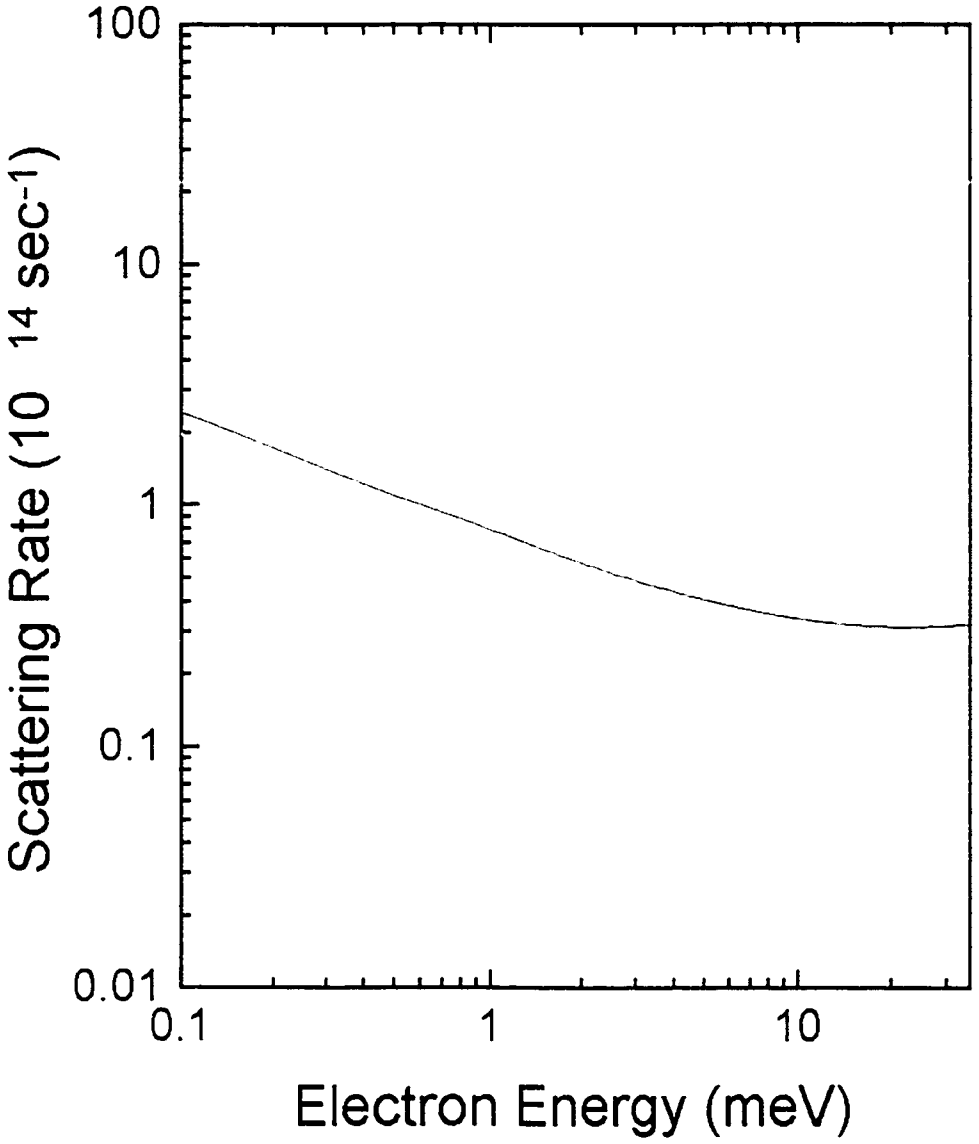

Fig. 2.4: Net scattering at electron energies below LO-phonon energy in 1D semiconductor structure.

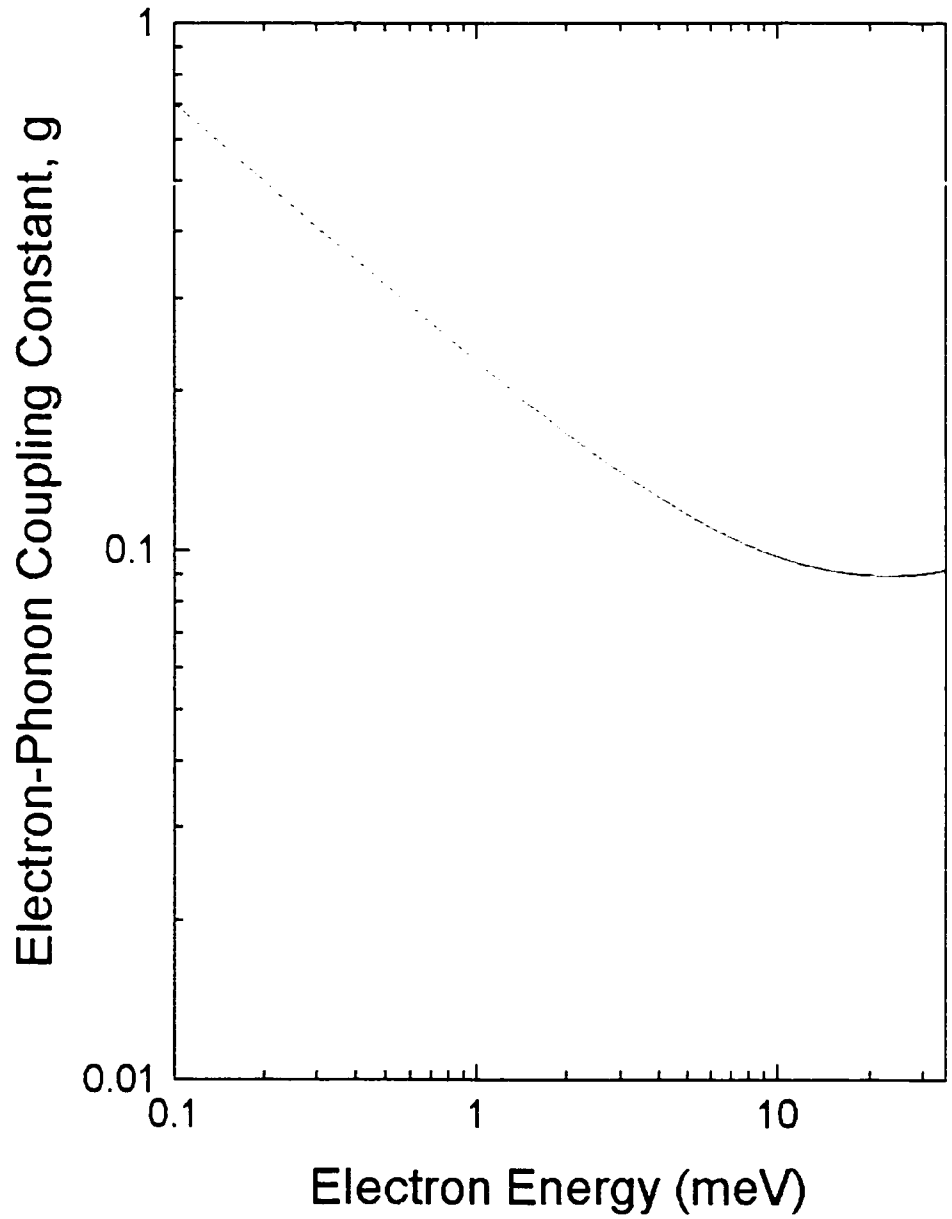

Fig. 2.5: The electron phonon coupling constant for low electron energies in 1D GaAs semiconductor structures.

CHAPTER 3

THEORY OF ELECTRON-PHOTON INTERACTION

3.1 Introduction

This chapter will mirror Chapter 2 in that an electron-photon Hamiltonian will be derived from electromagnetic theory[1]. The discretization of the Hamiltonian equations will be based on the results of Chapter 2.

3.2 Theory

The interaction Hamiltonian will be derived for an atom subject to external radiation.

The Maxwell's Equations are

(3.1a) $$\nabla \times \mathbf{E} = -\frac{\partial \mathbf{B}}{\partial t}.$$

(3.1b) $$\nabla \times \mathbf{H} = \mathbf{J} + \frac{\partial \mathbf{D}}{\partial t}.$$

(3.1c) $$\nabla \cdot \mathbf{D} = \rho.$$

(3.1d) $$\nabla \cdot \mathbf{B} = 0.$$

In an isotropic medium these relationships follow

(3.2a) $$\mathbf{B} = \mu \mathbf{H}.$$

(3.2b) $\mathbf{D} = \varepsilon \mathbf{E}$.

Thus the Maxwell's equations reduce to these equations for E and H

(3.3a) $$\nabla \times \mathbf{E} = -\mu \frac{\partial \mathbf{H}}{\partial t}.$$

(3.3b) $$\nabla \times \mathbf{H} = \mathbf{J} + \varepsilon \frac{\partial \mathbf{E}}{\partial t}.$$

(3.3c) $$\nabla \cdot \mathbf{E} = \frac{\rho}{\varepsilon}.$$

(3.3d) $\nabla \cdot \mathbf{H} = 0$.

For the case that there are no free charges or currents, they further reduce to

(3.4a) $$\nabla \times \mathbf{E} = -\mu \frac{\partial \mathbf{H}}{\partial t}.$$

(3.4b) $$\nabla \times \mathbf{H} = \varepsilon \frac{\partial \mathbf{E}}{\partial t}.$$

(3.4c) $\nabla \cdot \mathbf{E} = 0$.

(3.4d) $\nabla \cdot \mathbf{H} = 0$.

Take the curl of the Eq. (3.3a)

(3.5) $$\nabla \times \nabla \times \mathbf{E} = -\mu \frac{\partial \nabla \times \mathbf{H}}{\partial t} = -\varepsilon\mu \frac{\partial^2 \mathbf{E}}{\partial t^2}.$$

But,

(3.6) $$\nabla \times \nabla \times \mathbf{E} = -\nabla^2 \mathbf{E} + \nabla\nabla \cdot \mathbf{E} = -\nabla^2 \mathbf{E}.$$

Therefore,

(3.7a) $$\nabla^2 \mathbf{E} = \mu\varepsilon \frac{\partial^2 \mathbf{E}}{\partial t^2}.$$

(3.7b) $$\nabla^2 \mathbf{E} - \mu\varepsilon \frac{\partial^2 \mathbf{E}}{\partial t^2} = 0.$$

Let.

$$\mathbf{E} = \sqrt{\frac{2}{\varepsilon V}} p(t) \sin(kz) \mathbf{a}_y . \tag{3.8}$$

where p(t) will give the time variation and will later become an operator. Then it immediately follows that

$$\nabla^2 \mathbf{E} = -k^2 \mathbf{E} . \tag{3.9}$$

and thus proving the above equation has the correct spatial dependence. The parameter p can be found by differentiation with

$$\frac{\partial^2 \mathbf{E}}{\partial t^2} = \frac{\partial^2 p}{\partial t^2} \sqrt{\frac{2}{\varepsilon V}} \sin(kz) \mathbf{a}_y . \tag{3.10a}$$

$$-k^2 p - \mu\varepsilon \frac{\partial^2 p}{\partial t^2} = 0 . \tag{3.10b}$$

But.

$$k^2 = \omega^2 \mu\varepsilon . \tag{3.10c}$$

so p follows these equations

$$-\omega^2 p - \frac{\partial^2 p}{\partial t^2} = 0 . \tag{3.10d}$$

$$\omega^2 p + \frac{\partial^2 p}{\partial t^2} = 0 . \tag{3.10e}$$

$$\omega^2 p = -\frac{\partial^2 p}{\partial t^2} . \tag{3.10f}$$

Take the curl of the Eq. (3.3b)

$$\nabla \times \nabla \times \mathbf{H} = \nabla \times \varepsilon \frac{\partial \mathbf{E}}{\partial t} = \varepsilon \frac{\partial \nabla \times \mathbf{E}}{\partial t} = \varepsilon \frac{\partial}{\partial t} - \mu \frac{\partial}{\partial t} \mathbf{H} = -\varepsilon\mu \frac{\partial^2 \mathbf{H}}{\partial t^2} . \tag{3.11}$$

But.

(3.12) $$\nabla \times \nabla \times \mathbf{H} = -\nabla^2 \mathbf{H} + \nabla\nabla \cdot \mathbf{H} = -\nabla^2 \mathbf{H}.$$

And the relation for H becomes

(3.13a) $$-\nabla^2 \mathbf{H} = -\varepsilon\mu \frac{\partial^2 \mathbf{H}}{\partial t^2}.$$

(3.13b) $$\nabla^2 \mathbf{H} = \varepsilon\mu \frac{\partial^2 \mathbf{H}}{\partial t^2}.$$

Let.

(3.13c) $$\mathbf{H} = \omega \sqrt{\frac{2}{\mu V}} q(t) \cos(kz) \mathbf{a}_y.$$

Immediately we get the usual relationship for spatial coordinate

(3.14) $$\nabla^2 \mathbf{H} = -k^2 \mathbf{H}.$$

The time variable q(t) is

(3.15a) $$\frac{\partial^2 \mathbf{H}}{\partial t^2} = \frac{\partial^2 q}{\partial t^2} \omega \sqrt{\frac{2}{\mu V}} \cos(kz) \mathbf{a}_y.$$

(3.15b) $$\nabla^2 \mathbf{H} = \varepsilon\mu \frac{\partial^2 \mathbf{H}}{\partial t^2}.$$

(3.15c) $$-k^2 q = \varepsilon\mu \frac{\partial^2 q}{\partial t^2}.$$

(3.15d) $$k^2 = \omega^2 \mu\varepsilon.$$

(3.15e) $$-\omega^2 q = \frac{\partial^2 q}{\partial t^2}.$$

The electric energy density is

(3.16a) $$\frac{1}{2}\varepsilon E^2 = \frac{1}{2}\varepsilon \frac{2}{\varepsilon V} p^2(t) \sin^2(kz) = \frac{1}{V} p^2(t) \sin^2(kz).$$

The magnetic energy density is

(3.16b) $$\frac{1}{2}\mu H^2 = \frac{1}{2}\mu\omega^2\frac{2}{\mu V}q^2(t)\cos^2(kz) = \omega^2\frac{1}{V}q^2(t)\cos^2(kz).$$

The electric energy in volume V is (1/2 factor from the cos) simply

(3.17a) $$\frac{p^2(t)}{2}.$$

The magnetic energy in volume V is likewise

(3.17b) $$\omega^2\frac{q^2(t)}{2}.$$

The total energy is

(3.18) $$E = \frac{1}{2}\left[p^2(t) + \omega^2 q^2(t)\right].$$

Introduce the operators

(3.19a) $$a = \left(\frac{1}{2\hbar\omega}\right)^{1/2}(\omega q + ip).$$

(3.19b) $$a^* = \left(\frac{1}{2\hbar\omega}\right)^{1/2}(\omega q - ip).$$

with the relations

(3.19c) $$a + a^* = \left(\frac{1}{2\hbar\omega}\right)^{1/2}(2\omega q).$$

(3.19d) $$a + a^* = \left(\frac{2\omega}{\hbar}\right)^{1/2} q.$$

(3.19e) $$q = \left(\frac{\hbar}{2\omega}\right)^{1/2}(a^* + a).$$

Thus the magnetic field can be written

(3.20) $$\mathbf{H} = \sqrt{\frac{\hbar\omega}{\mu V}}(a^* + a)\cos(kz)\mathbf{a}_y.$$

Likewise for the electric field

(3.21a) $$a^{\dagger} - a = \left(\frac{1}{2\hbar\omega}\right)^{1/2}(-i2p).$$

(3.21b) $$i(a^{\dagger} - a) = \left(\frac{2}{\hbar\omega}\right)^{1/2} p.$$

(3.21c) $$p = i\left(\frac{\hbar\omega}{2}\right)^{1/2}(a^{\dagger} - a).$$

(3.21d) $$\mathbf{E} = i\sqrt{\frac{\hbar\omega}{\varepsilon V}}(a^{\dagger} - a)\sin(kz)\mathbf{a}_{\cdot}.$$

The time dependent of the creation and annihilation operators since in Heisenberg representation of quantum mechanics. the time development of operator O is

(3.22) $$\frac{d}{dt}O = \frac{i}{\hbar}[H.O].$$

Thus the time dependence of operator a is

(3.22a) $$\frac{d}{dt}a = \frac{i}{\hbar}[H.a].$$

(3.22b) $$H = \hbar\omega\left(a^{\dagger}a + \frac{1}{2}\right).$$

(3.22c) $$Ha = \hbar\omega\left(a^{\dagger}aa + \frac{a}{2}\right).$$

(3.22d) $$aH = \hbar\omega\left(aa^{\dagger}a + \frac{a}{2}\right).$$

(3.22e) $$[H.a] = Ha - aH = \hbar\omega(a^{\dagger}aa - aa^{\dagger}a) = \hbar\omega(a^{\dagger}a - aa^{\dagger})a = \hbar\omega(a^{\dagger}a - 1 - a^{\dagger}a)a = -\hbar\omega a.$$

(3.22f) $$\frac{d}{dt}a = \frac{i}{\hbar} - \hbar\omega a = -i\omega a.$$

with the solution

(3.22g) $$a(t) = \frac{a}{2} e^{-i\omega t}.$$

Likewise for operator $a^{\dagger}$

(3.23a) $$\frac{d}{dt} a^{\dagger} = \frac{i}{\hbar}[H, a^{\dagger}].$$

(3.23b) $$[Ha^{\dagger}] = Ha^{\dagger} - a^{\dagger}H = \hbar\omega(a^{\dagger}aa^{\dagger} - a^{\dagger}a^{\dagger}a) = \hbar\omega a^{\dagger}(aa^{\dagger} - a^{\dagger}a) = \hbar\omega a^{\dagger}.$$

(3.23c) $$\frac{d}{dt} a^{\dagger} = \frac{i}{\hbar}\hbar\omega a^{\dagger} = i\omega a^{\dagger}.$$

(3.23d) $$a^{\dagger}(t) = \frac{a^{\dagger}}{2} e^{i\omega t}.$$

Thus the time-dependent electric field is

(3.24) $$\mathbf{E} = i\sqrt{\frac{\hbar\omega}{2\varepsilon V}}(a^{\dagger}e^{i\omega t} - ae^{-i\omega t})\sin(kz)\mathbf{a}_{x}.$$

In the long-wavelength region, $k \cong 0$, it can be assumed that the electric field is

(3.25) $$\mathbf{E} = i\sqrt{\frac{\hbar\omega}{2\varepsilon V}}(a^{\dagger}e^{i\omega t} - ae^{-i\omega t})\,\mathbf{a}_{x}.$$

The interact Hamiltonian is the electric field times the dipole moment in the direction of the electric field. The dipole moment can be assumed to be

(3.26) $$\mathbf{m} = -ey\mathbf{a}_{y}.$$

and the interaction Hamiltonian is

(3.27) $$H_{e-p} = \mathbf{E}\cdot\mathbf{m} = -ie\sqrt{\frac{\hbar\omega}{2\varepsilon V}}(a^{\dagger}e^{i\omega t} - ae^{-i\omega t})y.$$

In my calculation, the electric field and the dipole moment are in z-direction. Further I take the reference point to be in center of quantum well.

(3.28) $$H_{e-p} = -ie\sqrt{\frac{\hbar\omega}{2\varepsilon V}}\left(a^{+}e^{i\omega t} - ae^{-i\omega t}\right)(z - z_0).$$

Introduce a constant, $g = e\sqrt{\frac{\hbar\omega}{2\varepsilon V}}$, the interaction Hamiltonian becomes

(3.29) $$H_{e-p} = -ig\left(a^{+}e^{i\omega t} - ae^{-i\omega t}\right)(z - z_0).$$

3.3 The Schrödinger equation with electron photon interaction

As before, the wavefunction for representing electron-photon coupling must include electron and photon terms. Here, the photon state can be either $|n>$, $|n-1>$ or $|n+1>$, which differ by a population of one, where $|n>$ is the incident radiation. There are three electronic states, $\psi^{(0)}$, $\psi^{(1)}$ and $\psi^{(2)}$, associated with each of three photon states which are separated by photon energy $\hbar\omega$. The wavefunction is

(3.30) $$\psi = \psi^{(0)}|n> + \psi^{(1)}|n-1> + \psi^{(2)}|n+1>.$$

The time-dependent Schrödinger equation is

(3.31) $$i\hbar\frac{\partial\psi}{\partial t} = H\psi(z,t).$$

The total Hamiltonian includes a purely electronic part and a part that deals with electron-photon interaction as

(3.32) $$H = H_e + H_{e-p}.$$

Using the electron-photon Hamiltonian in Eq. (3.29), this matrix equation is written

$$(3.33)\qquad i\hbar\frac{\partial}{\partial t}\begin{bmatrix}\psi^{(0)}\\ \psi^{(1)}\\ \psi^{(2)}\end{bmatrix}=\begin{bmatrix}H_e & -ig(z-z_0)\sqrt{n}e^{i\omega t} & ig(z-z_0)\sqrt{n+1}e^{-i\omega t}\\ ig(z-z_0)\sqrt{n}e^{-i\omega t} & H_e & 0\\ -ig(z-z_0)\sqrt{n+1}e^{i\omega t} & 0 & H_e\end{bmatrix}\begin{bmatrix}\psi^{(0)}\\ \psi^{(1)}\\ \psi^{(2)}\end{bmatrix}.$$

Equation (2.98) is rewritten here

$$(3.34)\qquad i\hbar\frac{\partial}{\partial t}\begin{bmatrix}\psi^{(0)}\\ \psi^{(1)}\\ \psi^{(2)}\end{bmatrix}=\begin{bmatrix}H_e & a(z,t) & b(z,t)\\ c(z,t) & H_e & 0\\ d(z,t) & 0 & H_e\end{bmatrix}\begin{bmatrix}\psi^{(0)}\\ \psi^{(1)}\\ \psi^{(2)}\end{bmatrix}.$$

Thus,

$$(3.35a)\qquad a(z,t)=-ig(z-z_0)\sqrt{n}e^{i\omega t}.$$

$$(3.35b)\qquad b(z,t)=ig(z-z_0)\sqrt{n+1}e^{-i\omega t}.$$

$$(3.35c)\qquad c(z,t)=ig(z-z_0)\sqrt{n}e^{-i\omega t}.$$

$$(3.35d)\qquad d(z,t)=-ig(z-z_0)\sqrt{n+1}e^{i\omega t}.$$

Finally the discretized equations, based on results of Chapter 2, are

$$(3.36a)\qquad A_j\begin{bmatrix}Q^{(0)\,r+1}_{j-1}\\ Q^{(1)\,r+1}_{j-1}\\ Q^{(2)\,r+1}_{j-1}\end{bmatrix}+\begin{bmatrix}B_j & D^{r+1}_j & E^{r+1}_j\\ F^{r+1}_j & B_j & 0\\ G^{r+1}_j & 0 & B_j\end{bmatrix}\begin{bmatrix}Q^{(0)\,r+1}_j\\ Q^{(1)\,r+1}_j\\ Q^{(2)\,r+1}_j\end{bmatrix}+C_j\begin{bmatrix}Q^{(0)\,r+1}_{j+1}\\ Q^{(1)\,r+1}_{j+1}\\ Q^{(2)\,r+1}_{j+1}\end{bmatrix}$$

$$=\begin{bmatrix}2p & D^{r+1}_j+DH^r_j & E^{r+1}_j+EH^r_j\\ F^{r+1}_j+FH^r_j & 2p & 0\\ G^{r+1}_j+GH^r_j & 0 & 2p\end{bmatrix}\begin{bmatrix}\psi^{(0)\,r+1}_j\\ \psi^{(1)\,r+1}_j\\ \psi^{(2)\,r+1}_j\end{bmatrix}.$$

$$(3.36b)\qquad Q^{(1)\,r+1}_j=\psi^{(1)\,r+1}_j+\psi^{(1)\,r}_j.$$

$$(3.36c)\qquad p=i\frac{2\varepsilon^2}{\hbar\delta}m_e.$$

$$(3.36d)\qquad A_j=\frac{m_e}{m_{j-1}+m_j}.$$

(3.36e) $$C_j = \frac{m_e}{m_{j-1} + m_j}.$$

(3.36f) $$B_j = p - A_j - C_j - \frac{\varepsilon^2}{\hbar^2} m_e V_j.$$

(3.36g) $$D_j^{r-1} = -\frac{\varepsilon^2 m_e}{\hbar^2} a_j^{r-1}.$$

(3.36i) $$DH_j^r = \frac{\varepsilon^2 m_e}{\hbar^2} a_j^r.$$

(3.36h) $$E_j^{r-1} = -\frac{\varepsilon^2 m_e}{\hbar^2} b_j^{r-1}.$$

(3.36j) $$EH_j^r = \frac{\varepsilon^2 m_e}{\hbar^2} b_j^r.$$

(3.36k) $$F_j^{r-1} = -\frac{\varepsilon^2}{\hbar^2} m_e c_j^{r-1}.$$

(3.36l) $$FH_j^r = \frac{\varepsilon^2}{\hbar^2} m_e c_j^r.$$

(3.36m) $$G_j^{r-1} = -\frac{\varepsilon^2 m_e d_j^{r-1}}{\hbar^2}.$$

(3.36n) $$GH_j^r = \frac{\varepsilon^2 m_e d_j^r}{\hbar^2}.$$

(3.36o) $$a_j^r = -ig\varepsilon(j - j_0)\sqrt{n}e^{i\omega\delta r}.$$

(3.36p) $$b_j^r = ig\varepsilon(j - j_0)\sqrt{n+1}e^{-i\omega\delta r}.$$

(3.36q) $$c_j^r = ig\varepsilon(j - j_0)\sqrt{n}e^{-i\omega\delta r}.$$

(3.36r) $$d_j^r = -ig\varepsilon(j - j_0)\sqrt{n+1}e^{i\omega\delta r}.$$

3.4 References

1. A. Yariv, *An Introduction to Theory and Applications of Quantum Mechanics* (John Wiley & Sons, New York, 1982), p. 133.

CHAPTER 4

VISUALIZATION OF ELECTRON TRANSPORT DYNAMICS IN SEMICONDUCTOR NANOSTRUCTURES

4.1 Introduction

Now that electron-phonon and electron-photon interaction Hamiltonians have been discussed, the most important element of the thesis concerning the visualization of electron transport dynamics in semiconductor nanostructures will be dealt with. A program, called Visual Quantum Project (VQP), will be used to display the calculated results in real time. Basically the important elements will be the inputs of a semiconductor nanostructure, setting of interaction within the device, and then setting up a calculation, *i.e.*, what elements are calculated. After the calculation, the program itself can be used for simple analysis. However for more complicated analysis, a series may be saved so a mathematical program can analyze the data. VQP will be used to analyze three devices mentioned in the next 3 chapters. However only the semiconductor superlattice structure is used in the illustrations of VQP in this chapter. All the steps in creating a project to view Bloch oscillations in semiconductor superlattices are detailed later in this chapter. The project file, which is an ACSII text file that can be modified by almost any other program, is included the Appendix.

4.2 Visualization program for quantum projects

A brief description of the program (VQP) follows. The program is a windows-based graphic user interface program and is written using Microsoft Visual C++ 6. When the program is launched, the following menu options are available: File, Setting, View, Window, and Help. The title bar indicates the name of the current quantum project with a short user note.

At this point the user may do two things. A saved project can be opened by selecting Open Project in File menu. A new project may be also be started by selecting Set Quantum Structure in the Setting menu. There are five options: square barrier or well, triangular barrier or well and import structure. If either of the four barrier or well structures are selected, several dialogs are displayed to get the potential energy and effective mass profile, for the number of regions in the device. The import structure will load an ASCII text file with a complex structure, where the text file can be written with almost any program such as Excel. Once a particular structure is set up, different options are now available in the Settings menu such as Modify Quantum Structure, Wavepacket (Traveling or Localized), Applied Bias, Interaction (electron-phonon or electron-photon) within device and Resolution (spatial and temporal) for the calculations. All have default values, which may be changed by choosing Default Settings in the Setting menu. For most of the parameters in the Setting menu, the program allows the user to enter a range of parameters by writing a start, step and stop value. The program will run the simulation the required number of times and cycle through all the variables.

Once the settings are set, a window titled 'Entire Structure' will show up showing the nanostructure. Also two new menu items will appear: Graph and Operation. Most of the operations in these 2 menus are available as toolbars. The program can display in real time five important results as electron wave function is being calculated: probability density (P), charge (Q), current (J), energy (E) and center of mass (X). These five options are available in the Graph menu as well as the new document toolbars with those letterings. The Operation menu is used to Run / Pause the calculation as well as Quit the calculation. The two options are available as toolbars with the blue arrow for Run / Pause and red stop sign for Quit.

The program allows for automatic saving of calculated data of current, charge, energy, or center of mass data after each calculation, *i.e.*, till the wavepacket is near the hard boundaries or after a selected time period, if and only if a series name is entered at the time the graphs were created. At any time, the Project Information option from the Help menu can be selected to see the current status of calculation. It will show what are the current values for the different variables and much calculation time is remaining.

The feature of saving a series is useful if the program loops for days. After program conclusion, the data in the series can be analyzed using a mathematical program such as MATLAB. Alternatively VQP can open the series by selecting Open Series option from the File menu. By right clicking on the graphs, the local minima and local maxima values can be found near a given point. Left clicking on a graph will give the value at a particular point, as well as the graph properties set at creation. The mouse options are also available for running calculations.

4.3 Semiconductor superlattice

In Chapter 6, I will discuss Bloch oscillations under electron-phonon interaction. In semiconductor superlattices under uniform electric field, time evolution of Wannier-Stark ladder (WSL) states leads to coherent quantum beats. Up to now, it is not clear how various phonon modes can affect the dynamics of Bloch oscillation. With this program, the subject can be easily investigated.

When VQP is launched a welcome screen will show up as shown in Fig. 4.1. Additionally if a project file is dragged into VQP icon, the saved quantum structure will be loaded. If this is not the case, the word 'Untitled' will appear in the Title bar. Then the structural information must be provided using the Setting menu. We first select the Default Settings in the Setting menu and enter the values shown in Fig. 4.2. The different structural parameters are the widths of well and barrier, how far the hard boundaries are from the structure, the length of the leads where the electric field is nonzero in case of applied bias, the effective mass for barrier and well and the conduction band discontinuity. For confined phonons, the interaction strength in the barrier is zero. Further the value in the well is the amplitude of sinusoidal distribution. Lastly the pen size indicates how wide the display lines will be. This is useful for large resolution monitors.

After the default settings are set, a 35-quantum-well structure can be set by selecting the options indicated on Fig. 4.3. We next enter 36 for the number of barriers / wells in the dialog box as shown in Fig. 4.4. After accepting the values in the next few dialog boxes, the structure shown in Fig. 4.5 will show up.

Next the Wavepacket is selected with the options shown in Fig. 4.6 and set with the values shown in Fig. 4.7. The wavepacket is centered within the superlattice structure with zero initial kinetic energy. The resulting quantum structure is shown in Fig. 4.8. Now select Applied Voltage from the Setting menu with the values shown in Fig. 4.9. A single voltage of 0.15 V is entered. The modified quantum structure is shown in Fig. 4.10. Finally the Resolutions are selected from the Setting menu and set with the values shown in Fig. 4.11.

Now that the different settings have been set, the project should be saved. Selecting Save Project from the File menu, the file save dialog comes up as shown in Fig. 4.12. After pressing save, the program prompts for project note as shown in Fig. 4.13. Both the project title and project note are displayed on Title bar. Next a new window is created through either the Graph menu or just by selecting the toolbar with the letter P. Enter the range shown in Fig. 4.14 to see only the superlattice structure and the new window is shown Fig. 4.15 with the 'Entire Structure' window closed.

A new window, for the center of mass, which is labeled X in toolbars, is opened with the values in Fig. 4.16. Now that we have set the windows, the calculation can be run by clicking on the arrow toolbar or selecting Run / Pause from the Operation menu. After running the calculation for about 3 ps, the graphs show that 3 Bloch oscillations have occurred as shown in Fig. 4.17. At that moment the center of mass graph is selected and printed using Print Graph from Graph menu or the print toolbar. The caption of graph and the margins of graph are set with the values shown in Fig. 4.18. The resulting graph will be printed as shown in Fig. 4.19.

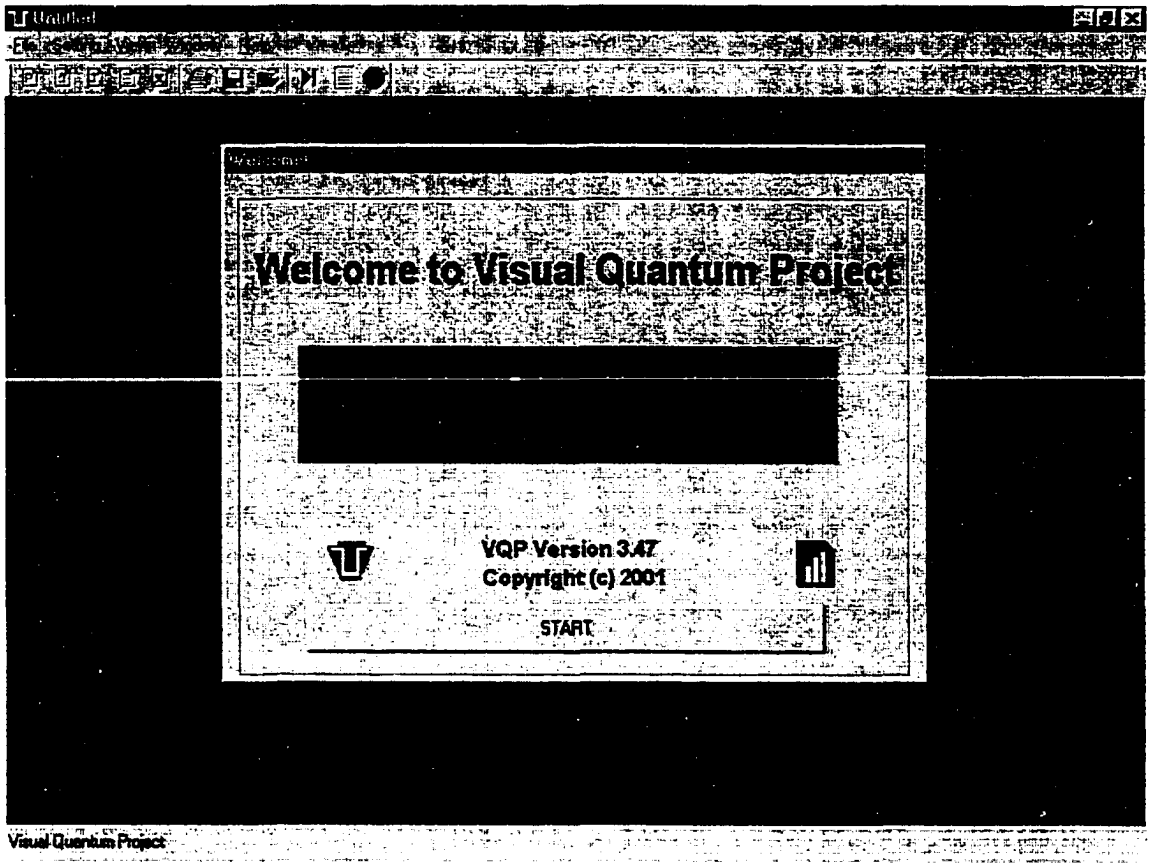

Fig. 4.1: A welcome dialog shows up when VQP is launched.

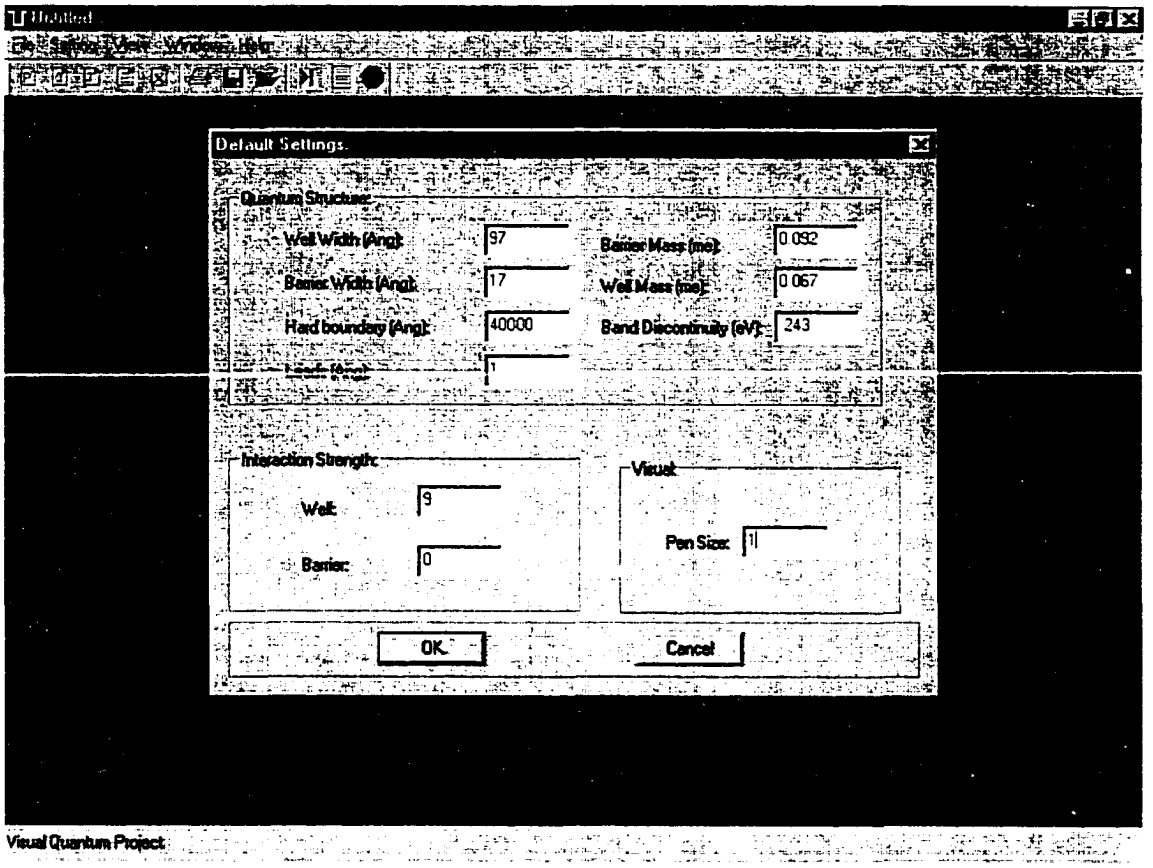

Fig. 4.2: The default settings can be changed by selecting Default Settings in the Setting menu and entering these values for a semiconductor superlattice.

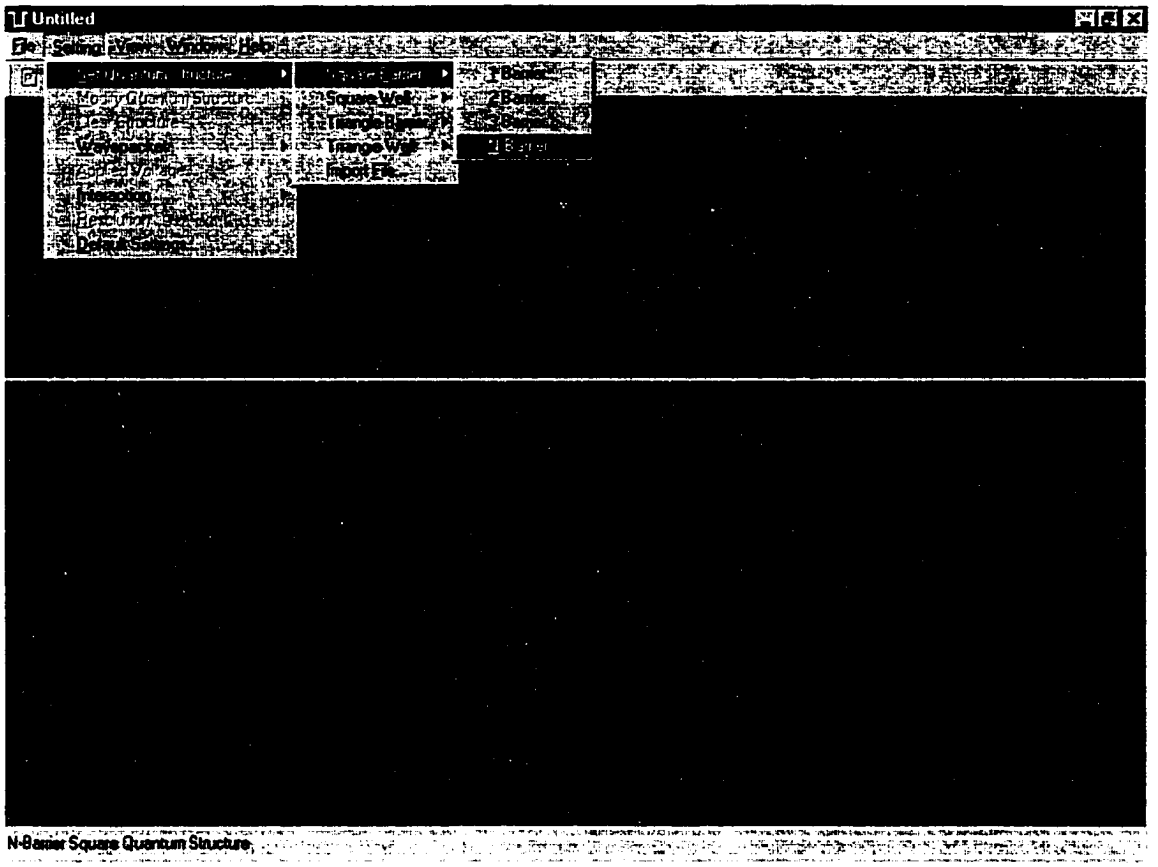

Fig. 4.3: A 36-barrier structure can be set by selecting the N-Barrier Square Barrier option.

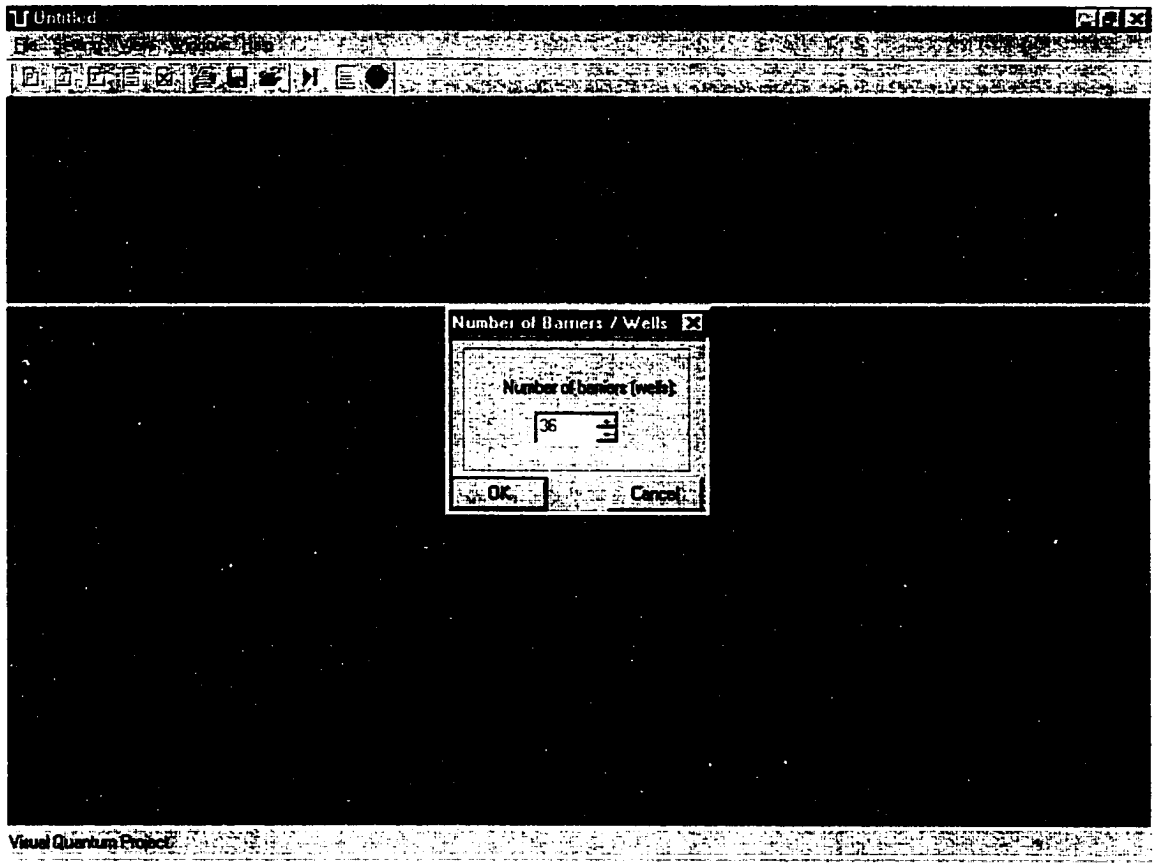

Fig. 4.4: Enter 36 barriers for a 35-QW structure.

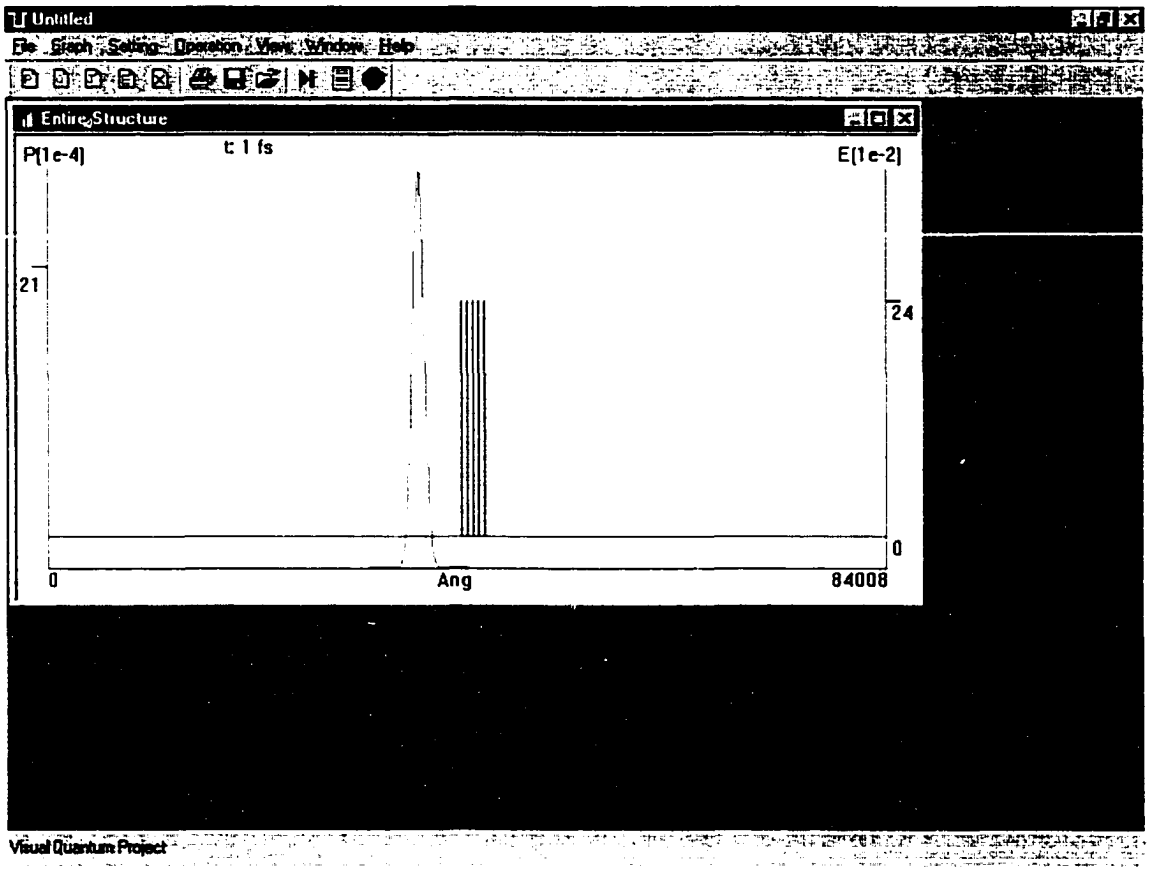

Fig. 4.5: After setting the structure, an 'Entire Structure' window shows up.

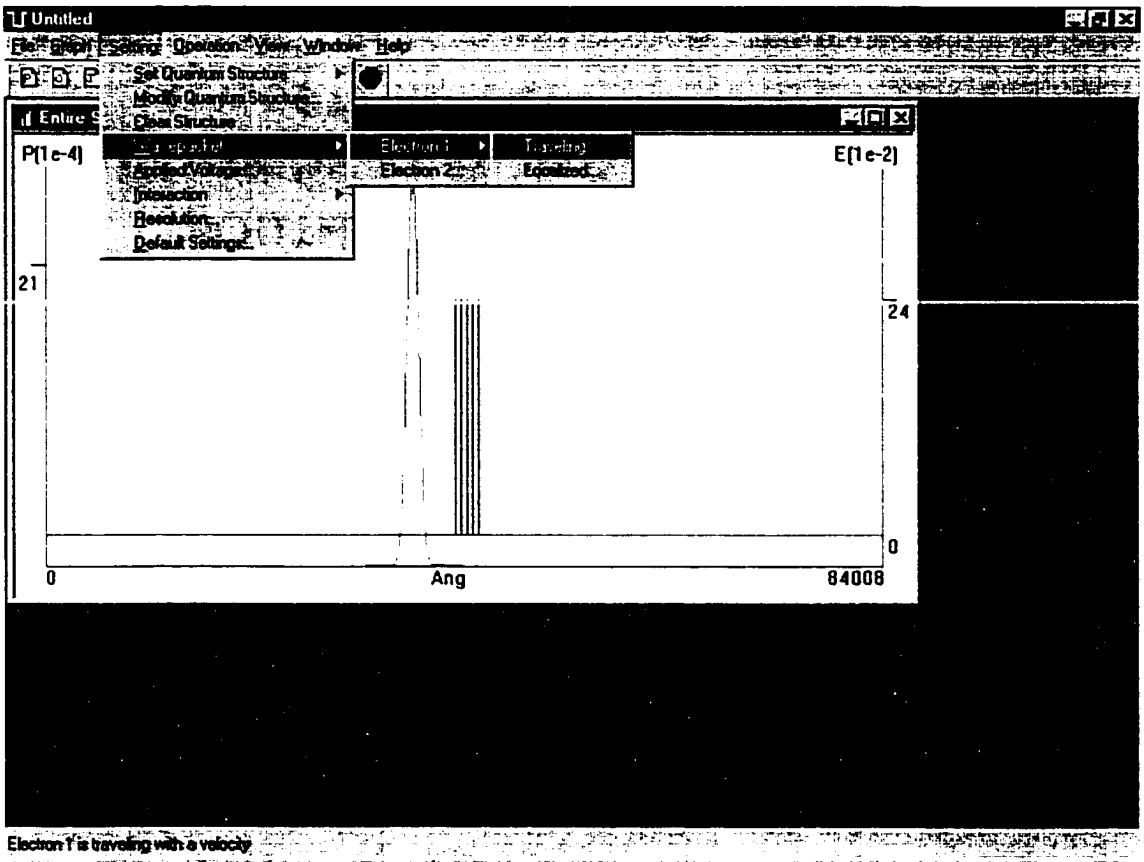

Fig. 4.6: We can change the wavepacket properties by selecting these options.

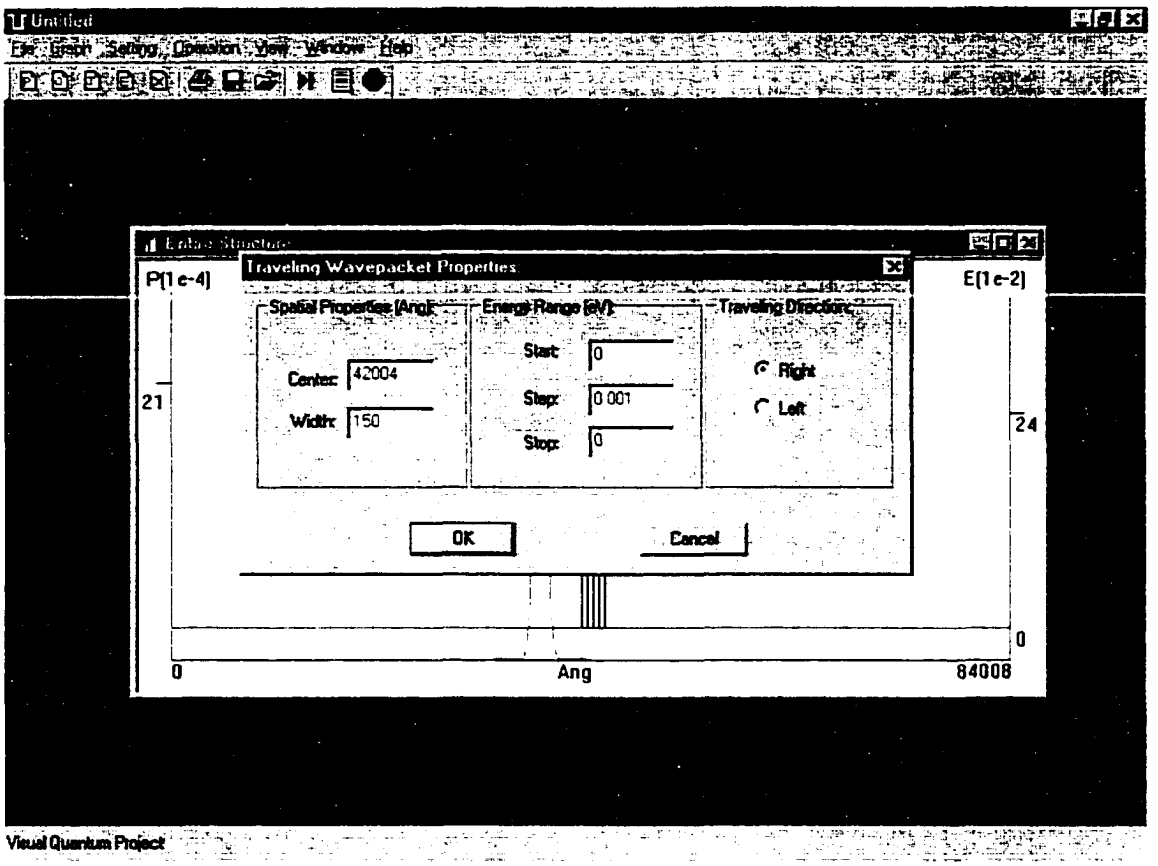

Fig. 4.7: Set the wavepacket properties so the electron is in middle of superlattice with zero kinetic energy.

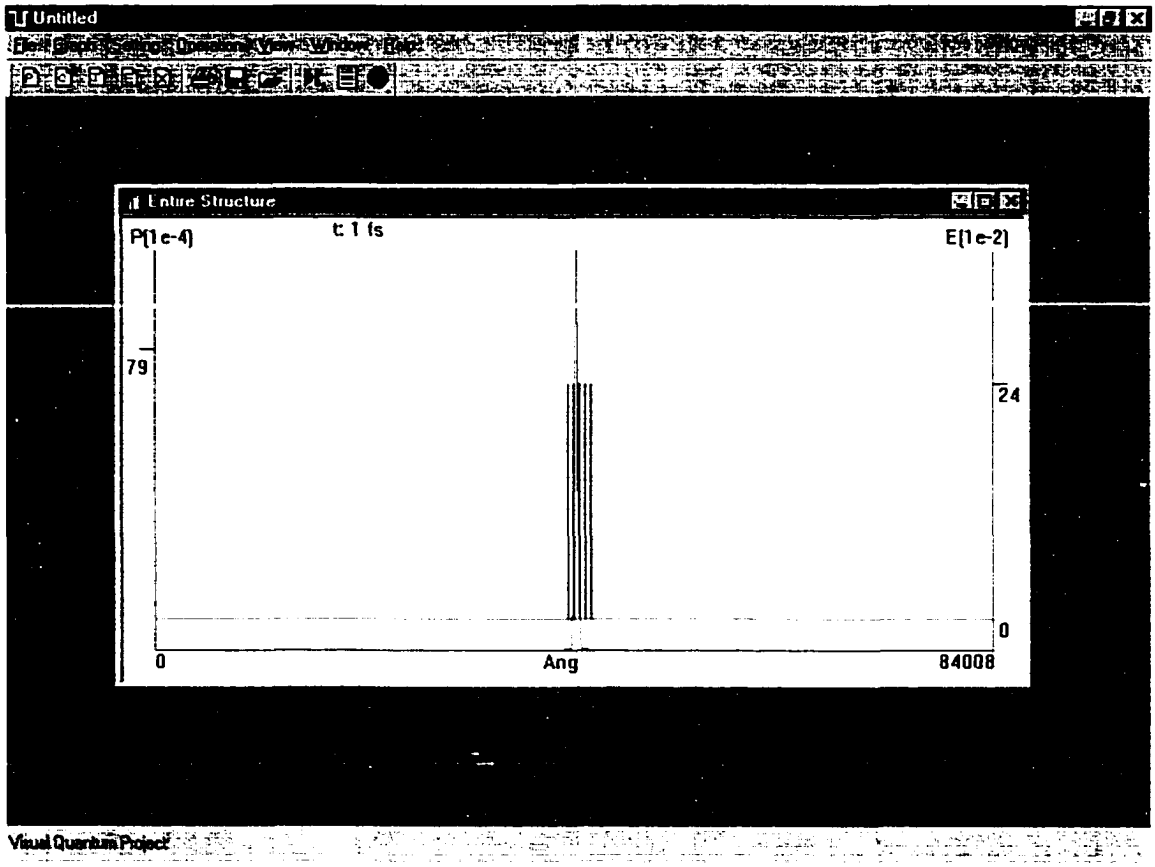

Fig. 4.8: The resulting quantum structure after setting the wavepacket properties.

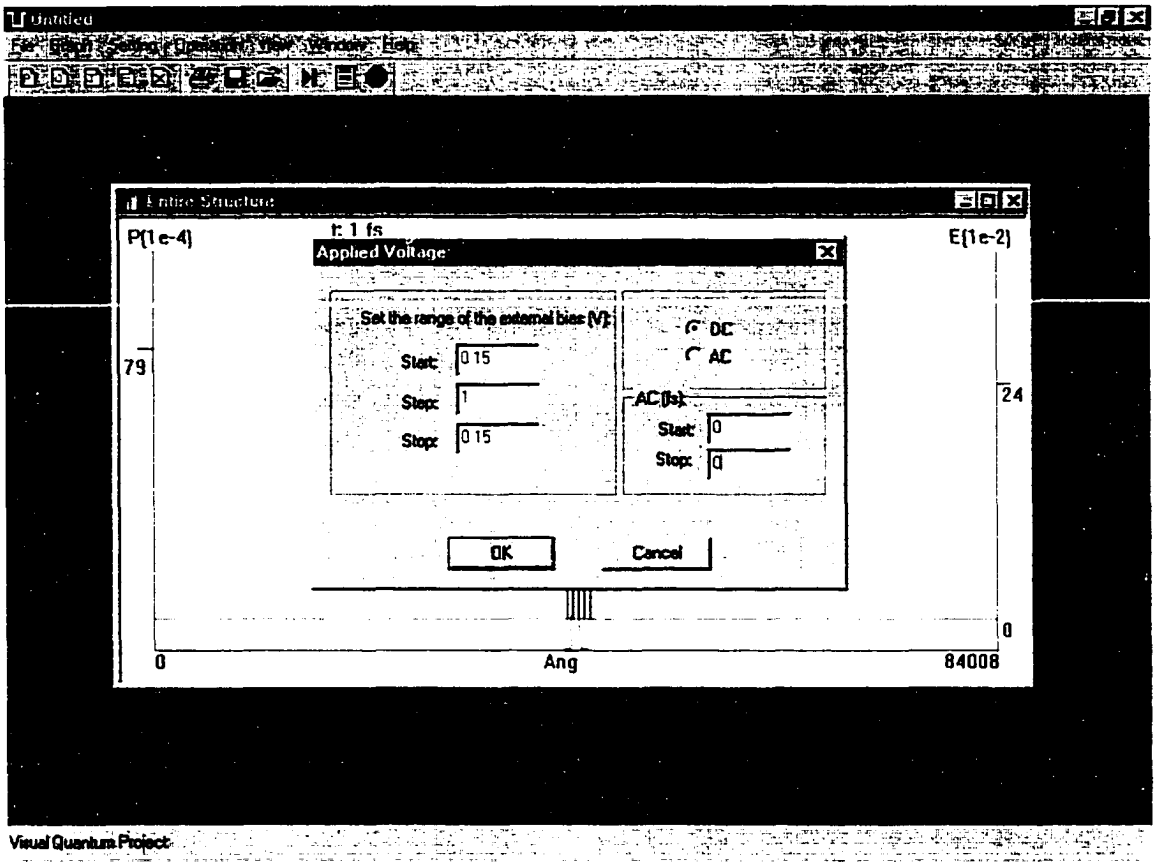

Fig. 4.9: Set the applied bias across the semiconductor superlattice as 0.15 V.

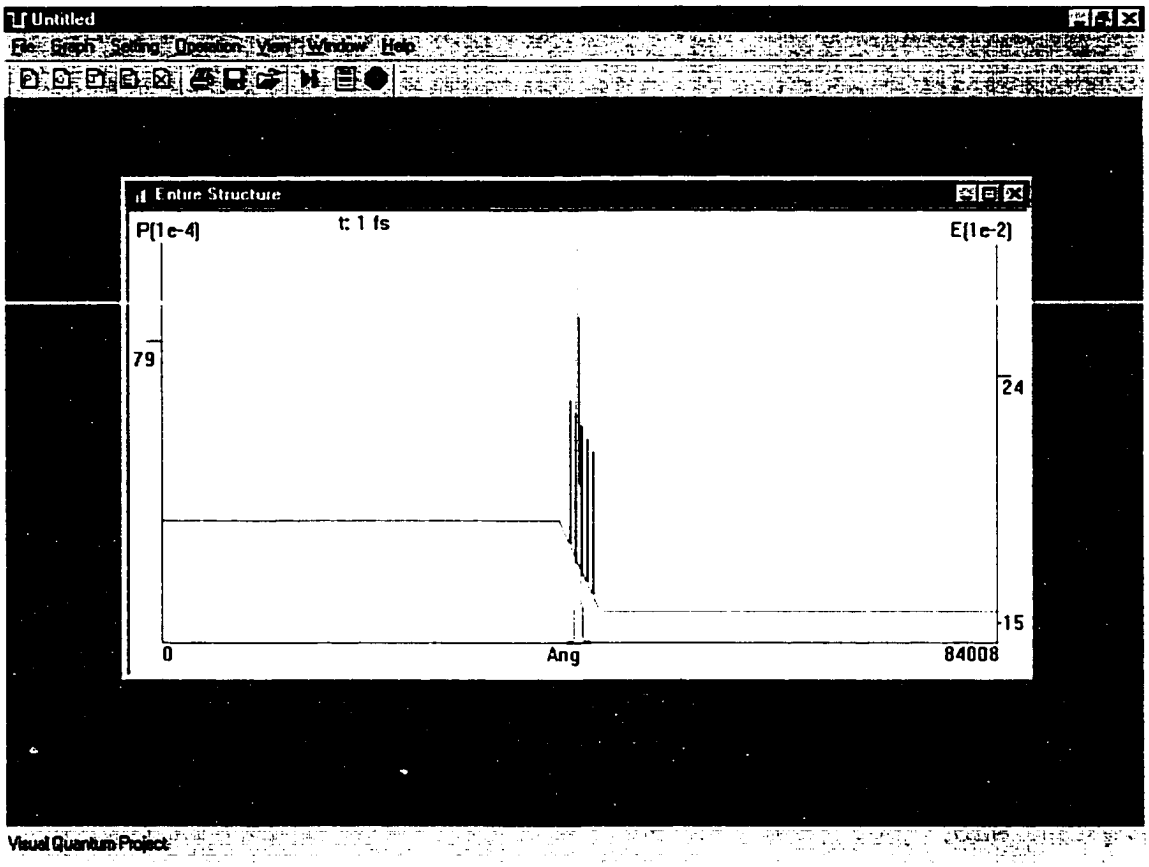

Fig. 4.10: The resulting quantum structure after setting the bias.

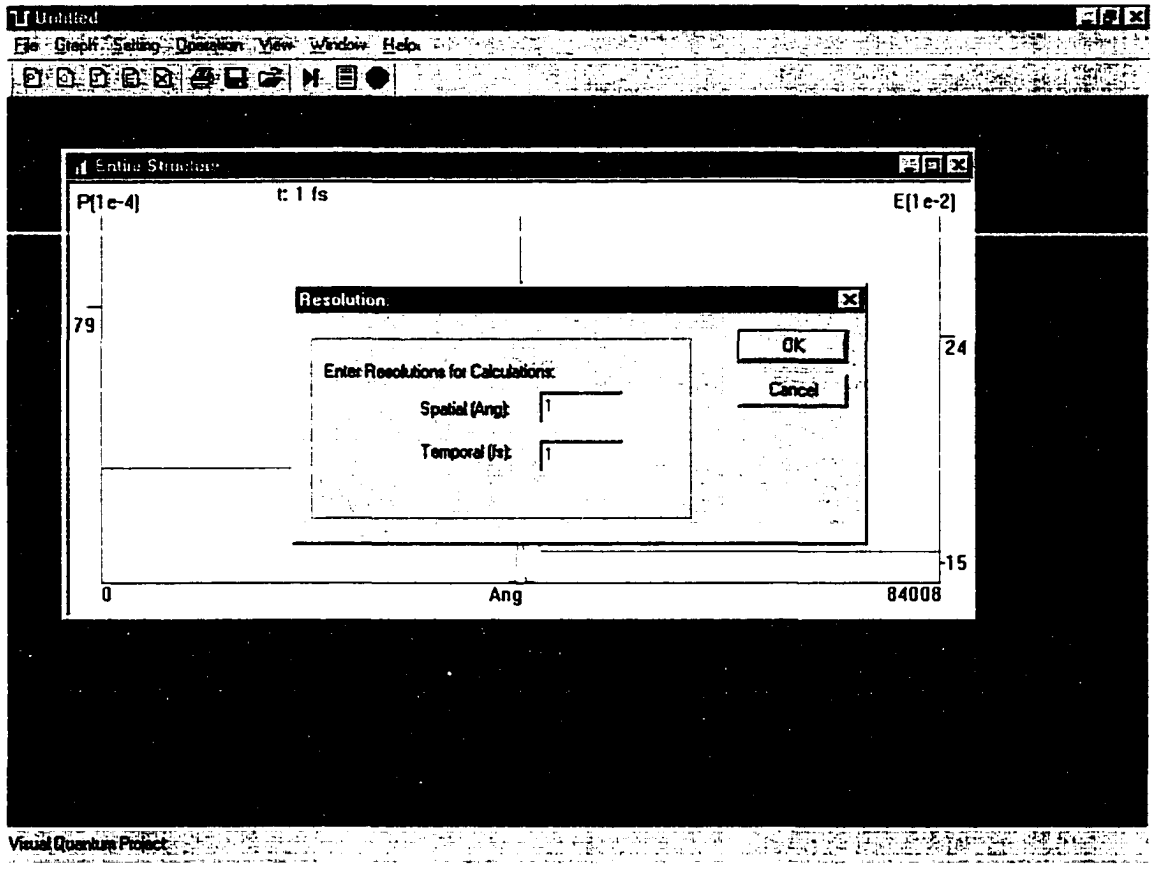

Fig. 4.11: Set the temporal and spatial resolutions for the calculation.

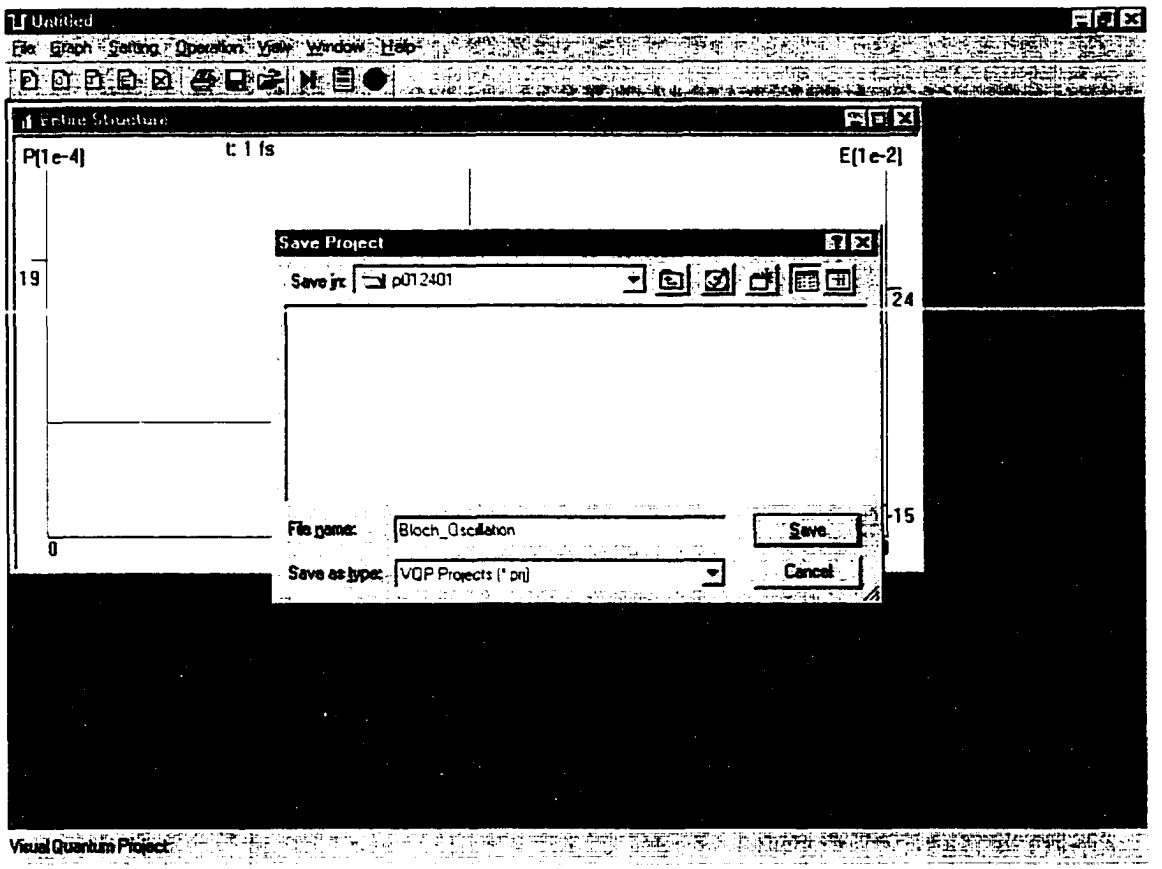

Fig. 4.12: After setting the quantum structure, the project should be saved by selecting Save Project from the File menu.

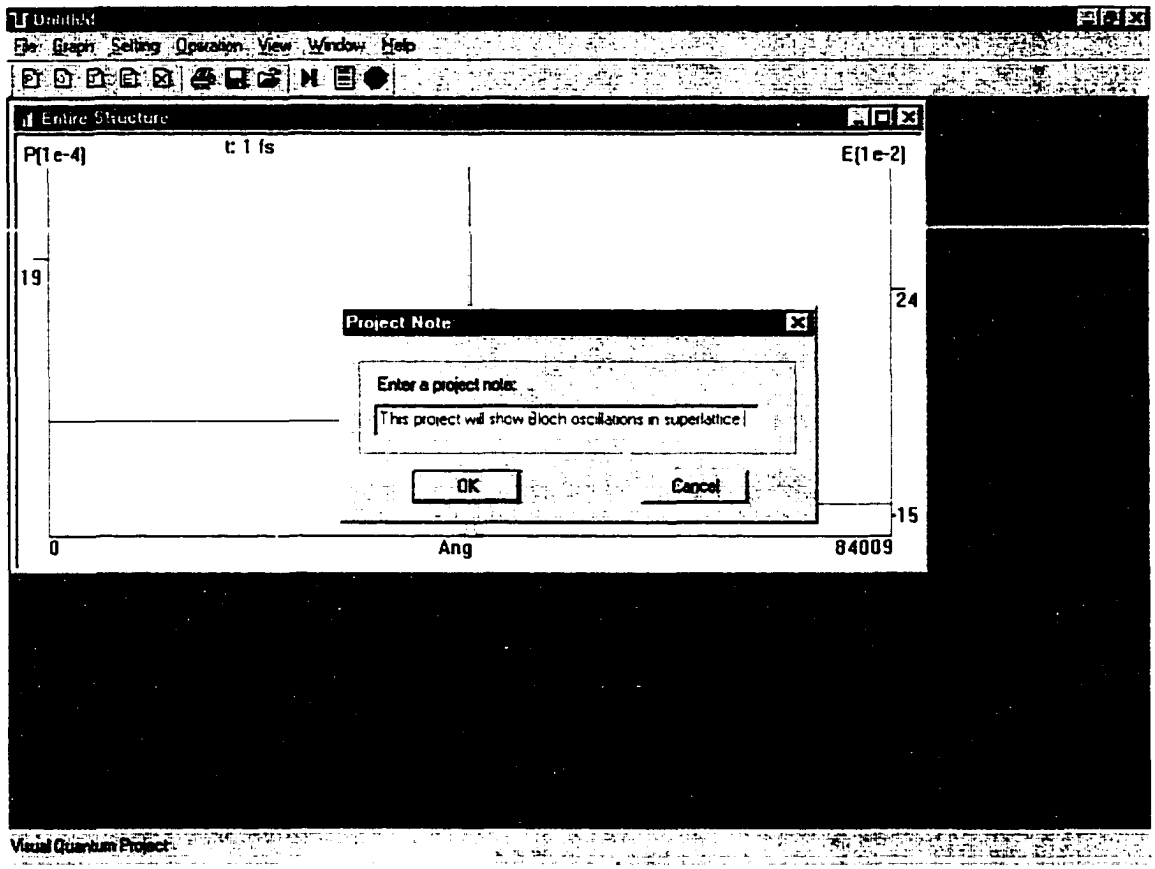

Fig. 4.13: After entering the project title, the program will ask for a project note.

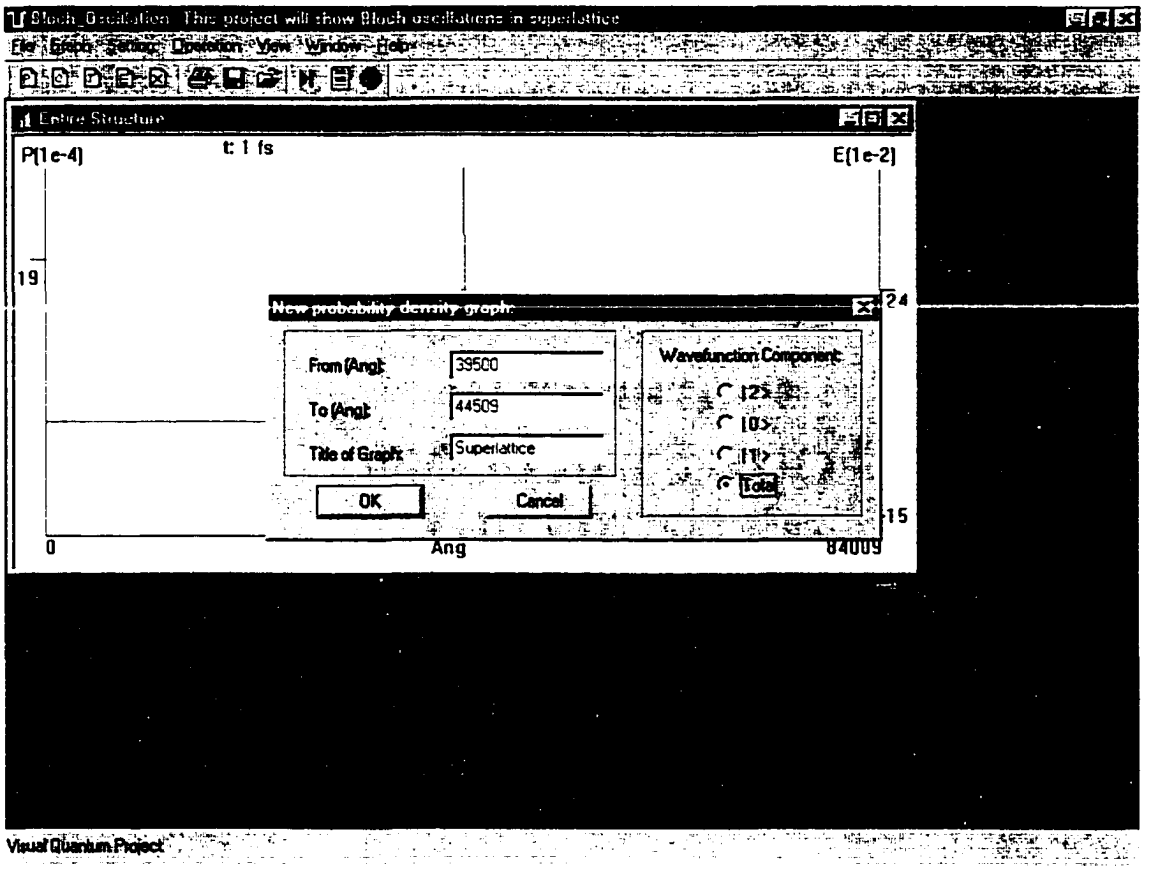

Fig. 4:14: Set up a new probability graph to zoom in on the superlattice structure.

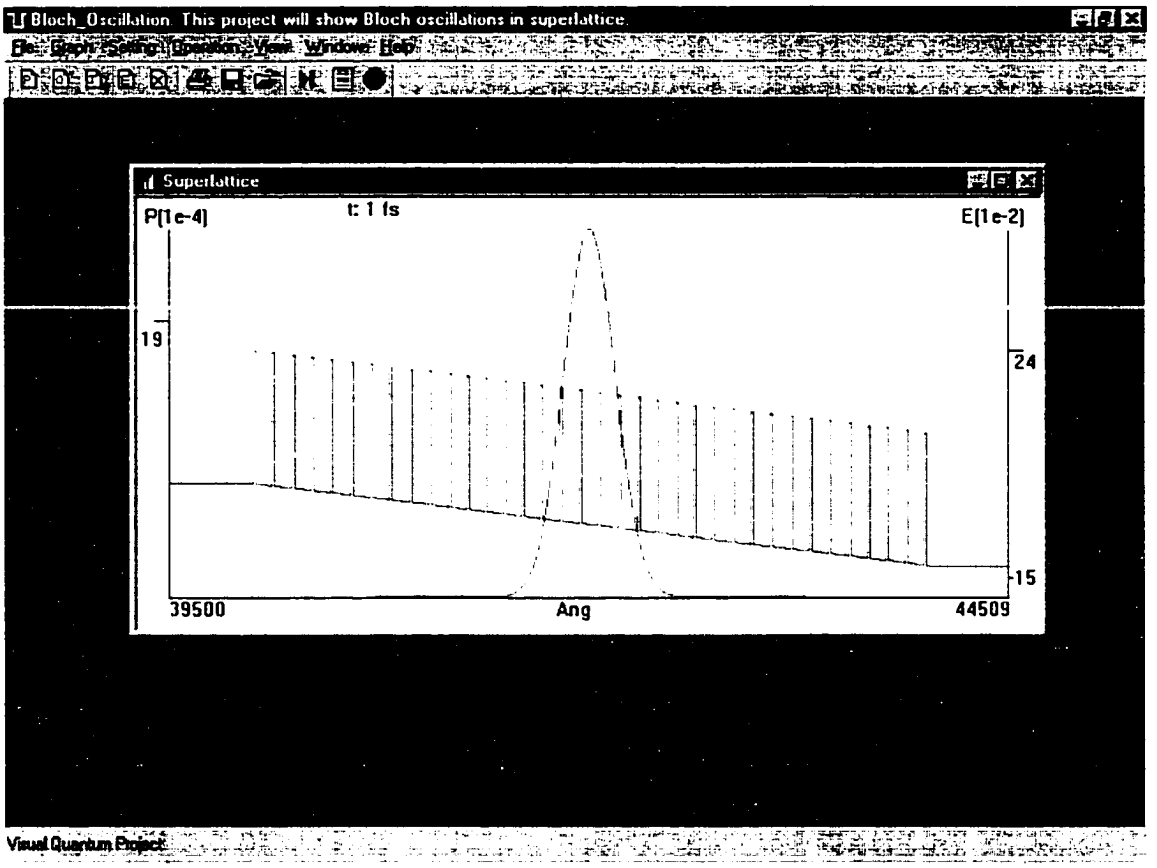

Fig. 4.15: The 'Superlattice' window pops up. Note that the 'Entire Structure window has been manually closed.

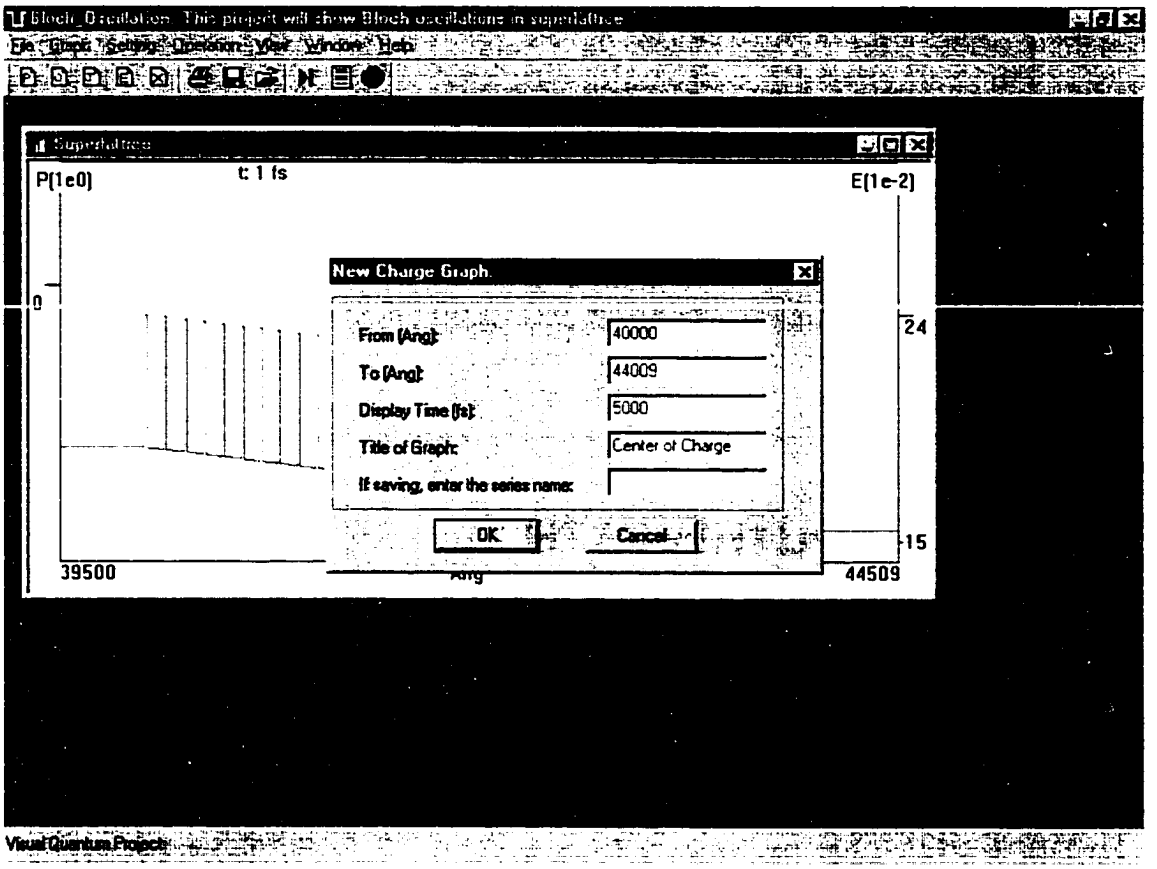

Fig. 4:16: A center of mass graph for finding the charge center within the superlattice.

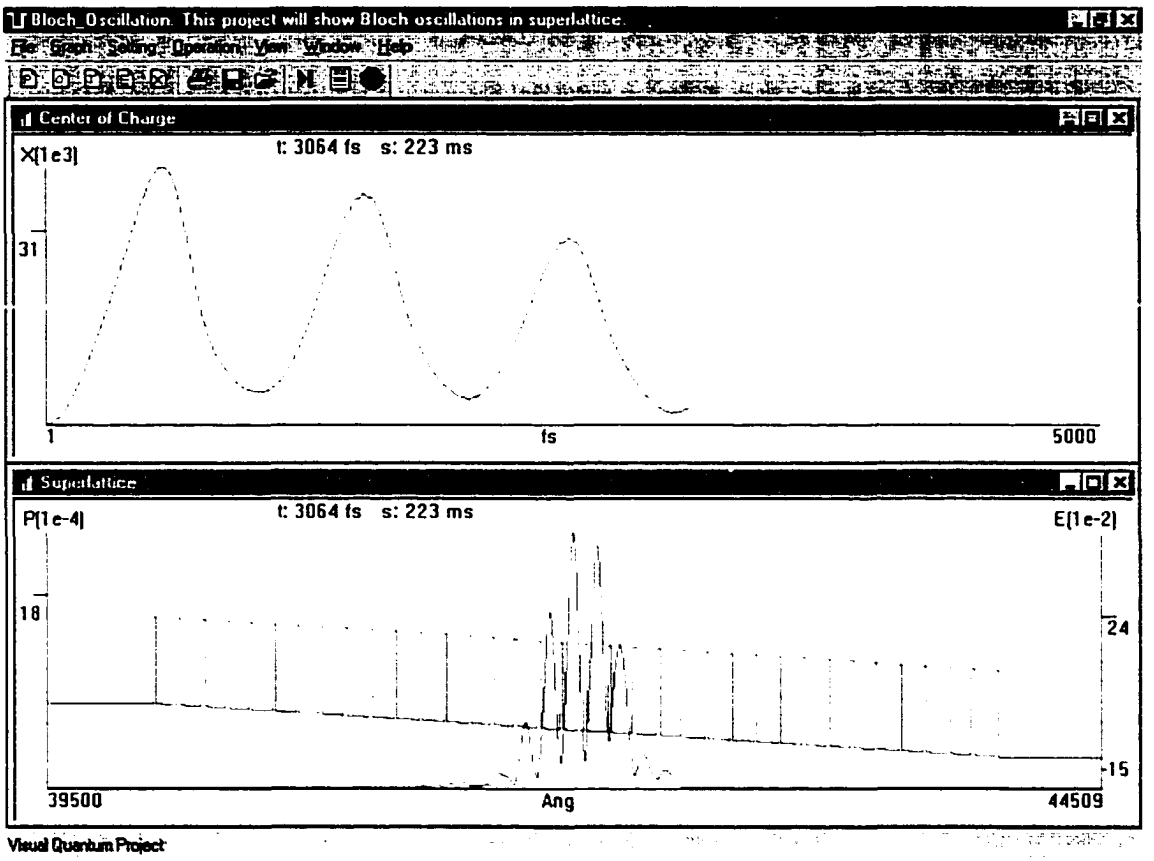

Fig. 4.17: The wavefunction and center of mass are shown in this tiled view after 3 Bloch oscillations.

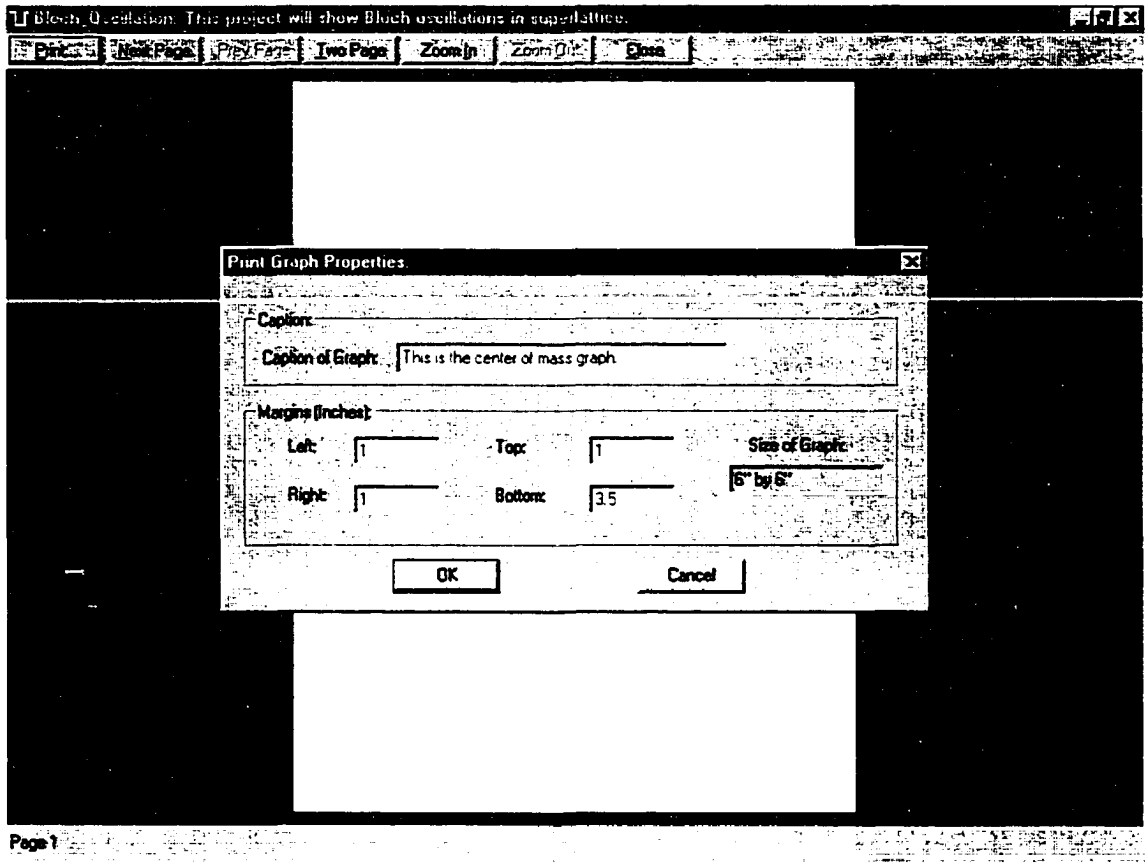

Fig. 4.18: The center of the mass is printed by entering the print properties.

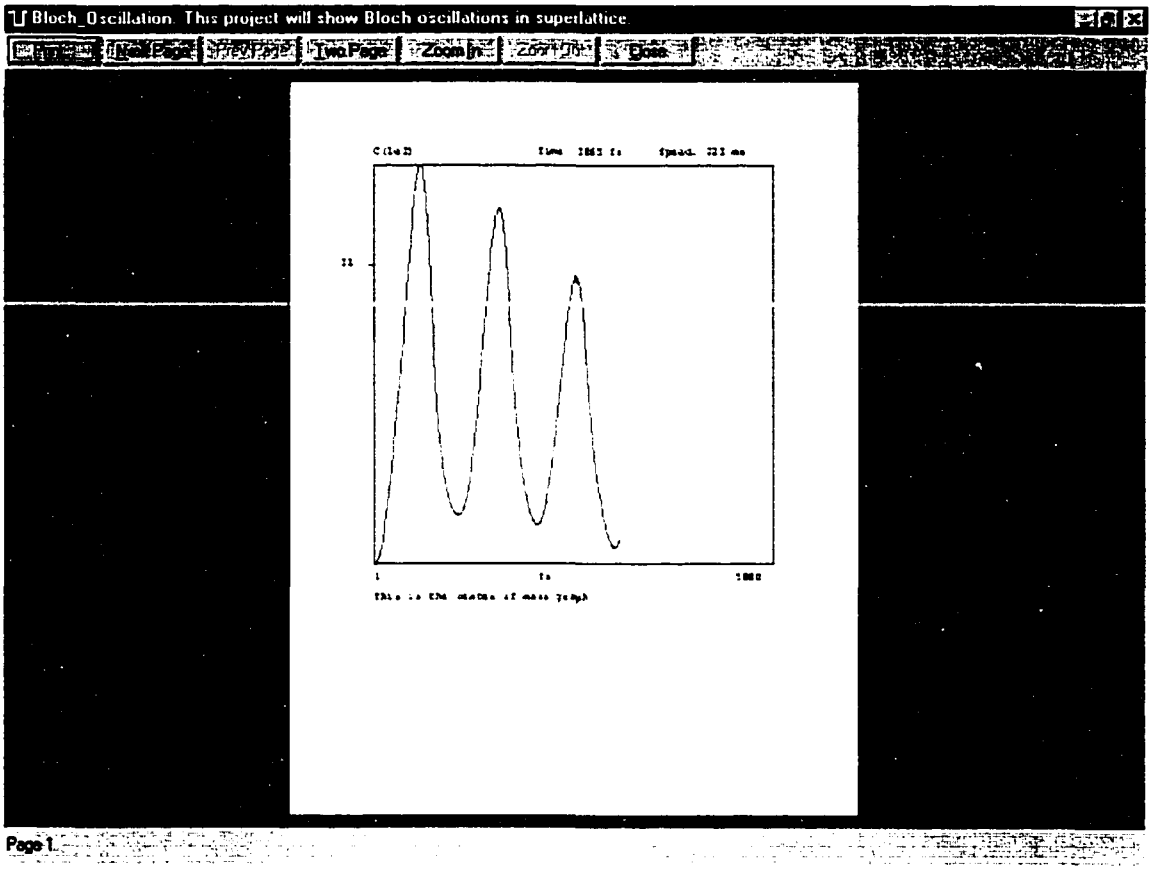

Fig. 4.19: Print preview window.

CHAPTER 5

ELECTRON-PHONON INTERACTION IN A SINGLE QUANTUM WELL

5.1 Introduction

A mixed three-quantum-state quantum mechanical model of a single quantum well under electron-phonon interaction will be used to study both electron capture and escape. The coupling of the three noncoherent states is based on the electron-phonon coupling constant. This model will be contrasted to others in terms of the information that can be obtained (capture and escape rates and electronic spectra, resonant energy, and density of states), as well as in terms of computational efficiency. The capture and escape rates are found to be strongly dependent on the number of eigenstates in the single quantum well. The effect of the interaction strength, or the electron-phonon coupling constant, on the electronic transport properties is linear for low values of interaction such that interaction energy is less than 1/100 of longitudinal-optical-phonon energy.

An understanding of electron - longitudinal-optical (LO)-phonon interaction in semiconductor nanostructures is important for determining the response of semiconductor devices. In quantum well (QW) lasers, the electron capture time determines the maximum modulation frequency. Meanwhile the escape time must be long enough for efficient light

emission through electron-hole recombination. The escape time also determines the maximum frequency of a quantum well infrared photodetector (QWIP). A numerical model of LO-phonons in the III-V GaAs/AlGaAs will be used to get the dynamics of an electron wavepacket.

The time-dependent Schrödinger equation (TDSE) must be used to get femtosecond dynamic behavior of electron wavepacket in semiconductor nanostructures. One of the first studies[1] solved the TDSE for the electron Hamiltonian without any interaction. Recently computers have become fast enough to consider scattering[2]. Here electron-phonon scattering will be considered with the electron being described by a one-dimensional (1D) system, in the z-axis. A thorough study of the different information that can be obtained from wavepacket analysis will form the body of this paper, as well as the advantages of this method over comparable methods.

5.2 Numerical Model

A mixed three-quantum-state system will be considered. The three states correspond to three different electronic wavefunctions, one corresponding to equilibrium population, and others to emission and absorption of one LO-phonon, respectively.

(5.1) $$\psi = \psi^0 \mid n > + \psi^1 \mid n-1 > + \psi^2 \mid n+1 > .$$

The coherence is maintained if the electrons remain in the initial channel. Decoherence sets in when significant leakage to the other channels has occurred. The effect of the electron phonon interaction is to transfer charge between the three electronic wavefunctions. The electron-phonon interaction Hamiltonian used is

$$H_{ep} = \hbar\omega\sqrt{g(z)}\left(a\exp(-i\omega t) + a^{+}\exp(i\omega t)\right). \quad (5.2)$$

where the lowering and raising operators are used. The exponential terms are the standard time development of these two operators. The spatially-dependent variable g(z) contains the spatial dependence of the phonon potential. The reason why the square root is used will become apparent when the Fermi golden rule (FGR) is used. The above treatment is a full quantum mechanical treatment as opposed to models just based on the FGR[3]. Thus the time dynamics from initial to final state can be found, how quickly dephasing is induced, and electronic density of states and energy spectra. The FGR requires knowledge of electronic density of states and the amplitude of transition matrix element between initial and final wavefunctions. The treatment of electronic resonances by this method have been questioned[4] because it cannot handle coherence-decoherence dynamics and overestimates the capture times. It should be noted that Monte Carlo calculations[5] employ the FGR-calculated probabilities. Monte Carlo methods may use the TDSE in the calculations, but become computationally extensive because of the large number of particles considered. Furthermore, there are several quantum mechanical plane-wave studies[6], where a mono energetic particle, or a plane wave, is studied. The assumption of mono energetic particle violates the uncertainty relationship thus giving unrealistic results. For example even though Reference 6 showed that the transmission coefficient changes from 0 to 1 at a electron-phonon resonance no matter how weak the dissipation, such results will not be obtained using a finite wavepacket with a range of energies. The use of time-dependent perturbation theory can also be used, but it cannot handle for all interaction strengths.

The function g(z) is the only variable in the interaction Hamiltonian and shall be called the electron-phonon coupling constant. The value of the interaction has been dealt with for semiconductor nanostructures[7,8,9,10] and how it related to the electron-phonon transition matrix. Several phonon modes in quantum structures have been found such as confined and interface. For confined phonons, g(z) is distributed within the QWs of a multiple quantum well structure. In the first approximation, it may be assumed to be distributed sinusoidally within the QW and zero at the interface. The amplitude of the distribution within the QW will be called the g-value and used in the rest of the paper. The interface phonons are exponentially decreasing from the interfaces. The relative importance of confined versus interface phonons increase with quantum well width[11]. A wide quantum well of 100 Angstroms is used in this study.

5.3 Capture and escape dynamics

A single quantum well (SQW) structure shown in Fig. 5.1 is studied. The variables are the electron-phonon coupling constant, g, and the confining potential, V. The variable, V, is varied from 25 meV to 350 meV. For a particular V within this range, there may be one, two, or three eigenstates within the SQW. If the electron kinetic energy is fixed at E_i = 24 meV as V is varied, the electron may resonantly emit a phonon leading to electron capture if the highest state is approximately one LO-phonon energy from E_i (where the slight shift is due to renormalization by electron-phonon interaction). The SQW is not biased (representing the intrinsic region) and the energetic particles are due to laser excitation or doped regions far from the SQW. In Fig. 5.2, the temporal dynamics

of an electronic wavepacket for a fixed g and V, are shown for three different times. In Fig. 5.2(a), the wavepacket has moved by 30 nm in the region to left of SQW corresponding to time t = 50 fs. The maximum captured charge in the SQW is shown in Fig. 5.2(b) for a time t of 1445 fs. The charge after significant escape, at time t = 4000 fs, is shown in Fig. 5.2(c) where there is a spike indicating the trapped charge in SQW. The Fourier spectra of Fig. 5.2(c) is shown in Fig. 5.3 for the transmitted wavefunction. The depression in the spectra from 20 to 30 meV, from the incident spectra, is at energy of 23.8 meV corresponding to the resonant electron energy. There is also a small component near 60 meV corresponding to phonon absorption. For a g-value of 0.05, the temporal dynamics of the ratio of captured charge in SQW to incident, capture probability, are shown for three V-values. These V-values correspond to one, two, or three states in SQW and the incident electron central energy being one LO-phonon energy above the highest resonant state. These particular V-values are found from analysis of capture probability vs. V-value for two times, one just after maximum capture and another one after significant escape in Fig. 5.5. It is seen why we pick the three V-values in the Fig. 5.4. From this diagram, the capture probability is greatest for V = 25 meV as well as the escape rate. This means that both trapping and escaping are faster if there is only one eigenstate in SQW. However, for most GaAs/$Al_xGa_{1-x}As$ structures where x greater than 0.25, the V value will be likely be greater than 250 meV corresponding to V = 265 meV case.

In Fig. 5.6, the temporal dynamics showing capture and escape are shown for different g-values for a fixed V-value of 25 meV, corresponding to first resonant eigenstate. The case of no interaction is shown by dashed line. It is a symmetric curve

with respect to a time of 1 ps. The original wavefunction (at time t = 0) is centered 3000 Angstroms from SQW. An electron with an energy of 24 meV will travel this distance in around 1 ps. The capture time can be defined as the difference between the time that the charge is maximum with reference to maximum charge for g = 0 case. This definition is consistent for g greater 0.02. For g = 0.01, the second maxima must be used as shown by visual inspection of the wavefunction. The escape time is the proportional to the slope of the tail end representing the escape process. The escape time corresponds to the best exponential fit and that is the reason the captured charge is shown logarithmally. The capture and escape times of Fig. 5.6 are shown in Fig. 5.7. The capture time, for these g-values, is a linearly decreasing line. The escape time meanwhile is proportional to the reciprocal of the g-value. We shall look in detail at both processes.

The resonant electron energies can be found from Fig. 5.8 where the maximum capture probability is shown as a function of electron energy. All resonant energies for the 10 nonzero g-values are near 24 meV for a V-value of 25 meV. In fact for g = 0.05, the maximum captured charge is at energy of 23.7 meV, which is only 0.1 meV different from the value obtained in Fig. 5.3. All the resonant energies are shown in Fig. 5.9, which shows the blue shift for increasing g-values.

The above showed that the different properties are linearly increasing with g-values. However in Fig. 5.10, the maximum captured probability, is shown as a function of g-values with g ranging from 0.01 to 0.5. It slows that the linear range extends till g = 0.1. Because of the square root dependence, this corresponds to interaction energy of 0.01 of LO-phonon energy. Above this g-value, the escape process is so efficient that charge is not being trapped and thus the resonance character of these states is lost.

The escape times for the Fig. 5.4 will now be examined in greater detail using the FGR. The escape times for the structure with one, two, and three eigenstates are 800 fs, 1859 fs, and 2098 fs. The escape rate can be found from the FGR provided the exact interaction Hamiltonian in known. A bound electron absorbs a phonon and the final state is 24 meV. The absorption can be written as

$$\Gamma^{(a)} = \frac{2\pi}{\hbar}\hbar^2\omega^2 g N_q \mathrm{dos}(24\ \mathrm{meV}). \tag{5.3}$$

The scattering time can be written as

$$\tau = \frac{1}{\hbar\omega^2 g}\left[\frac{1}{N_q \mathrm{dos}(24\ \mathrm{meV})}\right]. \tag{5.4}$$

which shows the 1/g dependence for a fixed energy.

The density of states at 24 meV has a mixture of 2D and 3D characters. If we let τ be 800 fs, the density of states at 24 meV can be found. For scattering times of 1859 fs and 2098 fs, the above formulas cannot be used because the time to go from ground to highest state must be accounted for. Furthermore, we do not know what is the appropriate length that must be used in calculating the density of states. An advantage of a direct method using Schrödinger equation is that confinement can be properly accounted for.

5.4 Conclusion

In conclusion, we have studied electron wavepacket dynamics in a SQW under electron-LO-phonon interaction. We can gain much information about the rates and electronic properties of the quantum nanostructure. This model is noted for its numerical

efficiency. The most common boundary conditions for quantum-mechanical wavepacket calculations is hard boundaries far away from device and the device typically takes only 1 percent of the total system. If there are N spatial divisions, then a matrix 3N by 3N must be solved. We have a sparse matrix with a band of 7 terms per row. The electron Hamiltonian induces terms in principal diagonal and terms to the left and right of the diagonal. Its an uncoupled problem, except in the middle region of device (where all 7 terms in row may be nonzero); thus the solution is approximately three N by N matrixes. For the interior points, corresponding to system, the algebraic equations must be solved with different time-dependent boundary conditions.

We studied electron transport as the depth of the SQW increased and for different electron-phonon interaction strengths. There is one resonant state, where capture takes place, if the electron energy is approximately one LO-phonon energy above the topmost eigenstate. The capture and escape rates are strongly dependent on the number of eigenstates in SQW. The electron-phonon interaction linearly affects electronic properties for low interaction strengths, *i.e.*, the maximum capture probability does not increase indefinitely with g-value but shows a strong nonlinear behavior. The capture time is linearly decreasing for small g-values while the escape rate is increasing for *all* g-values. The escape rate is inversely proportional to the g-constant as verified by using the Fermi golden rule.

5.5 References

1. A. Goldberg, H. M. Schey, and J. L. Schwartz, Am. J. Phys. **35**, 177 (1967).
2. Jon J. V. Maestri, R. H. Landau and M. J. Páez, Am. J. Phys. **68**, 1113 (2000).
3. J. A. Brum and G. Bastard, Phys. Rev. B **33**, 1420 (1986).
4. L. F. Register and K. Hess, Appl. Phys. Lett. **71**, 1222 (1997).
5. G. C. Crow and R. A. Abram, Semicond. Sci. Technol. **14**, 1 (1999).
6. W. Cai, P. Hu, T. F. Zheng, B. Yudanin and M. Lax, Phys. Rev. B **41**, 3513 (1990).
7. L. Wendler and R. Pechstedt, Phys. Stat. Sol. (b) **141**, 129 (1987).
8. L. Wendler and R. Haupt, Phys. Stat. Sol. (b) **143**, 487 (1987).
9. B. K. Ridley, J. Phys. C: Solid State Phys. **15**, 5899 (1982).
10. L. Wendler, Phys. Stat. Sol. (b) **129**, 513 (1985).
11. D. Y. Oberli, G. Böhm and G. Weimann, Phys. Rev. B **47**, 7630 (1993).

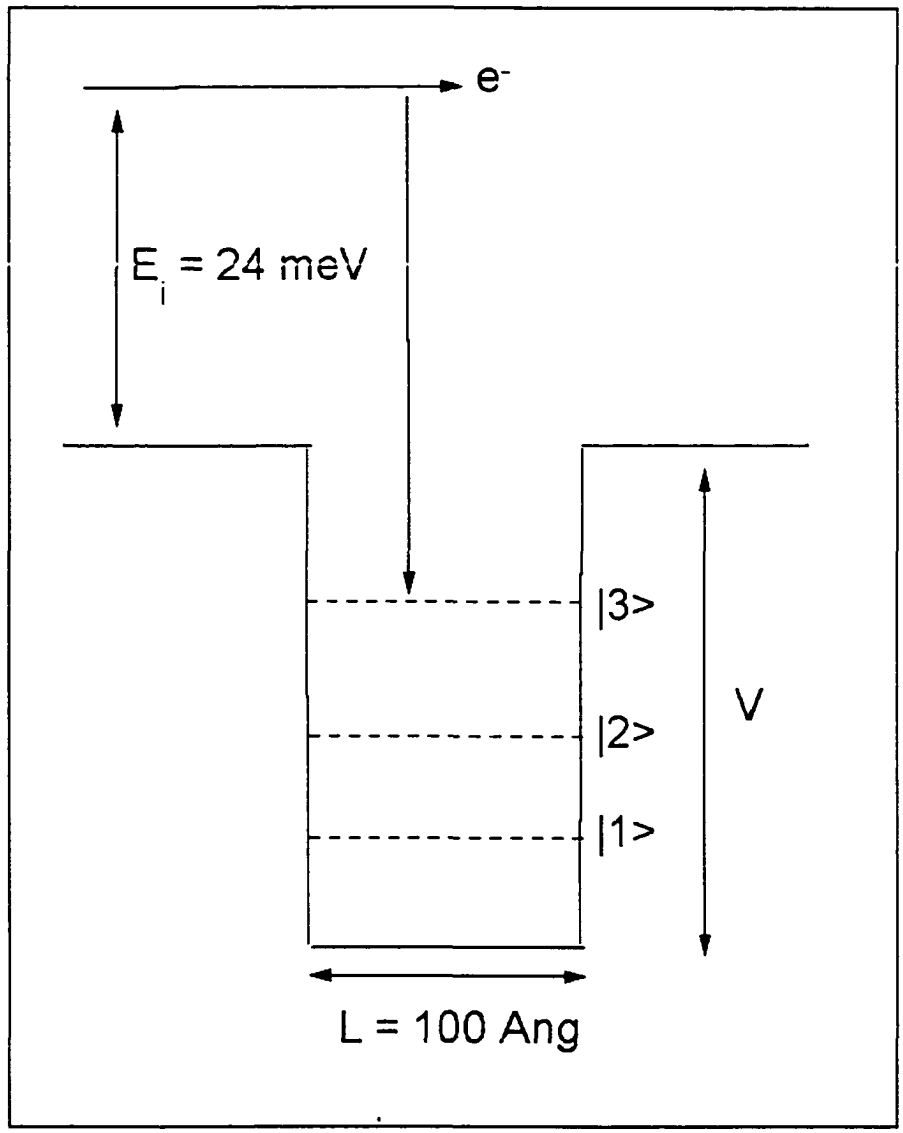

Fig. 5.1: An electron at energy 24 meV resonantly emits a phonon leading to capture of electron by a SQW of depth V.

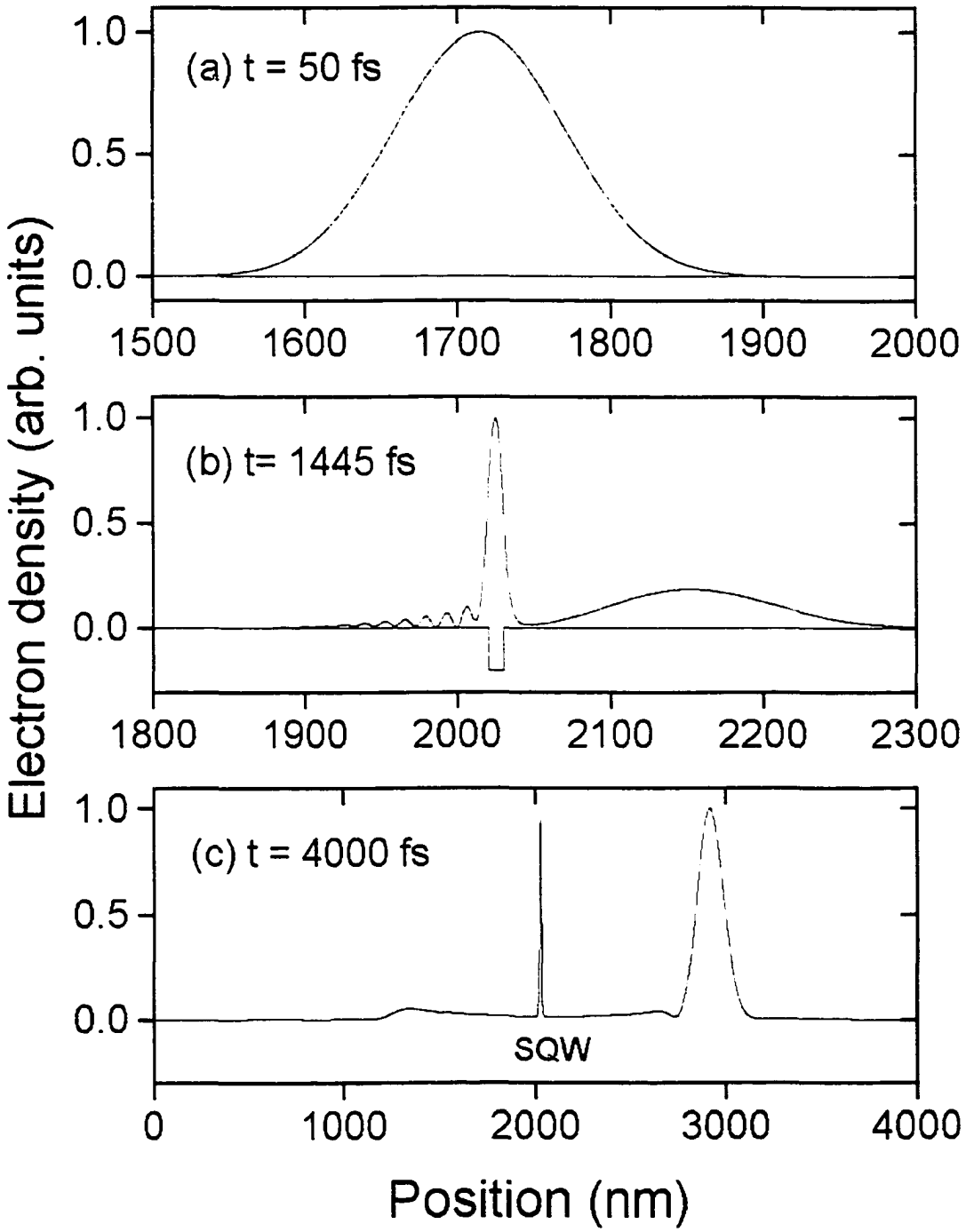

Fig. 5.2: The spatial variation of carrier density in a SQW for V = 25 meV and g = 0.05 at (a) t = 50 fs, (b) t = 1445 fs and (c) t = 4000 fs.

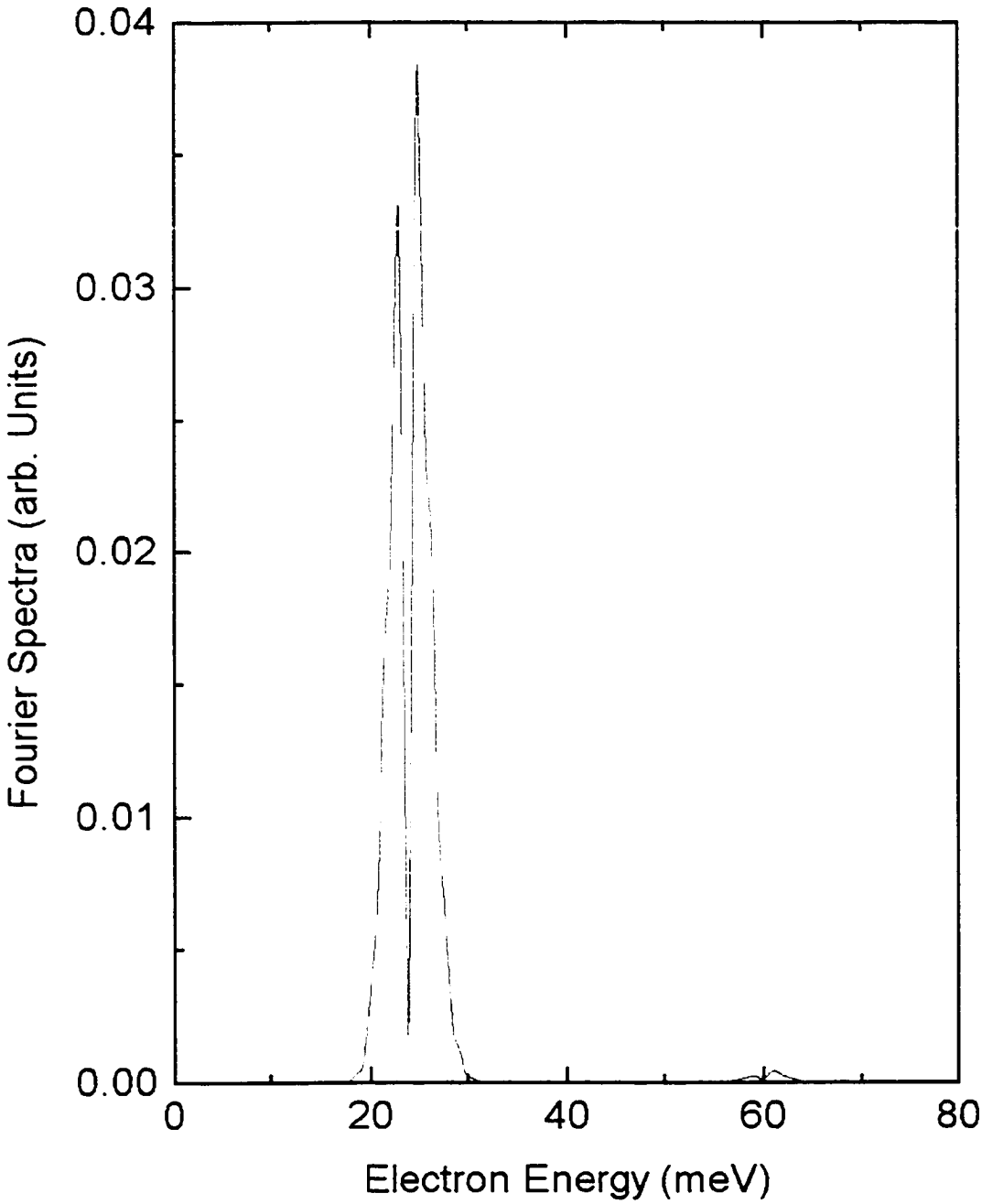

Fig. 5.3: The Fourier spectra of transmitted wavefunction (at t = 4000 fs) for V = 25 meV and g = 0.05. There is attenuation at a resonant electron energy of 23.8 meV, as compared to incident, with a small absorption component near 60 meV.

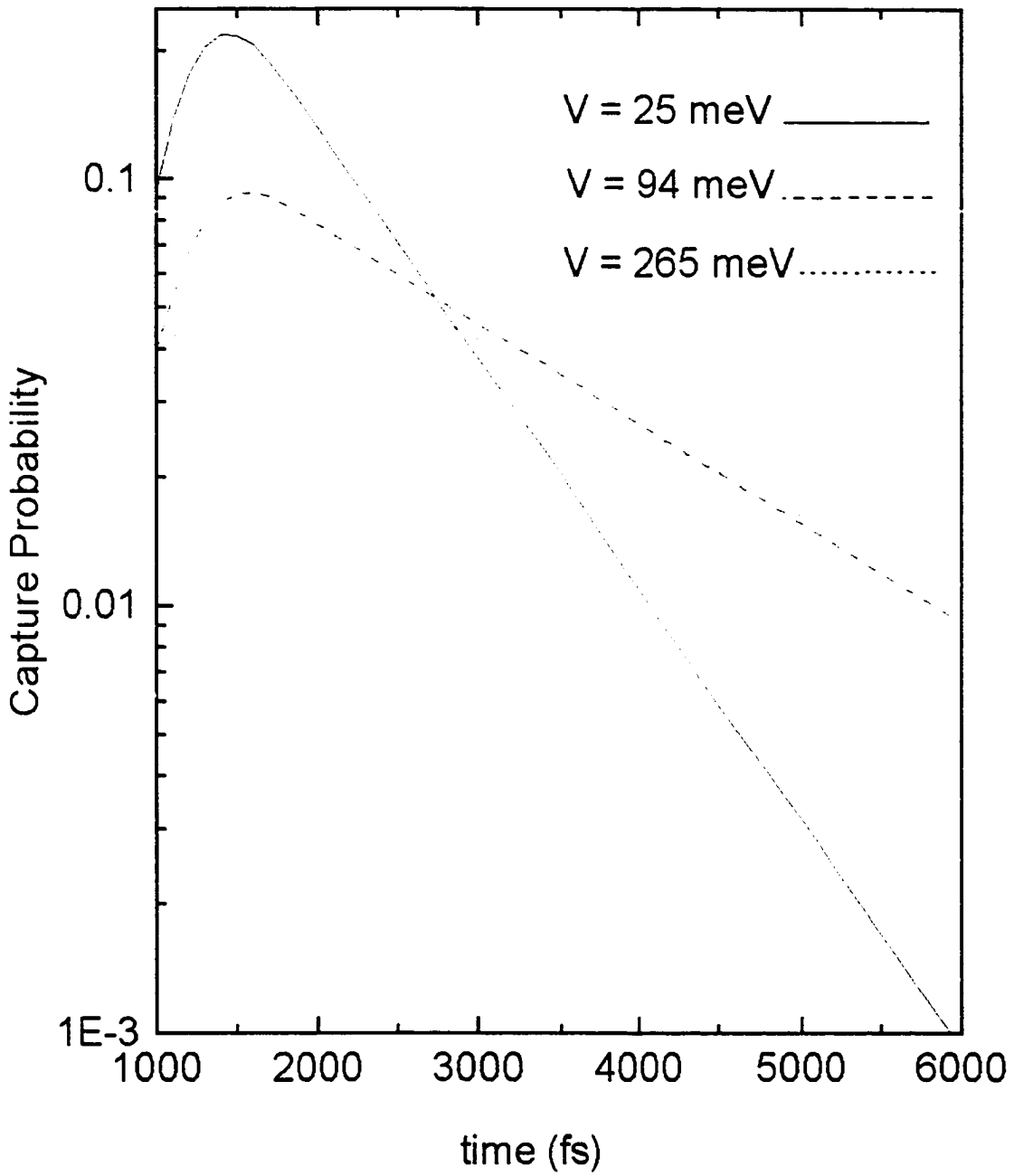

Fig. 5.4: The temporal dynamics of captured electron density for resonance conditions with the three states for g = 0.05. showing electron capture and escape.

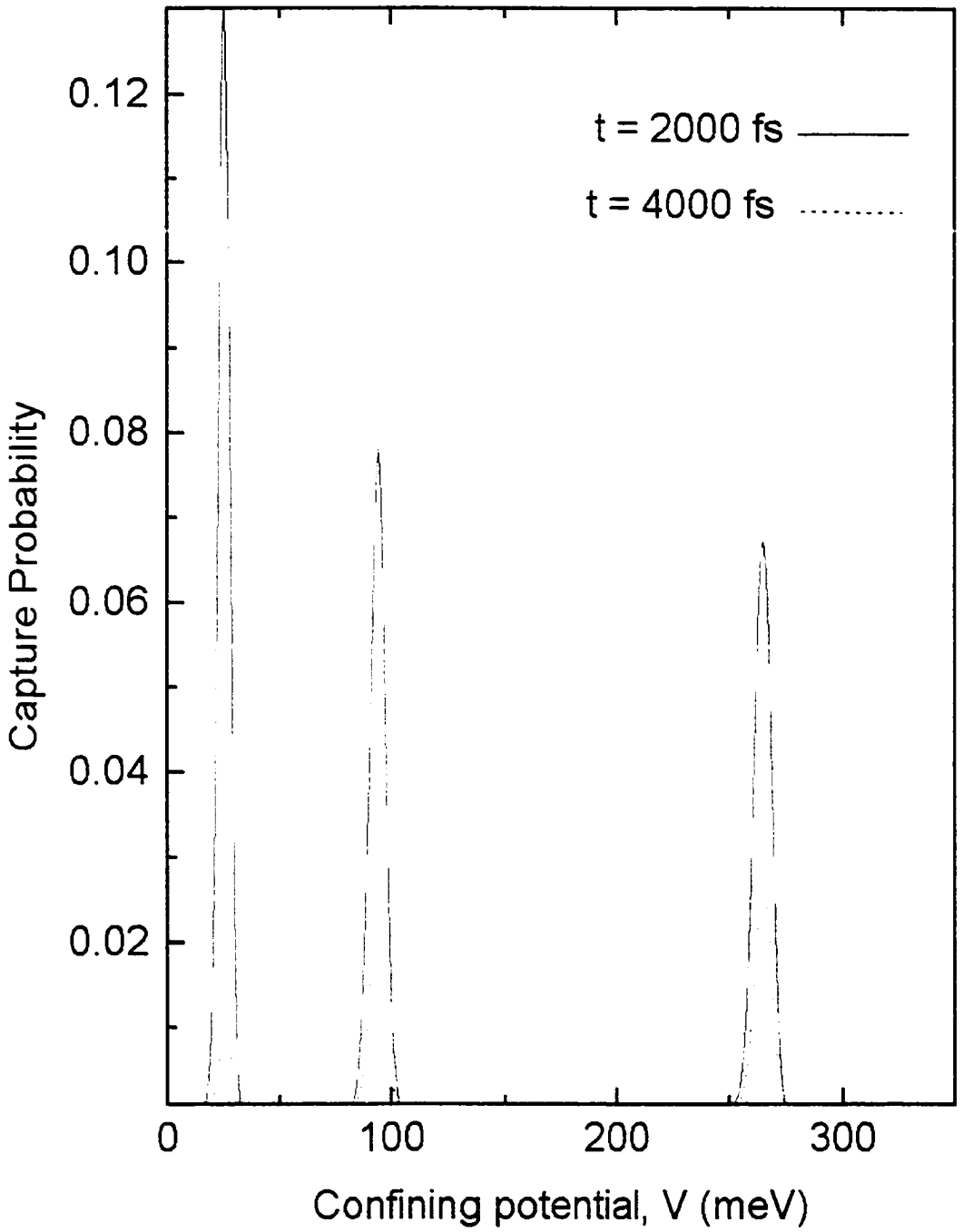

Fig. 5.5: The temporal dynamics of charge escaping due to LO phonon absorption for different confining potentials for g = 0.05.

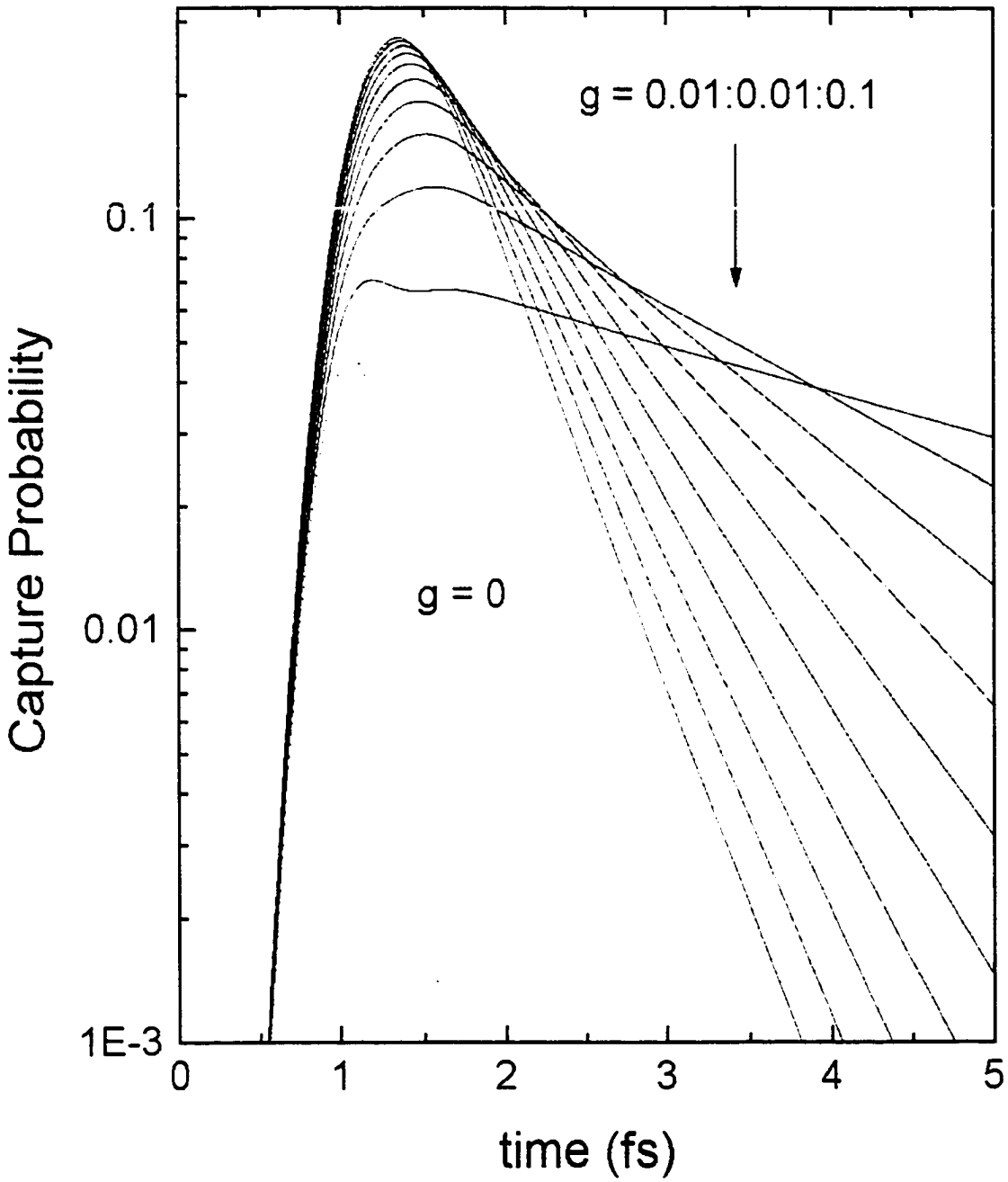

Fig. 5.6: The temporal dynamics for V = 25 meV and different interaction strengths from g = 0 to 0.1.

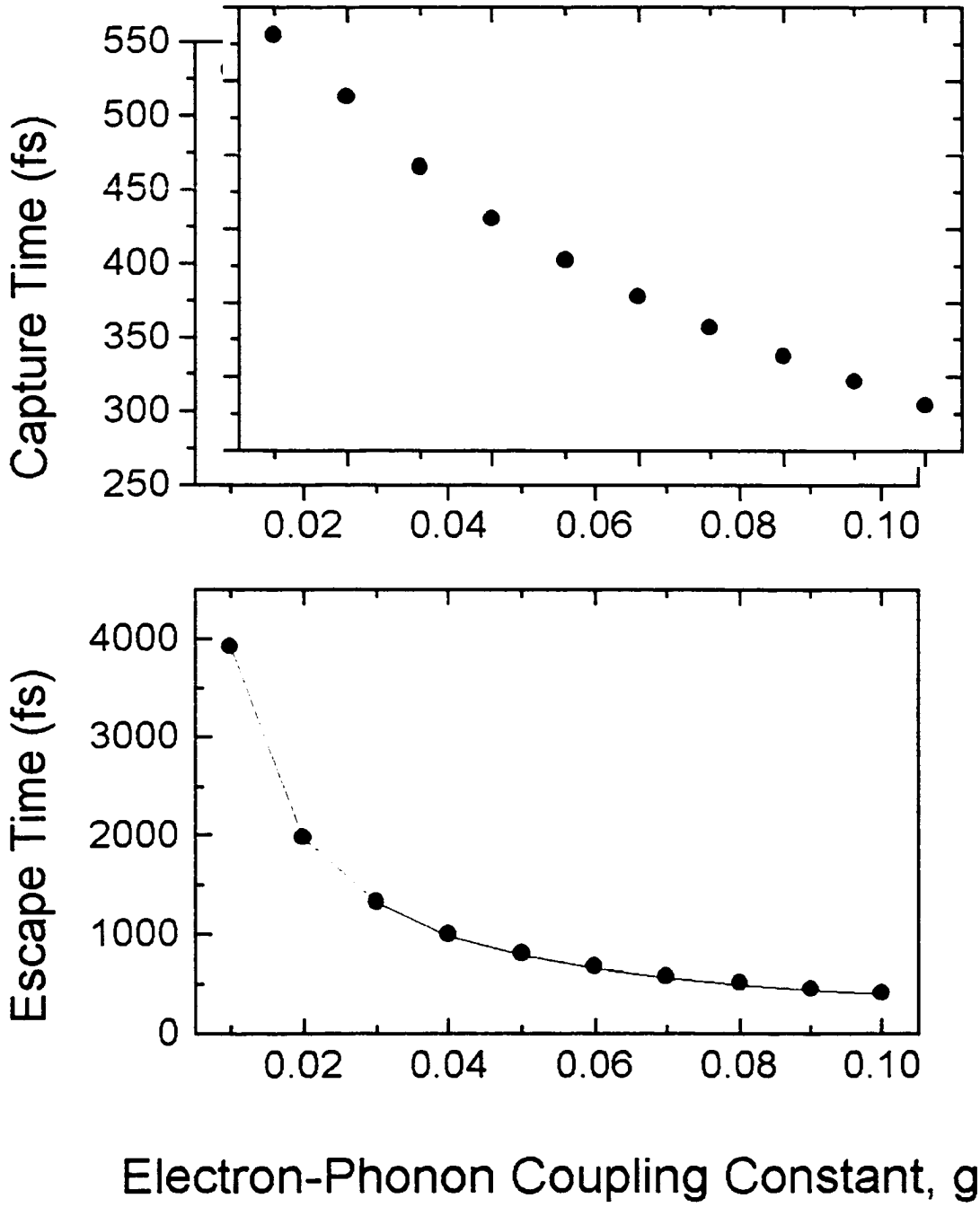

Fig. 5.7: Circles are calculated times for (a) capture and (b) escape. In (b). the solid curve is a fit using the expression of 40/g.

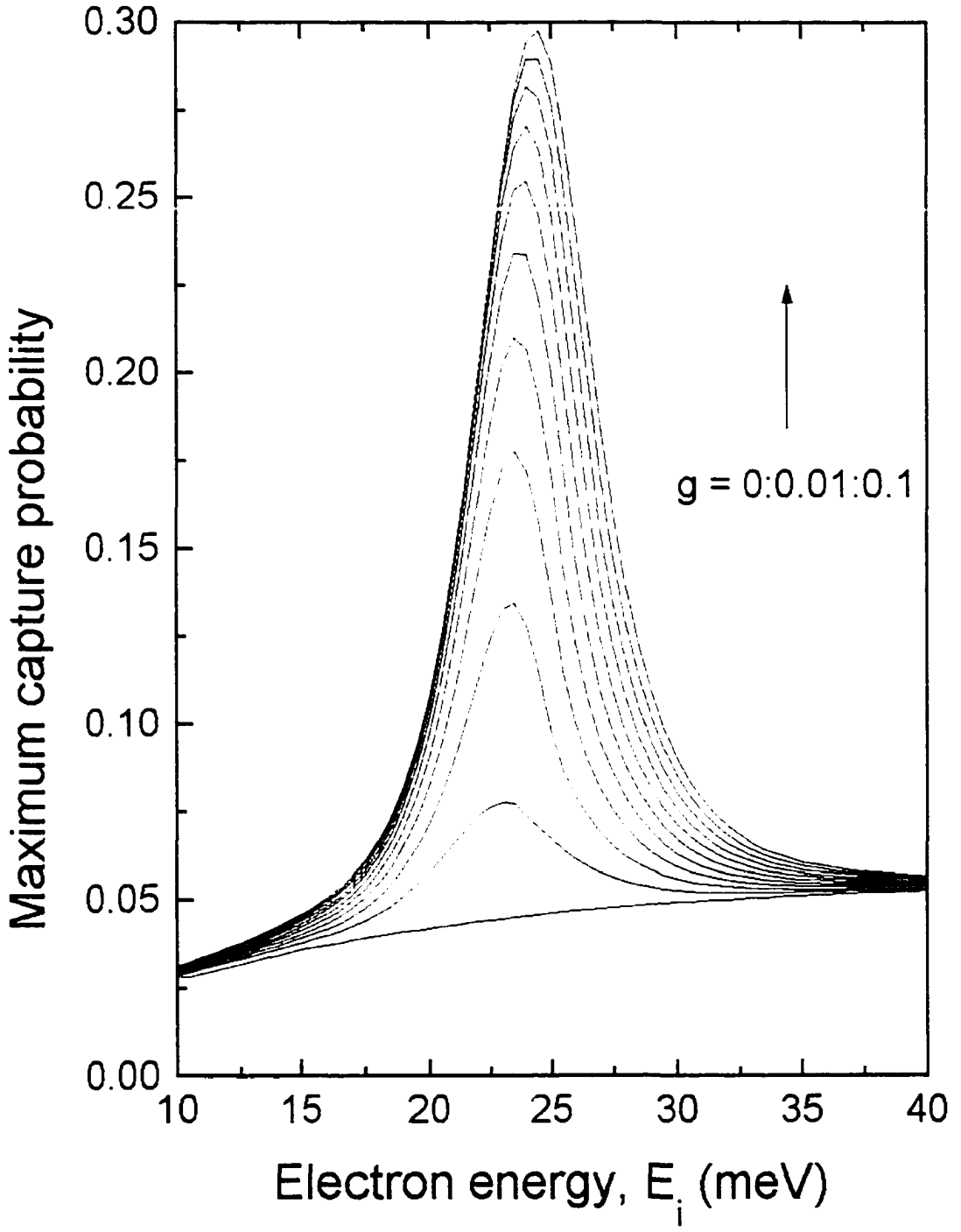

Fig. 5.8: Varying the electron energy, the resonant energy near 24 meV can be found for V = 25 meV and different interaction strengths from g = 0 to 0.1.

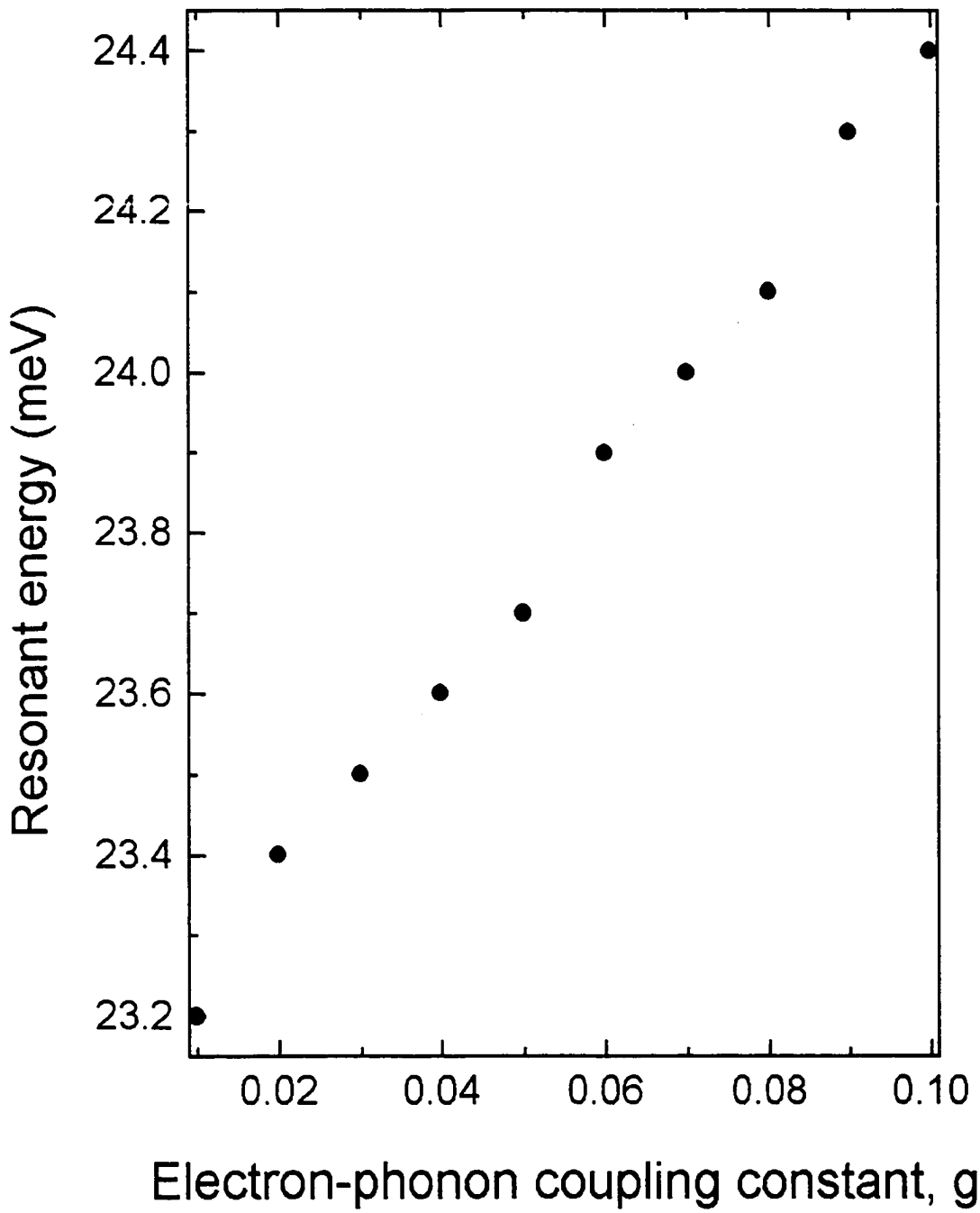

Fig. 5.9: The resonant energy is blue shifted for V = 25 meV with increasing electron-phonon interaction for small g-values.

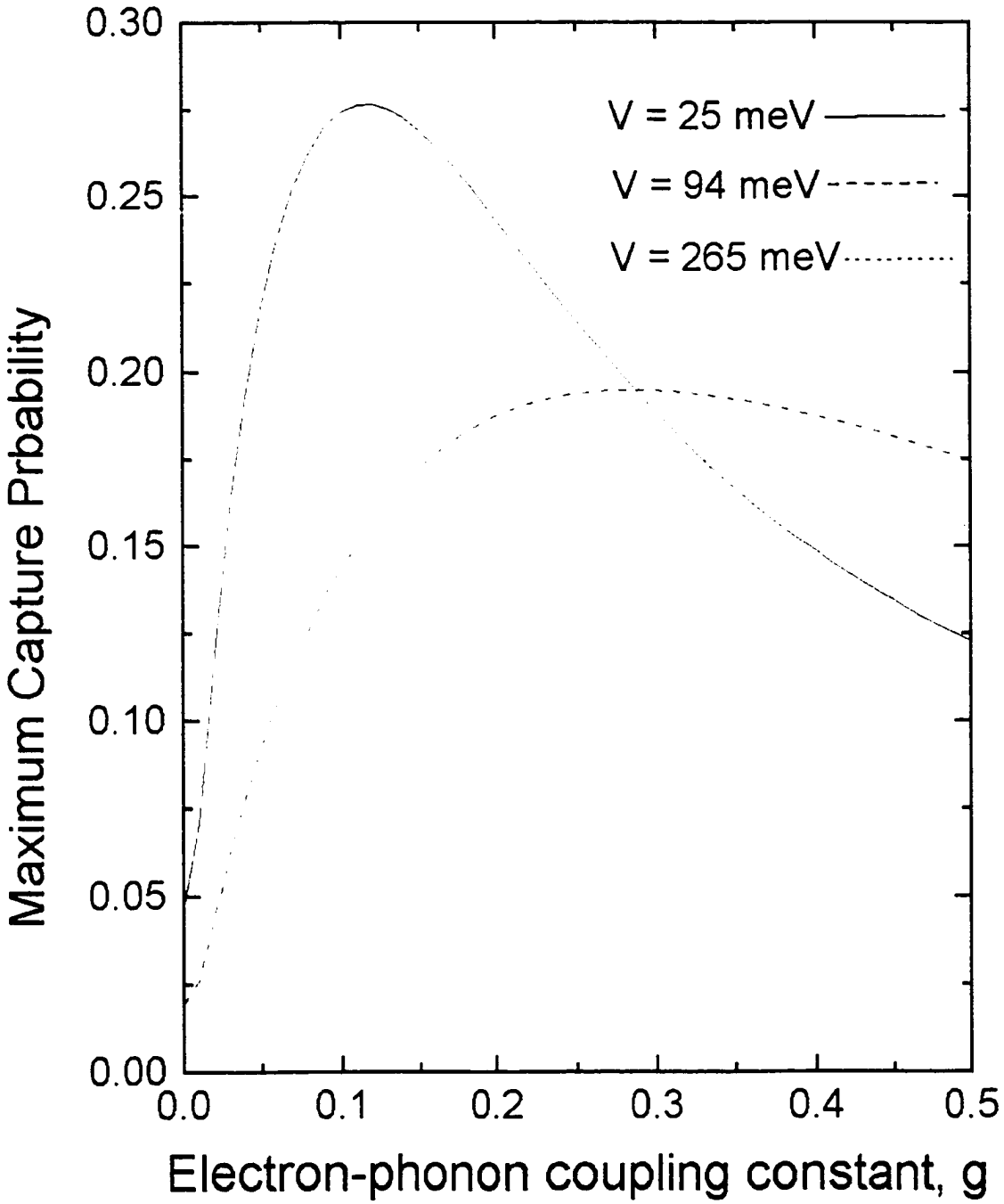

Fig. 5.10: The ratio of maximum captured electron probability in the SQW is a nonlinear function of the strength of interaction.

CHAPTER 6

BLOCH OSCILLATIONS IN SEMICONDUCTOR SUPERLATTICES

6.1 Introduction

The dephasing of electrons in biased semiconductor superlattices, due to LO-phonon emission, suppresses Bloch oscillations and is responsible for the oscillations due to negative differential velocity. We numerically solve the time-dependent Schrödinger equation with electron - LO-phonon interaction to study these related processes using a coupled set of three noncoherent quantum states. The scattering time shows an oscillating feature as the electric field increases with a period related to the bandwidth of the superlattice. The effective electric-field bandwidth increases linearly with increasing electric field. Further the electron energy corresponding to the oscillations is around 8.7% of the Wannier Stark ladder level at room temperature. The beating of unequal Wannier Stark ladders explains the rapid dephasing of the Bloch oscillations.

In the absence of scattering, Bloch electrons in semiconductor superlattices (SL) undergo Bloch oscillations with a time period h/eFd and spatial amplitude Δ/eF, where d is the period of superlattice, F is the electric field and Δ is the ground state bandwidth. Interface roughness dominates the scattering for low temperatures[1]. It is theoretically predicted this holds for the miniband widths smaller than the LO-phonon energy, at least

for low temperatures[2]. At high temperatures, polar optical phonon scattering becomes the most important scattering mechanism[3] in GaAs/$Al_xGa_{1-x}As$ heterostructures.

Negative differential velocity (NDV) in SL was considered by Esaki and Tsu as early as 1971[4]. Esaki and Chang observed oscillations in *I-V* curves[5] and attributed them to electric field domain (EFD) formation. Much progress in SL had to await the introduction of advanced growth technique of molecular beam epitaxy (MBE) and the first reported observation of Wannier Stark ladder (WSL)[6]. It is now believed that WSL and NDV are based on the same phenomena[7]. Electric field domains (EFD) are assumed to form in one well as the electric field induced a bias between wells greater than the minibandwidth of the superlattice. This would correspond to decreased tunneling and a region of NDV. There were a number of such regions equal to the number of quantum wells and thus there would be seen a number of oscillations. We instead consider the case where the electron loses energy to the phonon field so resonant tunneling exists for all electric fields and EFDs are not created or propagated in the simulation. However, in experiment, instabilities might exist that cause EFDs to form.

The dephasing due to LO phonons will be considered in this paper using a single-particle picture. Actually, Bloch oscillations are affected greatly by excitons and hole motion should be included. The excitons affect the spacing of the Wannier-Stark ladders via Coulomb field and lead to rapid dephasing[8]. Time-resolved study of Bloch oscillations by transient Four-Wave Mixing (FWM)[9] and Terahertz emission spectroscopy[10] measure the exciton decay. The influence of excitonic effects increases if the bandwidth is comparable to exciton binding energy[11]. In most cases, the bandwidth is much larger than the exciton binding energy of 5-10 meV. However the single-particle-

picture. with the hole localized. is still useful because of numerical complexity of the full two-body problem. Furthermore. it leads to insights not apparent from the two-body picture.

6.2 Electron-phonon model

The effect of electric field is to increase electron-phonon scattering by increasing carrier kinetic energy. This problem was originally analyzed in the study of electric breakdown[12,13,14] where the authors argued the scattering should increase logarithmically with the electric field. The confinement of phonons in 2D quantum structures has been actively studied[15]. It has been found that the dielectric continuum model is suitable for devices with wide QWs[16]. The electron phonon coupling function of a single electron to the long-wavelength optical phonons of mode j in a multilayer semiconductor nanostructure is[17]

$$\Gamma_j(q_\parallel, z) = -\frac{i}{q}\left(\frac{\varepsilon_0 e^2 \hbar}{2A\omega_j(q_\parallel)}\right)^{1/2} E^j(q_\parallel, z). \tag{6.1}$$

with the electron-phonon Hamiltonian being

$$H_{ep} = \sum_j \sum_{q_\parallel} e^{iq_\parallel r_\parallel} \Gamma_j(q_\parallel, z)(a(q_\parallel) + a^+(-q_\parallel)). \tag{6.2}$$

Using the long wavelength approximation ($q_\parallel \approx 0$). the above can be simplified

$$H_{ep} = \sum_j \Gamma_j(q_\parallel, z)(a + a^+). \tag{6.3}$$

Defining an electron-phonon coupling constant g(z) such that

$$\hbar\omega\sqrt{g(z)} = \sum_j \Gamma_j(q_\parallel, z). \tag{6.4}$$

the electron phonon interaction Hamiltonian can be written as

$$H_{e-p} = \hbar\omega\sqrt{g(z)}\left(ae^{-i\omega t} + a^{+}e^{i\omega t}\right). \tag{6.5}$$

The function g(z) is supposed to be a sum over interface and confined modes and can be related to the electron-phonon scattering matrix. The Fröhlich Hamiltonian is

$$H_{ep} = \sum_{q} M_q\left(a_q^{+}e^{iq\cdot r-i\omega t} + a_q^{-}e^{-iq\cdot r-i\omega t}\right), \tag{6.6}$$

and thus the g-value[18] is

$$g = \sum_{q}\left(\frac{|M_q|}{\hbar\omega}\right)^2. \tag{6.7}$$

We solve the time dependent Schrödinger equation (TDSE) in one dimension (1D), say z-axis, because of limited computation time. Thus scattering in x and y-directions is forbidden. By calculating the scattering matrix using 1D electron density of states we arrive at a value of g = 9 for a small electron energy, 0.5 meV, corresponding to a small net velocity of the motion of wavepacket in response to electric field. To simplify analysis only confined phonons are considered with boundary conditions that g(z) is zero at the interfaces and is sinusoidally distributed within each QW with the amplitude given by the g-value in Eq. (7). The relative importance of confined phonons versus interface phonons increases with quantum well width[19]. It is also predicted that the role of interface phonons can be suppressed in a SL[20].

The total Hamiltonian can be written as

$$H = H_e + \hbar\omega\sqrt{g(z)}\left(ae^{-i\omega t} + a^{+}e^{i\omega t}\right). \tag{6.8}$$

where H_e is the electron Hamiltonian and g(z) is the electron-phonon coupling constant. The electrons are assumed to be free in x and y directions and confined in the z-direction (along the layers). Thus H_e can be expressed as

$$H_e = \frac{\hbar^2}{2}\frac{\partial}{\partial z}\frac{1}{m^*(z)}\frac{\partial}{\partial z} + V_0(z) + eV_a . \tag{6.9}$$

where $V_0(z)$ is the potential profile of the selected quantum well, V_a is the applied potential and $m^*(z)$ is the position dependent electron effective mass.

A wavefunction with three components, corresponding to phonon states, will be used. The interaction between the three phonon states is assumed to be harmonic. The three phonon states are $|n>$, $|n-1>$, and $|n+1>$ differing in population as indicated with n being the equilibrium population with a population $n = [\exp(\hbar\omega / k_B T) + 1]^{-1}$. If more states were considered in the linear combination, multi-phonon absorption and emission can be considered. Electronic states are coupled to the phonon states as

$$|\psi> = \psi^{(0)}|n> + \psi^{(1)}|n-1> + \psi^{(2)}|n+1> . \tag{6.10}$$

The three electronic states are governed by the electron Hamiltonian. The three phonon states follow the standard harmonic equations with additional constraints due to fact only one-phonon absorption or emission can occur.

$$a|n> = \sqrt{n}\,|n-1> \qquad a^*|n> = \sqrt{n+1}\,|n+1> . \tag{6.11a}$$

$$a|n+1> = \sqrt{n+1}\,|n> . \qquad a^*|n+1> = 0 . \tag{6.11b}$$

$$a|n-1> = 0 \qquad a^*|n-1> = \sqrt{n}\,|n> . \tag{6.11c}$$

These equations have to changed appropriately for multi-phonon emission and absorption.

The resulting time-dependent Schrödinger equation, using orthogonality of the phonon states, is

$$(6.12)\quad i\hbar\frac{\partial}{\partial t}\begin{bmatrix}\psi^{(0)}\\ \psi^{(1)}\\ \psi^{(2)}\end{bmatrix}=\begin{bmatrix}H_e & \hbar\omega\sqrt{g(z)n}e^{i\omega t} & \hbar\omega\sqrt{g(z)(n+1)}e^{-i\omega t}\\ \hbar\omega\sqrt{g(z)n}e^{-i\omega t} & H_e & 0\\ \hbar\omega g\sqrt{g(z)(n+1)}e^{i\omega t} & 0 & H_e\end{bmatrix}\begin{bmatrix}\psi^{(0)}\\ \psi^{(1)}\\ \psi^{(2)}\end{bmatrix}.$$

This equation was discretized using a fast algorithm, and solved on a Pentium II processor with an initial electron wave packet inside a superlattice structure with zero initial kinetic energy.

6.3 Results

The superlattice is a 35 period superlattice with a quantum-well width of 97 Å and a barrier width of 17 Å of $GaAs/Al_{0.3}Ga_{0.7}As$ materials. This structure has been actively studied to view Bloch oscillations[21]. The effective mass is 0.067 electron mass in the quantum well and 0.092 electron mass in the barrier. The potential energy discontinuity at the interfaces is 243 meV. A spatial amplitude of 5 times the quantum well, or 481 Å, is predicted for a voltage of 0.15 volt applied over the semiconductor superlattice according to the semiclassical equation of Δ/eF. The bandwidth is around 18 meV and is less than the phonon energy of 36 meV as can be seen from Fig. 6.1 in which we plot both the eigenenergies for the finite structure and the infinite structure using Kronig-Penney model. In Fig. 6.2, the center of mass of the wavefunction, for the case of no interaction, is shown as a function of time, and two times corresponding to wavefunction being either at left or right-extrema are noted. In Fig. 6.3, the wavefunctions at these two times are depicted.

Figs. 6.4 and 6.5 are similar to the previous figures except here we have interaction with g = 9. The large leakage at the rightmost point should be noted and is due to escape mediated by phonon absorption. In Fig. 6.6, we show the temperature dependence of the confined phonons for temperatures between 5 and 300 K for an applied bias of 0.15 volt. The scattering time is defined here as the e^{-1} time of the damping of the modulation of the center of mass. An electron LO-phonon scattering time of 250 fs is usually given in literature for room temperature and which is range above[22].

In Fig. 6.7, the scattering time is shown as a function of applied bias. We can see an oscillating feature. It is seen that the period of the oscillating component is about 13 millivolts. The electron energy corresponding to the period is eV_p = 13 meV. This is less than the bandwidth of the first band. Thus electrons are scattered when they enter the negative effective mass region by LO phonons to k = 0. The inset shows that the period greatly changes as a function of applied bias. Thus for a constant voltage of 150 millivolts across the surface, the Wannier-Stark Ladder (WSL) spacing (eFd) is 150/35 or 4.268 millivolts. Thus the spread in WSL is 13/35 or 0.371 millivolts, which is 8.7% of the original spacing. Since the beats of the different equally-spaced ladders leads to Bloch Oscillations in the Quantum Mechanical picture, LO-phonon interaction leads to the change in spacing between the levels and the rapid dephasing. According to Ref. 4, the minimum electric field to observe WSL is $eF_{min}d = \hbar/\tau$. Because τ is between 3.25 ps and 0.25 ps in Fig. 6.7, this corresponds to a corresponding minimum WSL spacing of between 0.2 meV and 2.63 meV. Thus for a field of 0.15 V, with a corresponding to a WSL spacing of 4.268 meV, we should be able to observe Bloch oscillations.

6.4 Conclusion

In conclusion, Bloch electron scattering via LO-phonon interaction is studied by solving the time-dependent Schrödinger equation using a coupled set of 3 noncoherent quantum states to find how the Wannier Stark ladders are changed with interaction and lead to onset of negative differential velocity. Bloch oscillations are hard to observe since they need coherent dynamics with large scattering times. At low temperatures, up to 15 oscillations have been observed. However, the situation deteriorates with high temperatures where LO-phonon emission dominates. Here only one Bloch oscillation can be seen since the scattering time is similar to the Bloch period. It is seen that the main mechanism seems to be that the spacing of WSL are not equal leading to beats of slightly different frequency, rather than a single frequency. This is shown by the periodic modulation, with a period V_p, in scattering time versus applied bias. The electron energy, eV_p, corresponds to electrons entering the negative effective mass region and being reflected to k = 0. The above program could alternatively be used to get *I-V* curves. However in the absence of scattering there will no current. Furthermore even for the case of some scattering, the large times, in comparison to the femtosecond time resolution, after which there is significant leakage to measure a current are not possible for a limited-time numerical study.

6.5 References

1. H. Fröhlich. Proc. Roy. Soc. A **160**. 230 (1937).

2. H. Fröhlich. Proc. Roy. Soc. A **188**. 521 (1947).

3. H. B. Callen. Phys. Rev. **76**. 1394 (1949).

4. M. P. Chamberlain and M. Cardona. Semicond. Sci. Technol. **9**. 794 (1994).

5. T. Tsuchiya and T. Ando. Phys. Rev. B **47**. 7420 (1996).

6. L. Wendler and R. Pechstedt. Phys. Stat. Sol. (b) **141**. 129 (1987).

7. N. S. Wingreen. Karsten W. Jacobsen and J. W. Wilkins. Phys. Rev. Lett. **61**. 1396 (1988).

8. D. Y. Oberli. G. Böhm and G. Weimann. Phys. Rev. B **47**. 7630 (1993).

9. Insook Lee and C. Y. Fong. Phys. Rev. B **44**. 6270 (1991).

10. J. P. Reynolds and M. Luban. Phys. Rev. B **54**. 14301 (1996).

11. G. von Plessen. T. Meier. J. Feldmann. E. O. Göbel. P. Thomas. K. W. Goossen. J. M. Kuo and R. F. Kopf. Phys. Rev. B **49**. 14058 (1994).

12. K. Leo. Semicond. Sci. Technol. **13**. 249 (1998).

13. L. Esaki and R. Tsu. IBM J. Res. Develop. **14**. 61 (1970).

14. L. Esaki and L. L. Chang. Phys. Rev. Lett. **33**. 495 (1974).

15. E. E. Mendez. F. Agulló-Rueda. and J. M. Hong. Phys. Rev. Lett. **60**. 2426 (1988).

16. A. Sibille. J. F. Palmier and F. Mallot. Appl. Phys. Lett. **60**. 457 (1992).

17. M. Dignam. J. E. Sipe and J. Shah. Phys. Rev. B **49**. 10502 (1994).

18. J. Feldmann. K. Leo. J. Shah. D. A. B. Miller. J. E. Cunningham. T. Meier. G. von Plessen. P. Thomas and S. Schmitt-Rink. Phys. Rev. B **46**. 7252 (1992).

19. C. Waschke. H. G. Roskos. R. Schwedler. K. Leo. H. Kurz and K. Köhler. Phys. Rev. Lett. **70**. 3319 (1993).

20. A. M. Fox, D. A. B. Miller, J. E. Cunningham, W.Y. Jan, C. Y. P. Chao and S. L. Chuang, Phys. Rev. B **46**, 15365 (1992).

21. P. Leisching, T. Dekorsy, H. J. Bakker, H. Kurz and K. Köhler, Phys. Rev. B **51**, 18015 (1995).

22. P. Leisching, P. Haring Bolivar, W. Beck, Y. Dhaibi, F. Brüggemann, R. Schwedler, H. Kurz, K. Leo and K. Köhler, Phys. Rev. B **50**, 14389 (1994).

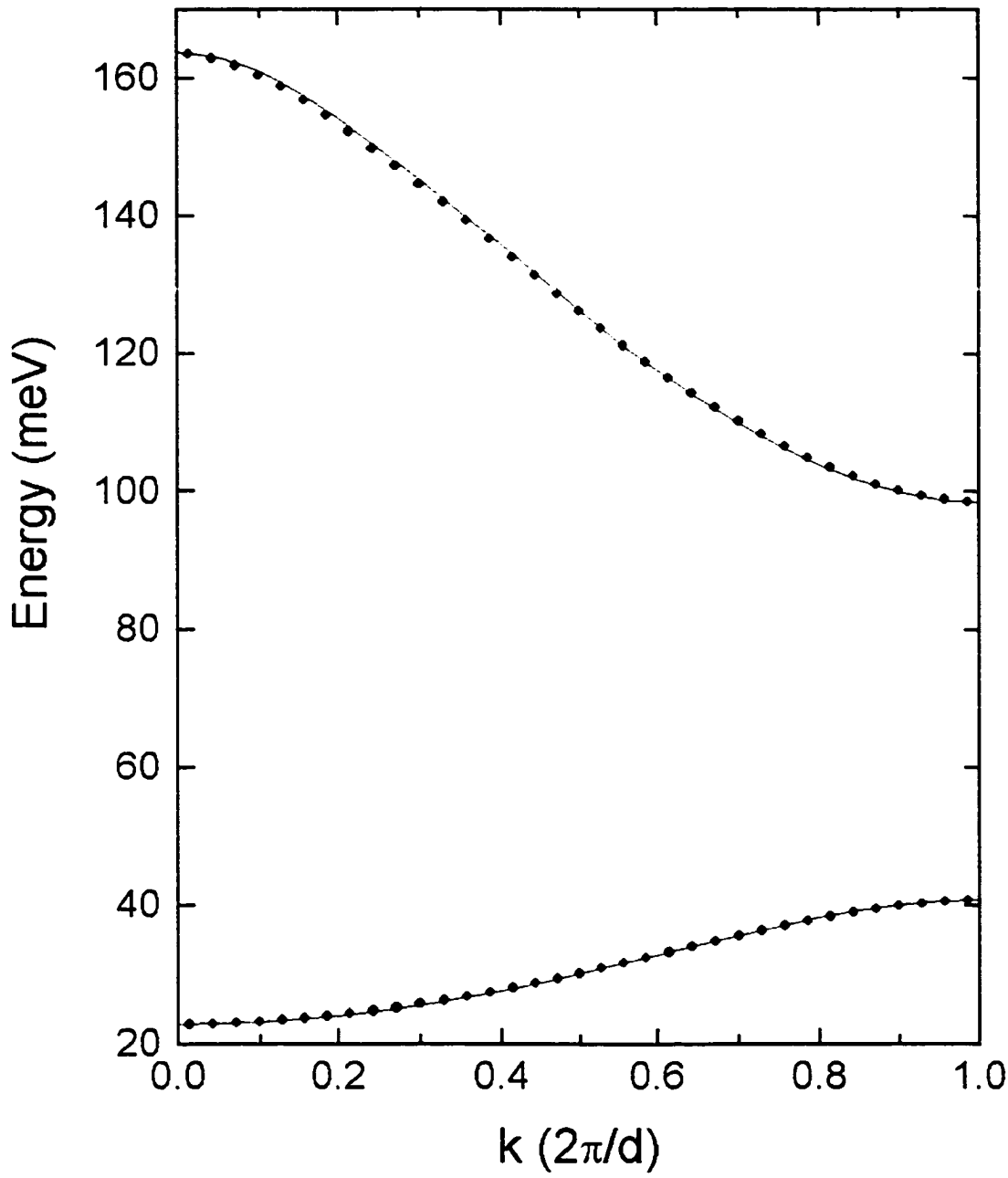

Fig. 6.1: The 35 eigenenergies per band are shown by the dots for the 35 quantum-well superlattice. For comparison the Kronig-Penney model is shown by solid line for the infinite superlattice.

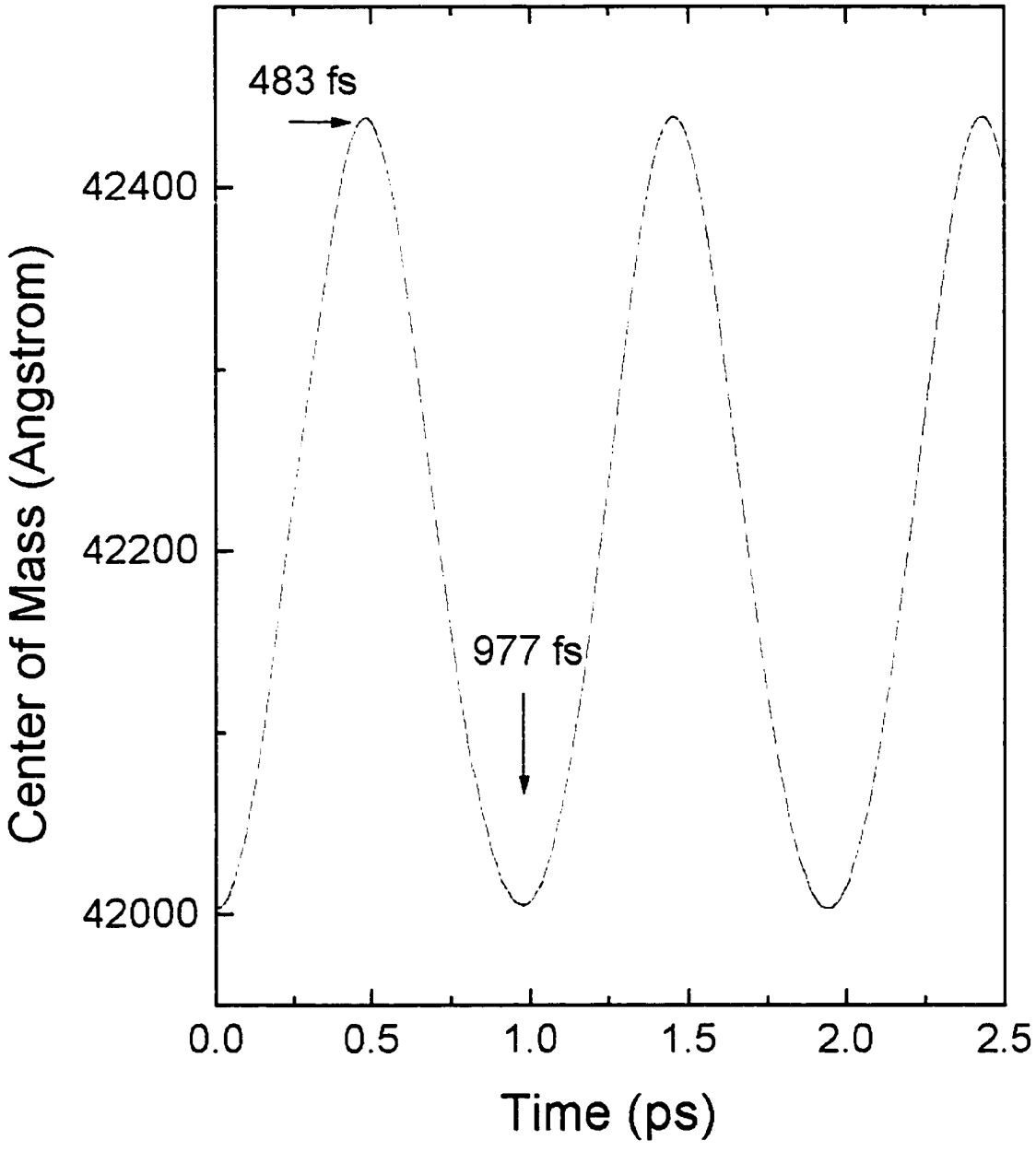

Fig. 6.2: The center of mass for the case of no scattering. The electron oscillates between two extreme positions in about 0.486 ps. The first rightmost position occurs at 483 fs and then the leftmost occurs at 977 fs.

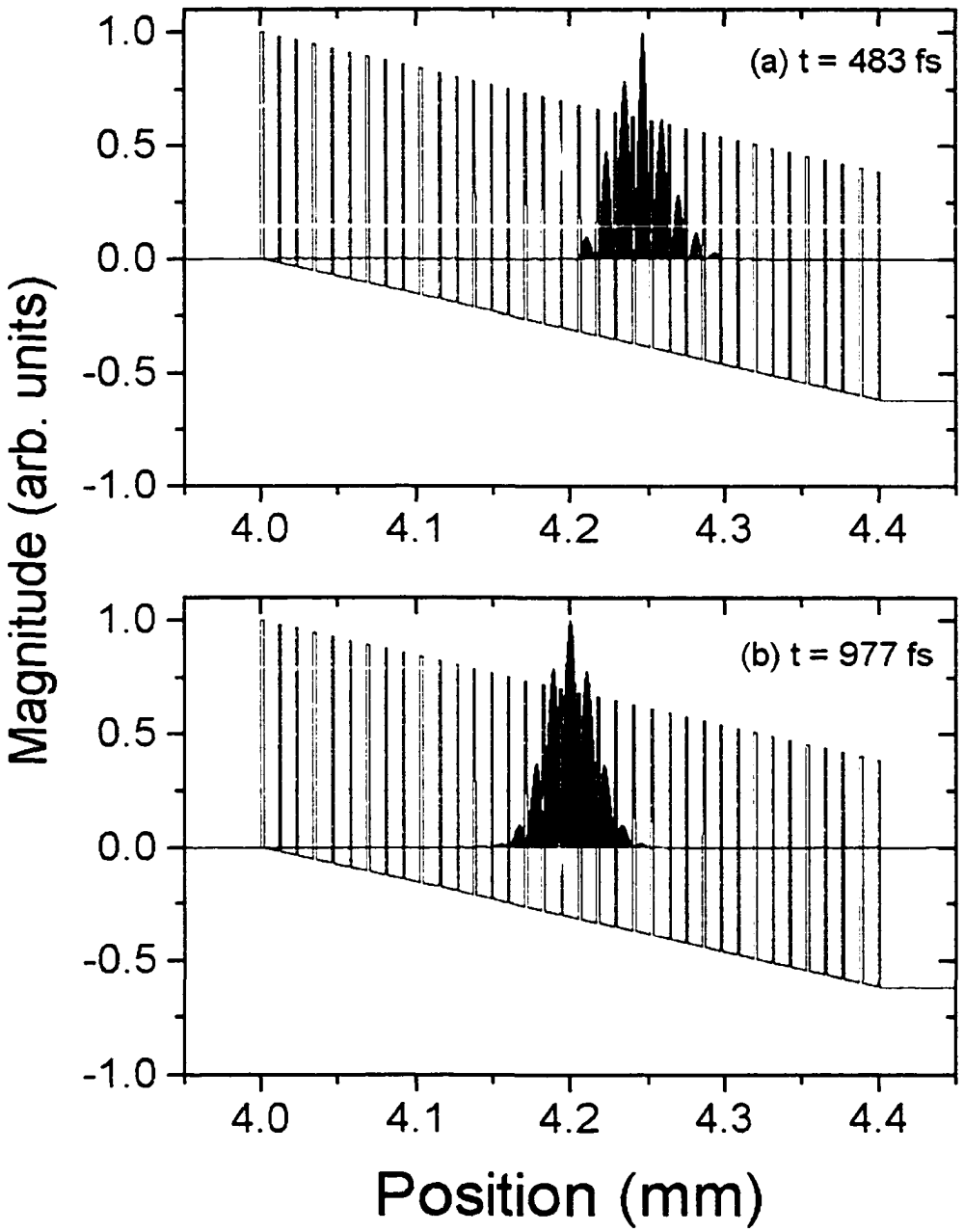

Fig. 6.3: The wavefunction without interaction for the two different times. (a) t = 483 fs and (b) t = 977 fs, which correspond to the center of mass at extreme right or left, respectively.

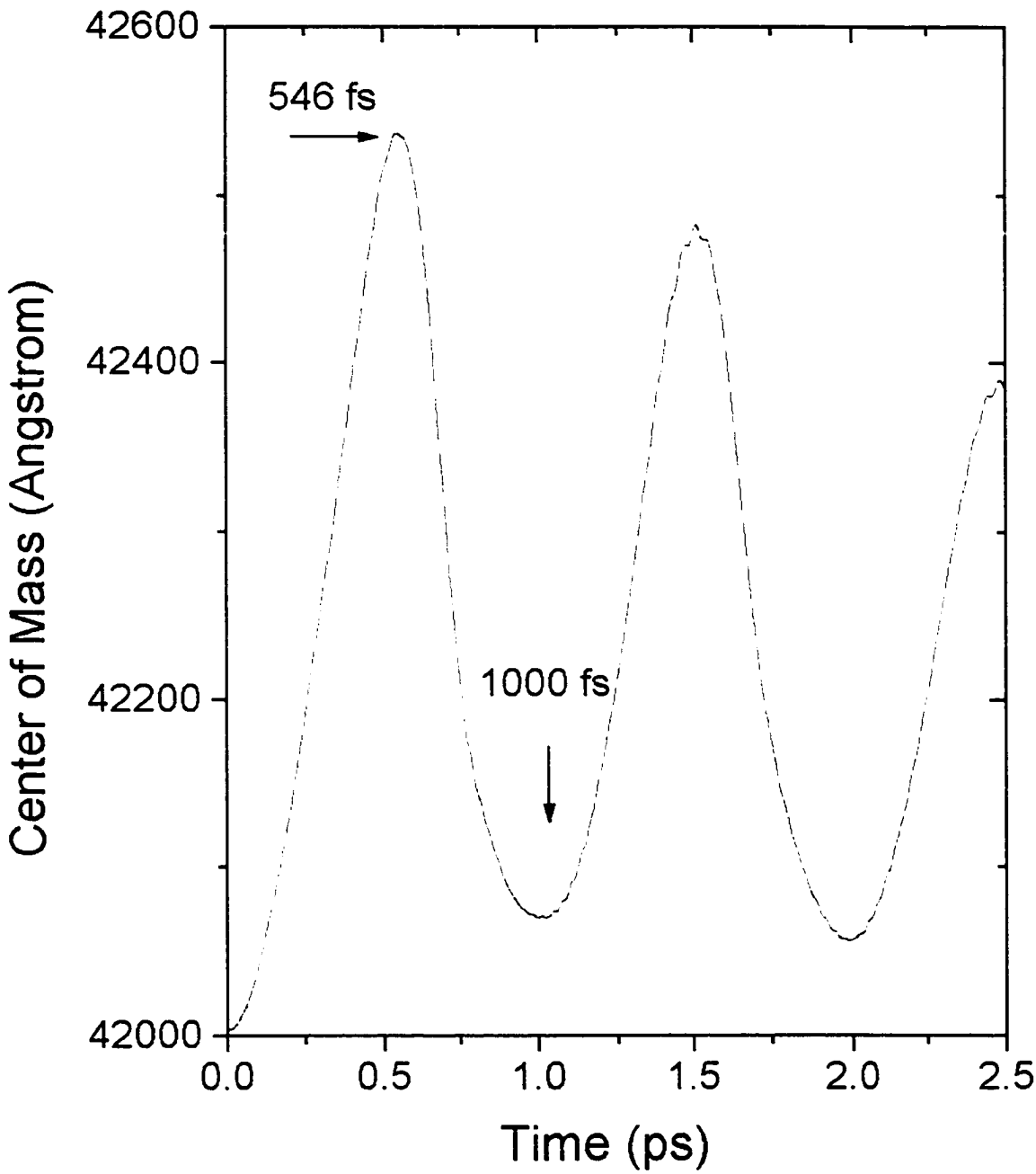

Fig. 6.4: The center of mass for the case of scattering with g = 9.0. The electron oscillates between two exteme positions in about 0.454 ps. The first rightmost position occurs at 546 fs and then the leftmost occurs at 1000 fs.

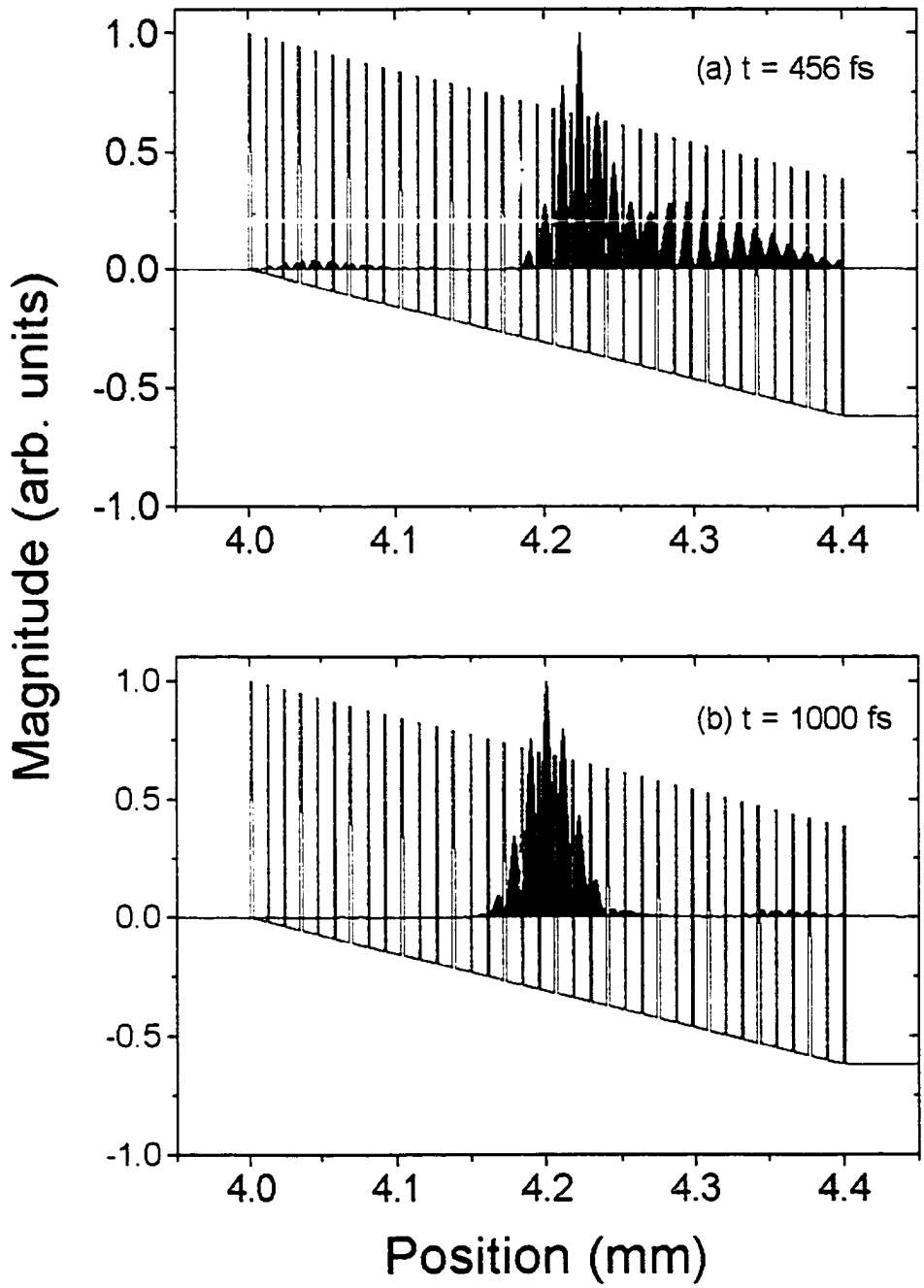

Fig. 6.5: The wavefunction with interaction for two different times. (a) t = 456 fs and (b) t = 1000 fs. which correspond to center of mass at extreme right or left, respectively.

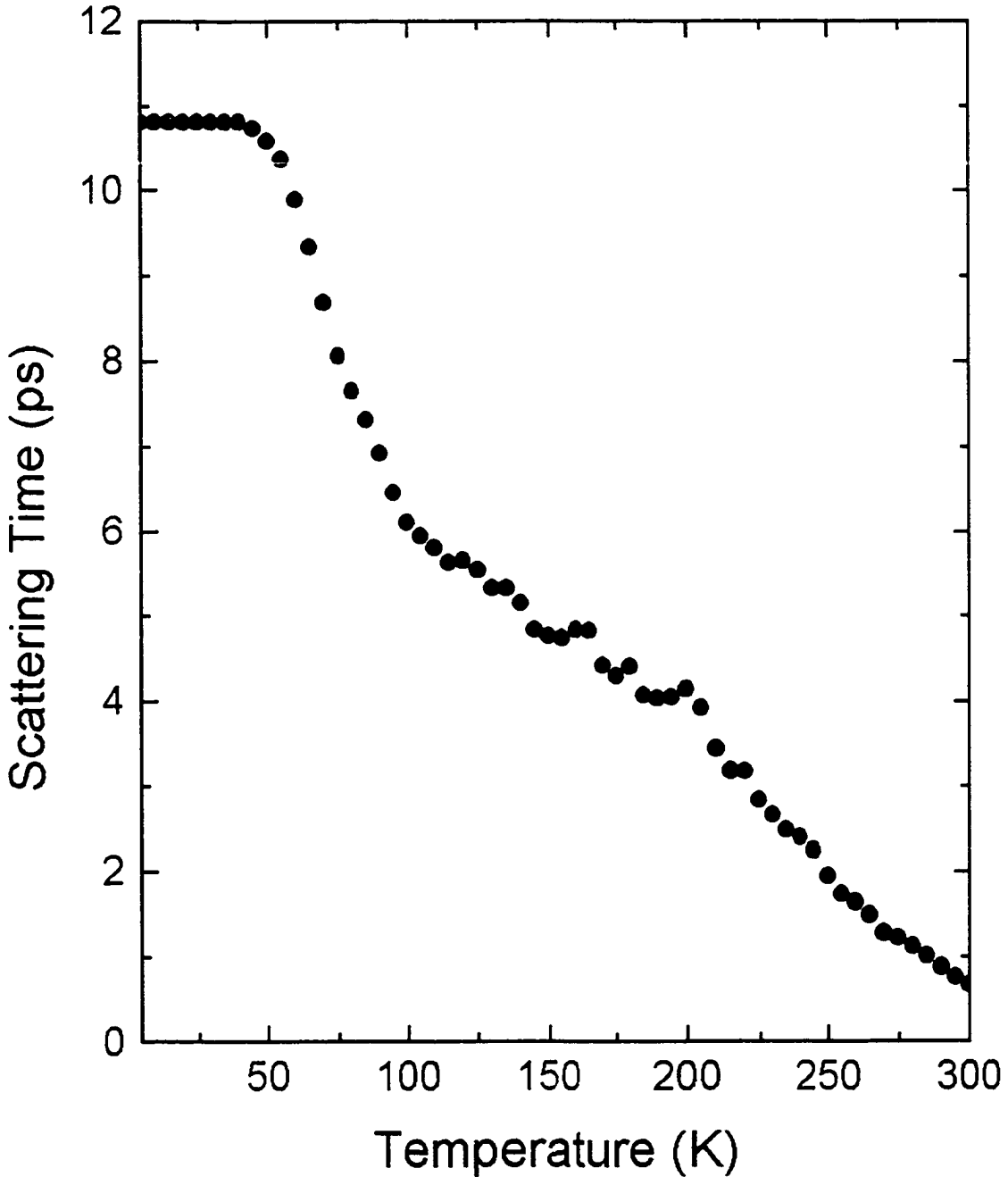

Fig. 6.6: The scattering time of confined phonons as a function of temperature for a bias of 0.15 V.

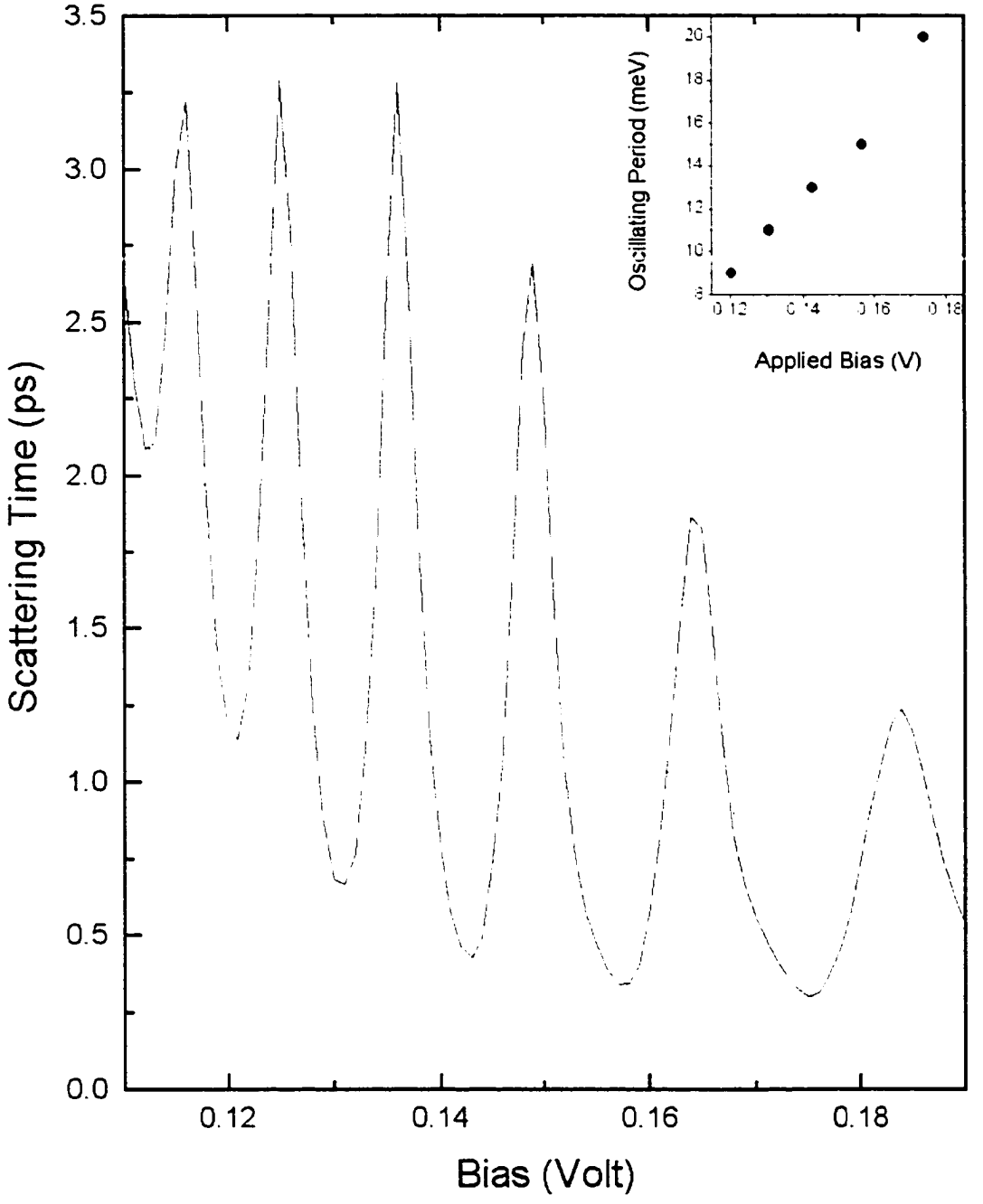

Fig. 6.7: The scattering time oscillates with electric field in a semiconductor superlattice. The dashed line shows that the average scattering time is decreasing with the electric field. The effective bandwidth also increases with the applied bias as shown in the inset.

CHAPTER 7

ELECTRON-PHOTON INTERACTION IN A SINGLE QUANTUM WELL

7.1 Introduction

An electronic switch controlled by the delay of an optical pulse is studied for use as an optical interconnect. The time-dependent Schrödinger equation with electron-photon interaction is used to study the characteristics of the switch. The switch is modulated by the time-delay, t_0, between when an electron pulse, that is modeled as a Gaussian wavepacket incident on a single quantum well, is released, and when a photon pulse is illuminated on the single quantum well. If this time delay corresponds to a time when most of the wavepacket is within the quantum well, there is maximum electron-photon interaction. Furthermore, the transmission and reflection coefficients are changed considerably due to increased electron-photon scattering for the resonant electron wavepacket. We have designed the switch so the transmission changes from 98% to 37% in 6 ps for an incident photon power of 10-mW and a width of 100 fs as the time-delay is increased from 2.5 ps to 3.3 ps. Better performance can be achieved by choosing different quantum structures with an ultimate switching time of 300 fs.

Optical interconnects for massive parallel processing computing tasks is an active area of a research[1] For chip-to-chip communications, the simplest implementation includes the transmitting chip's laser sending an optical signal which impinges on a photodetector in the receiving chip. The signal may travel either by a waveguide, a holographic mask for complicated connections, or in free-space. The photodetector thus acts like an optical switch and the output current corresponds to the voltage on the transmitting chip driving the laser.

A switching system utilizing a single quantum well (SQW) will be designed as an optical interconnect. The use of a low-dimensional semiconductor nanostructure, such as a SQW, in optoelectronic switching has been extensively studied[2] using the quantum confined Stark effect (QCSE)[3]. Among the several devices, the Self Electro-Optic Effect Devices (SEED)[4], is the most developed of the different technologies.

The electrooptic switch, here, is based on Mach-Zehnder interferometer, with the undelayed and delayed signals impinging on a semiconductor grading region and a single quantum well (SQW), rather than combining, as shown in Fig. 7.1. The transmitting chip's output voltage, V, is applied to a delay element to produce a variable delay τ which in turn controls the resonant transmission of electron wavepacket.

The time-dependent Schrödinger equation with electron-photon interaction is used to study the proposed switch. The switch is modulated by the time-delay t_0 between when an electron pulse, modeled as a Gaussian wavepacket incident on a SQW, is released, and when a photon pulse is illuminated on the SQW. If this time delay corresponds to a time when most of the wavepacket is within the SQW, there is

maximum electron-photon interaction and the transmission coefficient is decreased considerably for resonant transmission.

Photoillumination has been used in semiconductor superlattices (SL) to suppress current[5]. On the other hand, it is known that photoillumination leads to increased conduction in photoconductors. Photoconductors are optimized, mostly by doping, for the trapped electrons in quantum wells escaping by photoionization while the reverse takes place in our SQW, *i.e.*, traveling resonant electrons are trapped in a SQW. Most of the escaped electronic wavepacket contributes to reflected wave, after suffering a phase change, and there is decreased transmission.

We directly solve the time-dependent Schrödinger equation including electron-photon interaction. The solution is similar to a method used for electron-phonon interaction[6]. The Hamiltonian includes an electron-photon interaction term proportional to the electric field and the dipole moment (with respect to center of SQW z_c) and is given by[7]

$$H_{e-p} = -ig\left(a^{+}e^{i\omega t} - ae^{-i\omega t}\right)(z - z_c). \tag{7.1}$$

where the constant g is given as $e\sqrt{\frac{\hbar\omega}{2V\varepsilon}}$. Here $a(a^{+})$ is the photon annihilation (creation operator), $\hbar\omega$ is the photon energy, V is the volume of the interacting system and ε is the permittivity of the SQW. The time-dependent Schrödinger equation, with incident radiation *n* and terms for emission and absorption, leads to the matrix equation

$$i\hbar\frac{\partial}{\partial t}\begin{bmatrix}\psi^{(0)}\\ \psi^{(1)}\\ \psi^{(2)}\end{bmatrix} = \begin{bmatrix} H_e & -ig(z-z_0)\sqrt{n}e^{i\omega t} & ig(z-z_0)\sqrt{n+1}e^{-i\omega t}\\ ig(z-z_0)\sqrt{n}e^{-i\omega t} & H_e & 0\\ -ig(z-z_0)\sqrt{n+1}e^{i\omega t} & 0 & H_e\end{bmatrix}\begin{bmatrix}\psi^{(0)}\\ \psi^{(1)}\\ \psi^{(2)}\end{bmatrix}. \tag{7.2}$$

This equation was solved numerically on a Pentium II processor with an initial electron wave packet impinging on a SQW. By monitoring the temporal development of the wavepacket, electron transmissions with different photon pulses may be studied.

7.2 Ultrafast electronic switching via a photon pulse

In the numerical calculations, a spatial mesh size of 0.4 nm, a time mesh size of 5 fs, and the photon energy, $\hbar\omega$ = 36.2 meV (terahertz photons) are used. Zero boundary conditions are applied at the two end-points 2-μm away from the SQW, which are at coordinates z = 0 nm and z = 4010 nm. The 2-μm distance is far enough for the time scale considered to insure that the packet will not hit the boundaries and bounce back.

Fig. 7.2 shows the electronic spatial distribution of the quantum system. A Gaussian wavepacket is centered at $z_0 = 1000$ nm with a width of 110 nm. It is released at time t = 0. There are current probes at $z_1 = 1500$ nm and $z_4 = 2510$. These are placed so they are 500 nm away from the 10-nm SQW, which is bounded by coordinates $z_2 = 2000$ nm and $z_3 = 2010$. The depth of the SQW, ΔE_c, is 25 meV. This value is chosen to insure that there is only one electron eigenstate in the SQW, which has been calculated as $E_1 = 14.3$ meV (using time-independent Schrödinger equation without electron-photon interaction). A 100 fs photon pulse is shone on the SQW with a temporal center at t_0 denoted by $n_p(t, t_0)$. If the time t_0 is such that the wavepacket is traveling over the SQW, electron-photon interaction will decrease transmission, by increasing reflection and trapping. The incident energy E_i = 24 meV is chosen so that there is

electron-photon interaction if both the electrons and photons are inside the SQW. However if the incident energy is very far from the resonant condition, $\hbar\omega - (\Delta E_c - E_1) = 25.5$ meV, no electron-photon interaction will take place and the transmission will be independent of the photon pulse profile.

The effect of electron-photon interaction on the transmission spectra is shown in Fig. 7.3. Here the photon flux is a constant number and there is a measurable decrease in transmission near the resonant energy, which is about 24 meV. A volume of 1 μm^3 is used throughout this study.

Fig. 7.4(a) shows the temporal profile of the incident electron current at the left probe and Fig. 7.4(b) similarly shows the temporal profile for three different photon pulse delays. For comparison the width of electron current is 450 fs. The three photon pulses have these t_0 values: t_{01} = 2500 fs, t_{02} = 3300 fs and t_{03} = 4100 fs. The three times correspond to when the wavepacket is to the left of the SQW, partly inside the SQW, and partially transmitted from the SQW. It can be assumed that the electron photon interaction will be greatest for the middle value.

Fig. 7.5 shows the results for different t_0 values under various photon power levels. Basically the power levels determine what is the peak photon population of the pulse for a given time step. It can be seen that around t_0 = 3300 fs, the interaction is greatest, leading to decreased transmission. The inset shows how the maximum transmission differential (change in transmission from the non-interaction case) varies with the power levels.

Fig. 7.6 shows the current profiles for two different t_0 values for a photon pulse power of 0.1 mW. The current for t_{03} is identical to that for t_{01} and is not shown here. The current for t_{02} shows that there is decreased transmission, and increased reflection. It can be seen that the transmitted current has two major peaks, probably indicating that it has been split so there is a below resonant energy and above resonant energy component. The switching time is seen to be around 6 ps, when the transmitted current has decayed to zero. As the above switching speed is dependent on the width of the leads used in the device, the net charge capture in the SQW for delay t_{02} is shown in Fig. 7.7. Thus the ultimate switching speed of the device is 300 fs.

7.3 Conclusion

In conclusion, we have designed a novel electro-optic switch that is modulated by the delay time between an electric and optical pulse. The calculations have shown a transmission differential of 61 percent for an optical pulse of power 10 mW and width of 100 fs. The numerical model can easily account for the effect of changing various parameters for making optimum switches. The switching time can be reduced considerably from the 6 ps in this calculation, by placing the electronic leads closer to the SQW and it goes to 300 fs. Multiple quantum well structures can be tailored to yield an arbitrary transmission spectra and may be useful for wavelength division multiplexing (WDM). The optical source does not necessarily have to be on the transmitting chip and could be a part of the global clock system.

7.4 References

1. D. A. B. Miller, Proc. of the IEEE **88**, 728 (2000).

2. H. Haug and L. Bányai, Eds., *Optical Switching in Low-Dimensional Systems* (Plenum Press, New York, 1988).

3. D. A. B. Miller, D. S. Chemla, T. C. Damen, A. C. Gossard, W. Wiegmann, T. H. Wood and C. A Burrus, Phys. Rev. B **32**, 1043 (1985).

4. C. R. Giles, T. Li, T. H. Wood, C. A. Burrus and D. A. B. Miller, Electron. Lett. **24**, 848 (1988).

5. E. Schomburg, A. A. Ignatov, J. Grenzer, K. F. Renk, D. G. Pavel'ev, u. Koschurinov, B. Ja. Melzer, S. Ivanov, S. Schaposchnikov and P. S. Kop'ev, Appl. Phys. Lett. **68**, 1096 (1996).

6. J. M. Mohaidat, K. Shum and R. R. Alfano, Phys. Rev. B **45**, 3822 (1992).

7. A. Yariv, *An Introduction to Theory and Applications of Quantum Mechanics* (John Wiley & Sons, New York, 1982), p. 133.

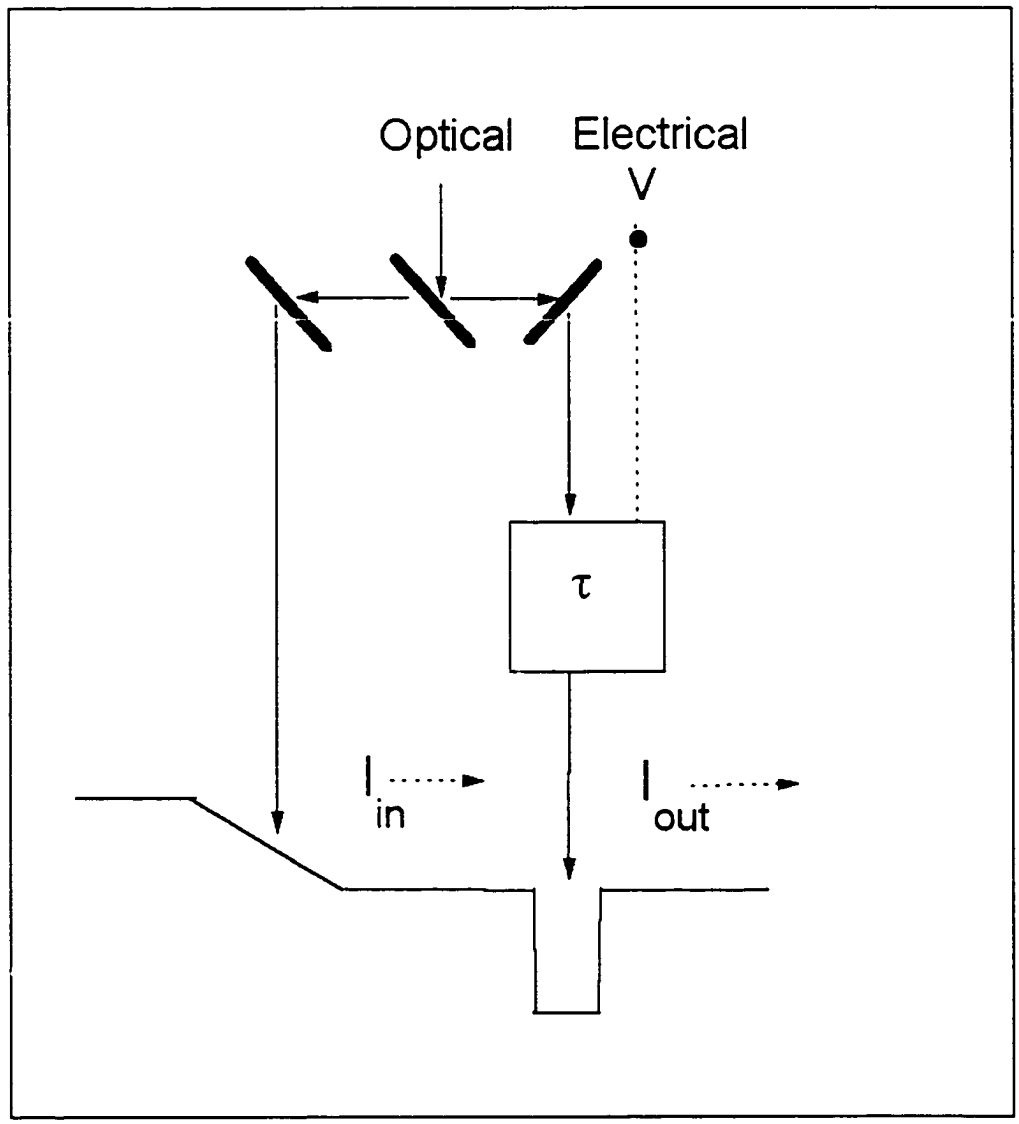

Fig. 7.1: An electrooptic switch is modulated by the delay τ induced by voltage, V, in the transmitting chip to drive a current I_{out} in the receiving chip.

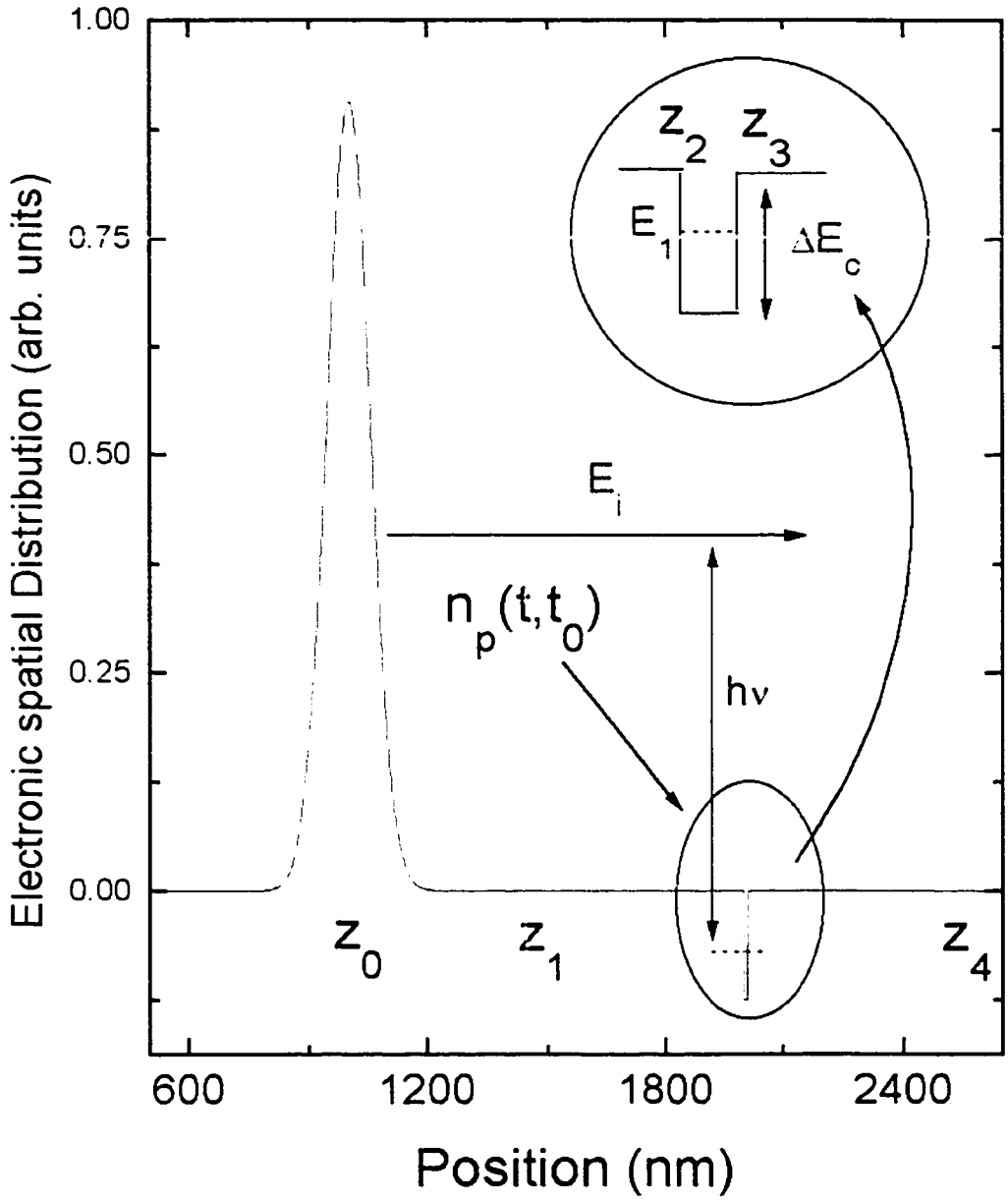

Fig. 7.2: Electron spatial distribution of the calculation. An electronic Gaussian pulse, with a center at z_0 and a kinetic energy of E_i, interacts inside a SQW with a delayed optical pulse $n_p(t,t_0)$.

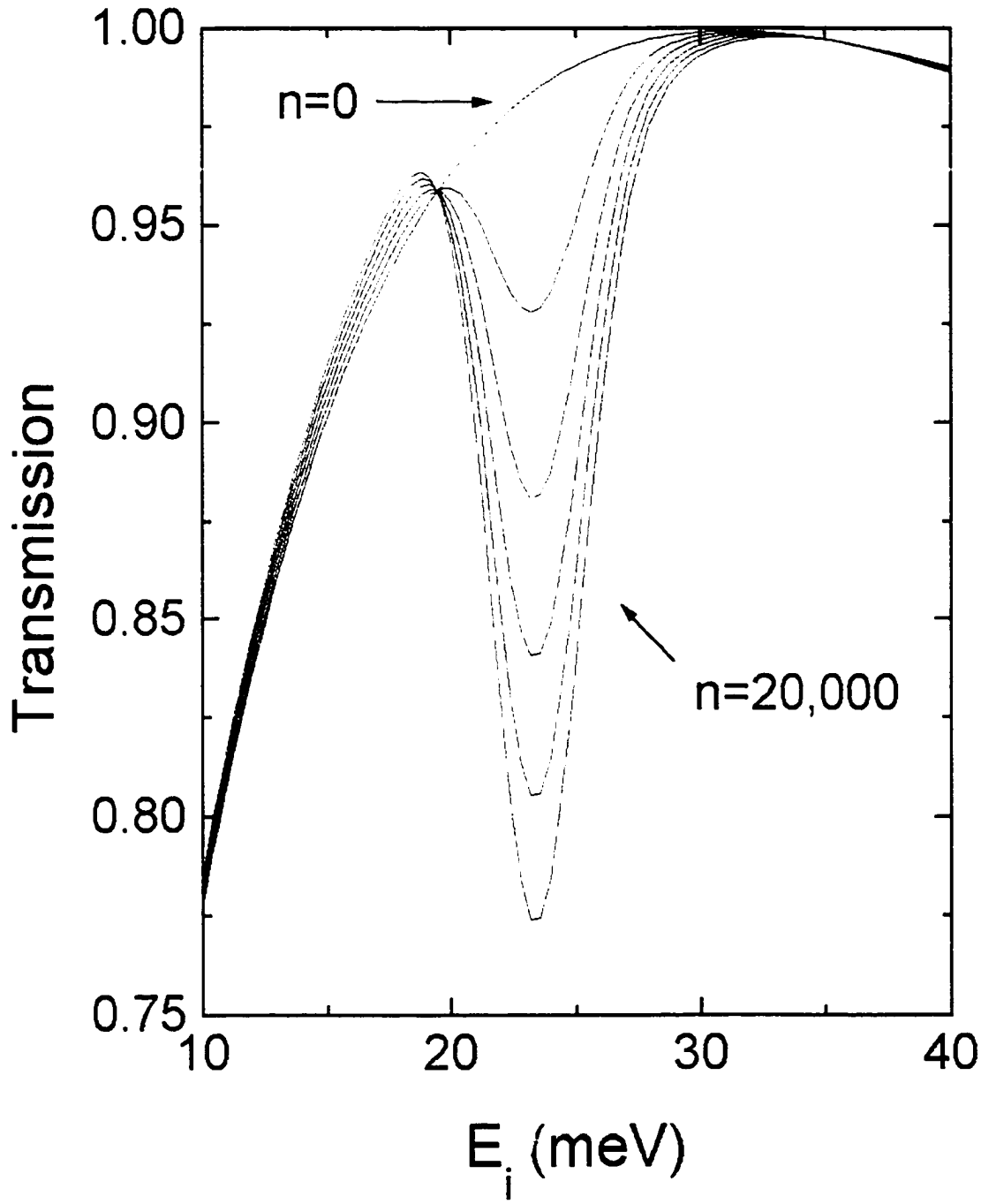

Fig. 7.3: The steady-state transmission for a constant photon flux of n photons over the SQW with a resonant energy of 24 meV.

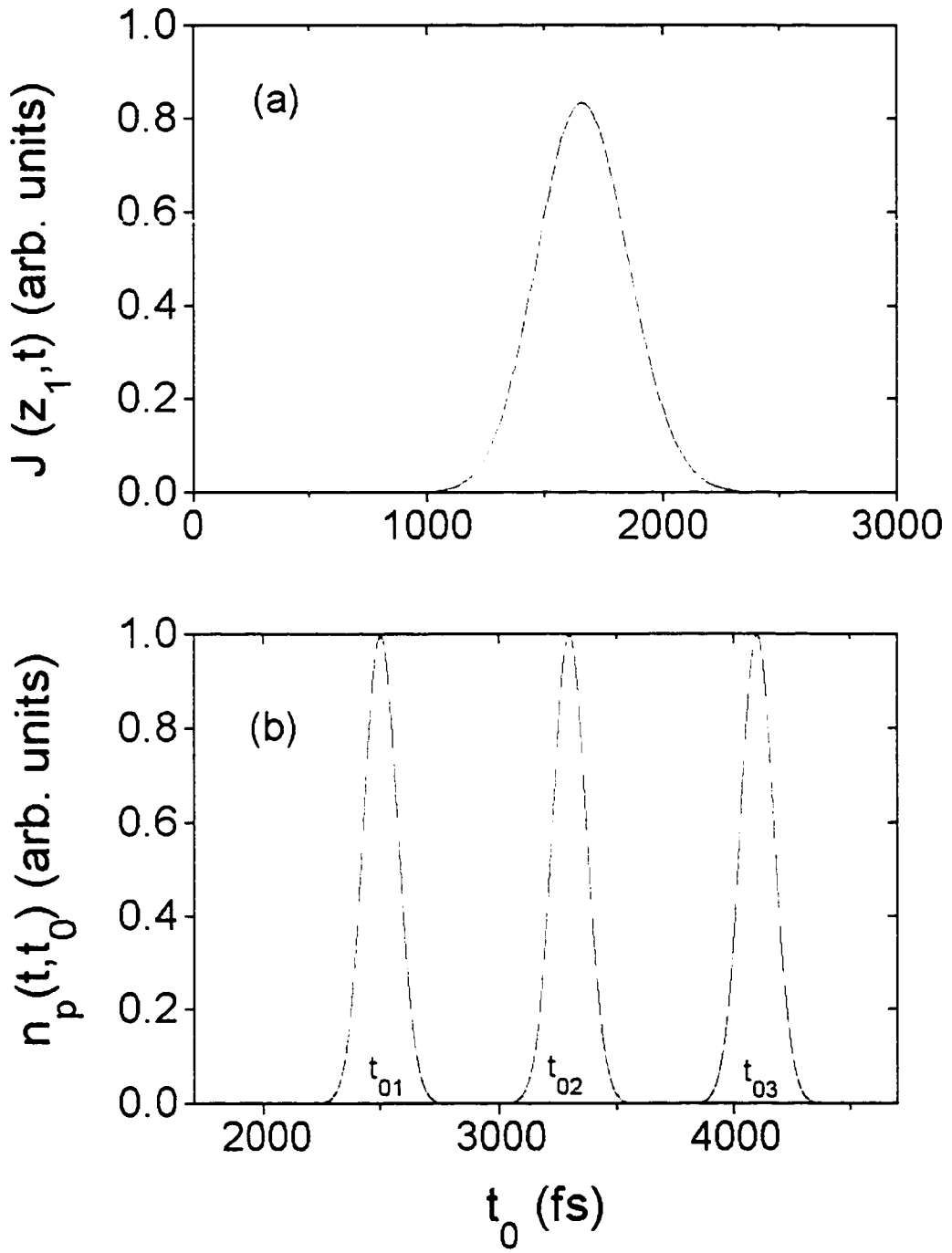

Fig. 7.4: Temporal distribution of (a) incident current at z_1 and (b) three different photon pulses with temporal centers at t_{01}, t_{02} and t_{03}.

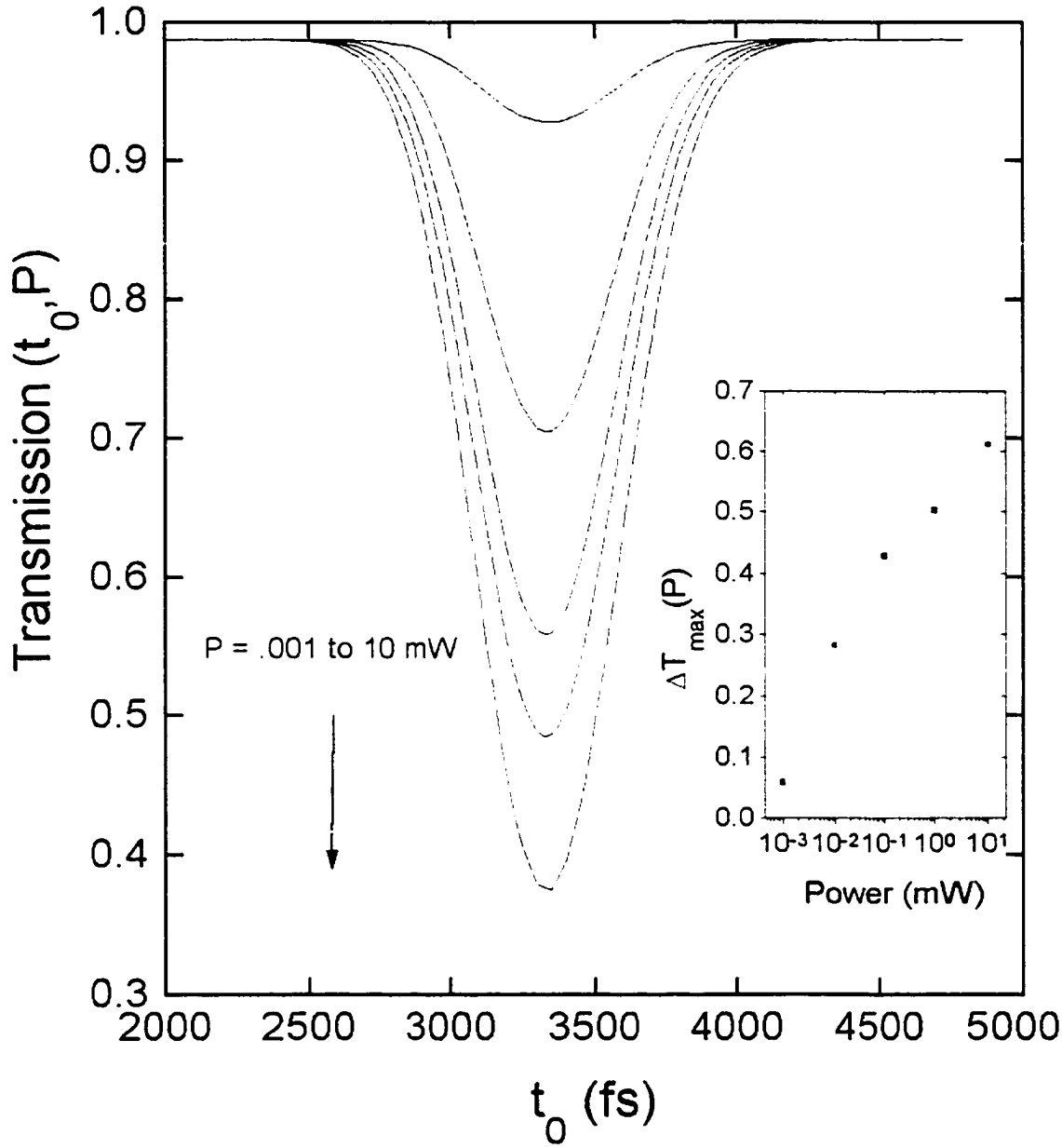

Fig. 7.5: Transmitted wavefunction as a function of optical pulse delay, t_0, for five different power levels. The inset shows the maximum transmission differentials for the various power levels.

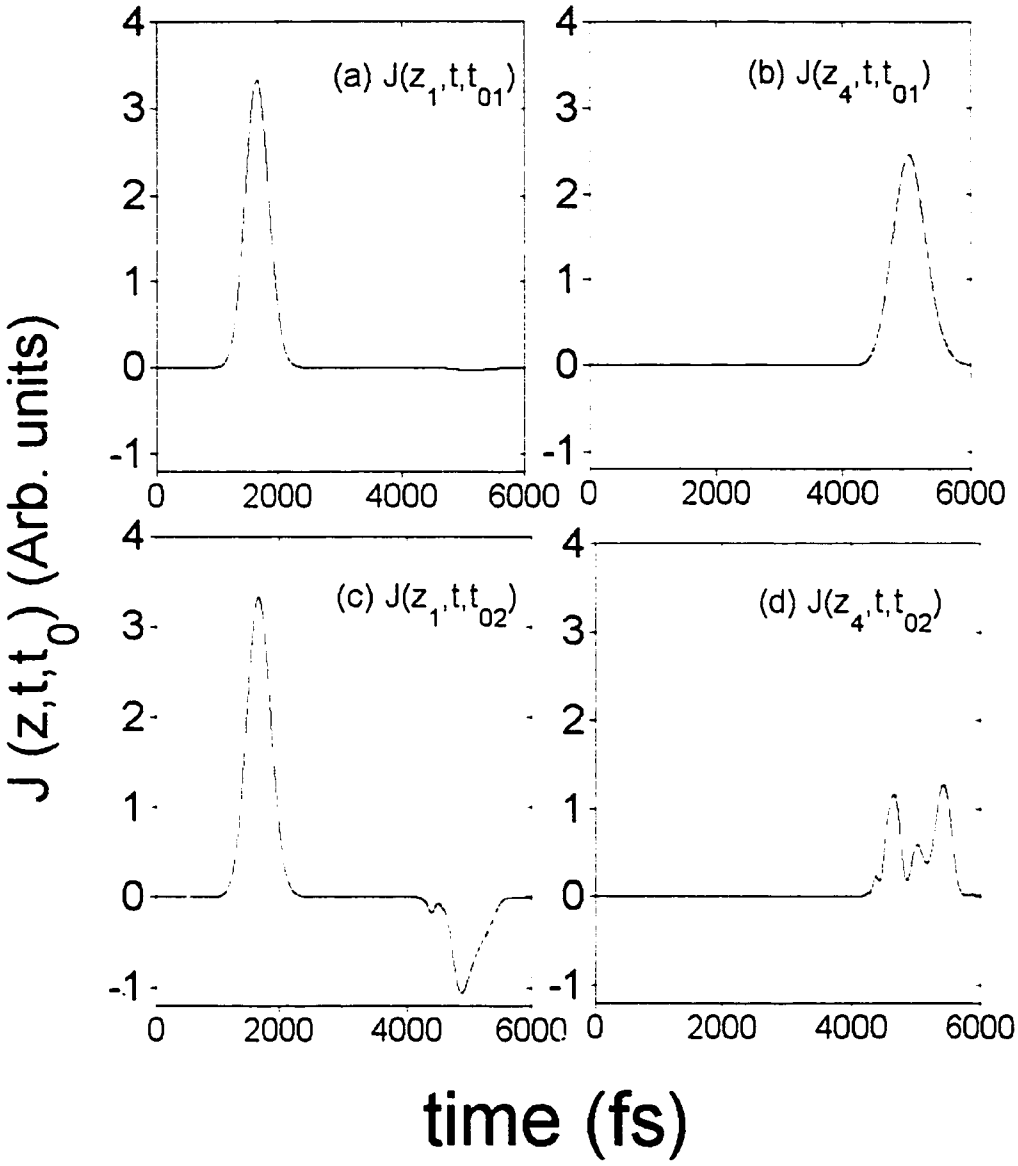

Fig. 7.6: The incident, transmitted and reflected electron currents as measured by the input and output probes for photon delays t_{01} and t_{02}.

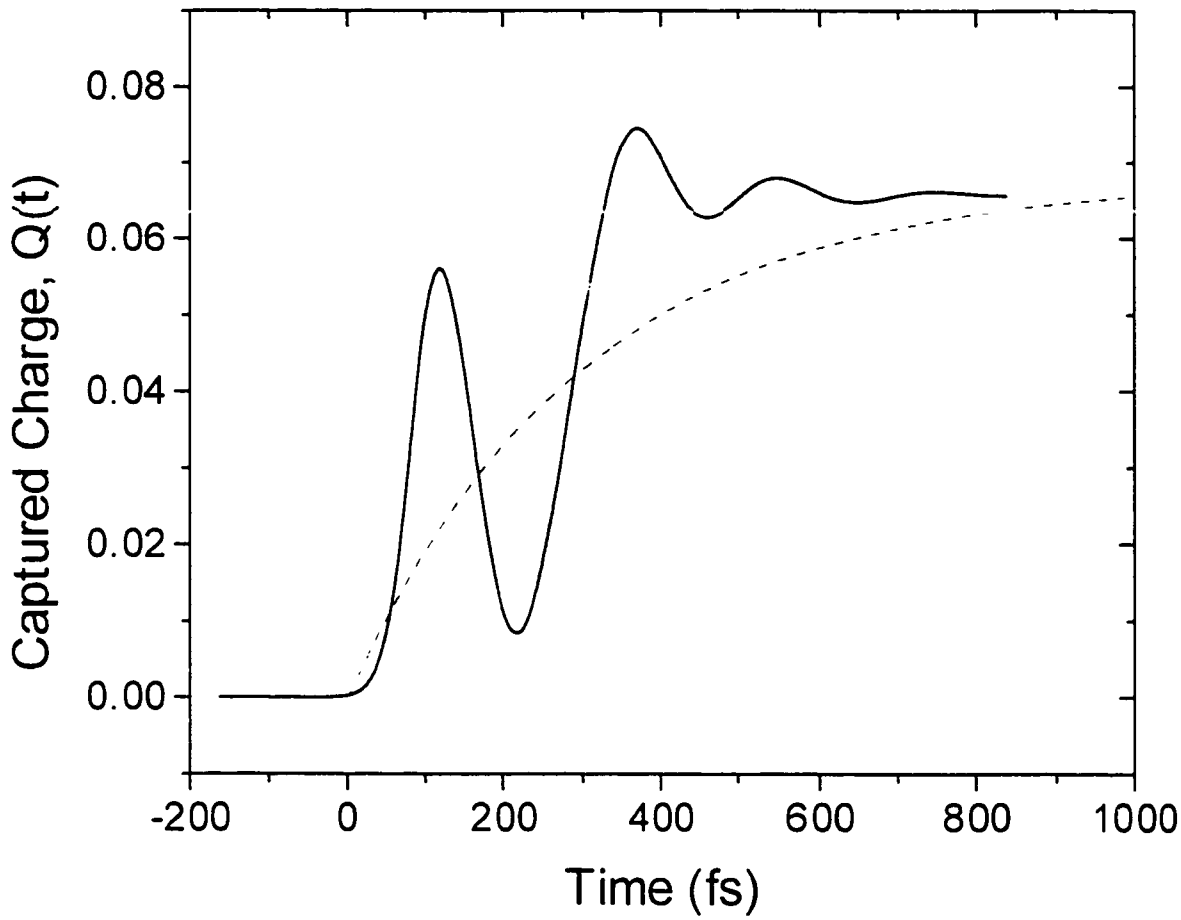

Fig. 7.7: Captured charge in the quantum well (solid curve). The dashed curve is a plot of the expression $0.068(1-\exp(t/\tau_c))$, where $\tau_c = 300$ fs.

CHAPTER 8

RECURSIVE ERROR METHOD FOR SOLVING ARBITRARY HAMILTONIAN

8.1 Introduction

A stationary iterative method is reported that can solve the time-dependent Schrödinger equation for any Hamiltonian, while being efficient and accurate. Forward-time (U_N^+) and backward-time (U_N^-) operators based on the Taylor series expansion for the propagation operator, $\exp(\pm \Delta t\, H / i\hbar)$, are employed in our method, where N is the number of terms in the expansion. We find that the iterative sequence, $\psi^{r+1}(t+2\Delta t) = (1 - U_N^- U_N^+)\psi^r(t+2\Delta t) + U_N^- U_N^+ \psi(t)$, converges to the actual wavefunction. The stability of the method arises from the usage of both forward-time and backward-time operators in an innovative iterative procedure. The efficiency and parallelism of this method compares favorably to other iterative procedures and the split-operator technique.

As semiconductor devices become smaller and faster, physical models for carrier transport dynamics should include the time-dependent Schrödinger equation (TDSE). The prohibitive amount of computation-time needed for solving this partial differential equation limits the current models. Recent progress in the use of distributed-memory parallel processors (DPPs)[1] promises to change this situation. DPPs use a large array of

processors, each with separate memory, connected via a high-speed network to carry out a massive computation task. In order to effectively use DPPs, innovative methods for solving the TDSE should be explored with which parallel algorithms can be designed and implemented. In this paper, an innovative recursive error method (REM) is reported. A highly parallel and efficient algorithm based on the REM to solve the TDSE is illustrated with several examples and its performance is compared with the various existing methods.

The classical method for solving the TDSE is the Crank-Nicolson method[2]. This method yields an array of n equations, where n is the number of spatial divisions. It can be solved implicitly by a direct method such as Gaussian elimination or by an explicit iterative method. For a multidimensional or many-body Hamiltonian, explicit methods must be used, as direct methods become computationally intensive requiring extensive memory. The most widely used iteration methods are based on stationary Jacobi or non-stationary Conjugate Gradient (CG)[3].

Even though the Jacobi method is highly parallel, it converges very slowly. Some extensions of the Jacobi method include the Gauss-Seidel method and the Successive Over-Relaxation (SOR) method. The Gauss-Seidel method can converge twice as fast while the SOR method can converge up to n times faster[4]. However, this convergence rate will only be possible if the optimum relaxation constant is known by calculating the eigenvalues of a matrix. The CG method can also converge with a similar number of iterations as SOR method although it requires the massive calculation of dot products for computing a new iteration matrix. This causes delays due to the need for extensive communications among the various processors. Stationary methods require less

communication overhead and are preferable for developing parallel algorithms, provided the convergence is fast.

All iteration methods solve the TDSE in the real space. However, the split-operator technique[5] solves the TDSE both in reciprocal and real spaces. Most of the calculations are done to get the FFT of initial-time wavefunction and its inverse after simple modifications. Parallel computers can compute the FFT and its inverse in a number of stages that depend logarithmally on the size of problem. This is in contrast to iterative methods where the total number of stages depends on the number of iterations required for convergence. The split-operator method requires the Hamiltonian to be easily expressible in reciprocal space, *i.e.*, it should form a diagonal matrix in reciprocal space. Otherwise, it becomes an inefficient method.

The REM has converging properties similar to SOR and CG while requiring far fewer calculations. It remains highly accurate even as the time step, Δt, is increased without the need for vastly more calculations. The underlying principle for this novel method is a unique error minimization procedure. Such a procedure finds a minimum difference between the wave function $\psi(t)$ and the assumed wave function $\psi(t+2\Delta t)$, after they are projected to the same time coordinate at $t + \Delta t$ using N-term forward-time and backward-time operators, respectively. The minimization of the difference between the projections yields an optimum approximation to the actual wave function.

The paper is organized as follows. The REM is developed in §8.2. In §8.3 an algorithm is described to find an iterative sequence for solving the TDSE. In §8.4 and §8.5 the accuracy and speed of REM are given and compared with that of Jacobi method.

One-dimensional (1D) and two-dimensional (2D) Hamiltonians are used in our demonstrations. In §8.6. the advantages of REM are summarized for solving the TDSE.

8.2. Recursive error method for solving the TDSE

The TDSE for the propagation of a wavefunction ψ by a Hamiltonian H. is

$$i\hbar \frac{\partial \psi}{\partial t} = H\psi . \tag{8.1}$$

A numerical solution to the TDSE starts by discretizing (8.1). The time derivative that appears in the TDSE can be approximated as

$$i\hbar \frac{\partial \psi}{\partial t} \cong i\hbar \frac{\psi(t+\Delta t) - \psi(t-\Delta t)}{2\Delta t} . \tag{8.2}$$

Eq. (8.2) is equal to the product of Hamiltonian and wavefunction. $H\psi$. *Different approximations to this product result in widely varying methods of solution.* Three approximations are listed in Table 8.1. The first method is explicit Second-Order Differencing (SOD) method[6]. while the second method is Crank-Nicolson[2]. The third method is the new method. REM.

The SOD method is not unitary leading to error accumulation as a wavefunction evolves in time. Most iterative methods are based on the unitary Crank-Nicolson. However. the Crank Nicolson method involves a matrix equation relating the product of $H(t-\Delta t)\psi(t-\Delta t)$ and the product of $H(t+\Delta t)\psi(t+\Delta t)$. *This method can only deal with a selective number of simple Hamiltonians because the expression for the latter time is too complicated to setup.*

Using the REM approximation. the TDSE leads to the following equation.

$$\psi(t+\Delta t) = U(2\Delta t)\psi(t-\Delta t). \tag{8.3}$$

where $U(2\Delta t)$ is a double-time-step propagation operator and is given by

$$U(2\Delta t) = \frac{1+aH(t)}{1-aH(t)}. \tag{8.4}$$

where $a = \Delta t/i\hbar$. In the following analysis H will be denoted as the Hamiltonian at time t.

For $aH << 1/2$, the Taylor Series for $(1 + aH)/(1 - aH)$ approaches the series expansion of $\exp(2aH)$, which is the exponential propagation operator for time-independent Hamiltonians[7]. The condition $aH << 1/2$ can be approximated as $\Delta t << \hbar / 2\Delta V_{max}$ where ΔV_{max} is the maximum potential-energy discontinuity in the structure under study, which is the same time step requirement as in the split-operator technique[5]. The potential energy discontinuities are on the order of electron volt for most semiconductor structures, thus the condition $aH << 1/2$ requires that the time step, Δt, be less than 0.3 fs. Under these conditions, the double-time-step propagation operator can be written as

$$U(2\Delta t) = \exp(2aH). \tag{8.5}$$

Equation (8.5) allows us define the single-time-step propagation operator simply by the relation $U(2\Delta t) = U(\Delta t)U(\Delta t)$. For convenience, the forward-time U^+ operator and the backward-time operator U^- are defined as

$$U^+ = \exp(aH),\ U^- = \exp(-aH). \tag{8.6}$$

With the above definitions as well as a change in variable from t to $t + \Delta t$, Eq. (8.3) becomes

$$U^-\psi(t+2\Delta t) = U^+\psi(t). \tag{8.7}$$

where the double-time-step operator is separated into the single-time-step operators on each side using the identity $U^{-}U^{+}=1$. This equation establishes a base for the REM algorithm.

8.3. Algorithm to implement REM

The operators U^{+} and U^{-} have an infinite number of terms. However, any numerical solution will use a finite number of terms. A finite-operator method based on (8.3) is unstable because the truncated operator U is not unitary. However, a finite-operator method based on (8.7) is stable when the method is implemented using the error minimization strategy described below.

The solution vectors $\psi(2k\Delta t)$ can be found using equation (8.7), where k is a positive integer, by knowing the initial wavefunction $\psi(0)$. If N is the number of terms in our approximation to exponential operator, the forward-time operator for $N=4$ is

$$U_4^{+}=1+aH+\frac{a^2}{2}H^2+\frac{a^3}{6}H^3+\frac{a^4}{24}H^4. \tag{8.8a}$$

and the backward-time operator for $N=4$ is

$$U_4^{-}=1-aH+\frac{a^2}{2}H^2-\frac{a^3}{6}H^3+\frac{a^4}{24}H^4. \tag{8.8b}$$

The implementation of U_4^{+}, in terms of Hamiltonian operations, is shown in Fig. 8.1. By using these operators, equation (8.7) can be expressed as this relation between input and output vectors

$$U_N^{-}\psi_{out}\equiv U_N^{+}\psi_{in}. \tag{8.9}$$

Here ψ_{in} is the initial-time wavefunction and ψ_{out} is an assumed wavefunction a time $2\Delta t$ later.

We define an error in the assumed wavefunction, ψ^r, as

(8.10) $$e^r = U_N^- \psi^r - U_N^+ \psi_{in}.$$

In this equation, the variable r refers to the iteration index. For some iteration index $r = s$, the value of error is less than a tolerance and $\psi_{out} = \psi^s$.

Eq. (8.10) gives the error of the wavefunction at time $t + \Delta t$. This is seen by the following analysis. The assumed wavefunction at time $t + 2\Delta t$, ψ^r, is operated by the backward-time operator U_N^- to get an assumed wavefunction at time $t + \Delta t$. This is compared with the wave function obtaining by operating the forward-time operator U_N^+ on initial-time wavefunction ψ_{in}.

The wave function for next iteration, ψ^{r+1}, must be chosen so that the error is zero. This wave function is given by

(8.11) $$\psi^{r+1} = \psi^r + Ke^r.$$

Replacing ψ^r in (8.10) by the ψ^{r+1} given in (8.11), the error at iteration $r + 1$ is

(8.12) $$e^{r+1} = U_N^-\left(\psi^r + Ke^r\right) - U_N^+\psi_{in} = U_N^-\psi^r + U_N^-Ke^r - U_N^+\psi_{in} = e^r + U_N^-Ke^r.$$

This suggests that if $e^r + U_N^-Ke^r = 0$, the new error would become zero or

(8.13) $$U_N^-Ke^r = -e^r. \qquad U_N^+U_N^-Ke^r = -U_N^+e^r. \qquad K \equiv -U_N^+.$$

In the above analysis, the product of $U_N^+U_N^-$ is assumed to be 1. In Table 8.2, the analytic values of this unitary operator are shown for the first five N values.

From Table 8.2, it can be seen that the unitary condition requires that aH be much less than one. Furthermore, the unitary condition is satisfied to a high power of Δt for large N.

The REM algorithm is shown in Table 8.3. The total number of time steps is given by the variable *last*. The variable *max* is given to check whether the iterative solutions are actually converging within a reasonable number of iterations. The error loop can be terminated if either the error norm is less than a small value *tol* (around 10^{-15} for 32-bit computers) or if the total number of iterations is greater than *max*. For the later case, the program will have to be restarted with a smaller time step.

The above algorithm yields the following iterative sequence

$$\psi^{r+1}(t+2\Delta t) = \left(1 - U_N^{\dagger} U_N^{\dagger}\right)\psi^{r}(t+2\Delta t) + U_N^{\dagger} U_N^{\dagger}\psi(t). \tag{8.14}$$

This sequence is much faster to implement on computers. However it requires knowledge of Δt, N, and *max* needed for convergence. Thus if we go through a few time steps with the REM algorithm and find these parameters, we can implement the faster iterative sequence based on equation (8.14).

8.4 Accuracy of REM

In the REM algorithm, the error is defined as the difference between left-hand and right-hand sides of (8.9). The right-hand side, corresponding to $U_N^{\dagger}\psi_{in}$ is our guess to the value of the wave function at time $t + \Delta t$ and is represented by vector RHS. We can check for accuracy of REM method by monitoring the difference in magnitude between a calculated value and an exact solution for the right-hand side.

A 100 Å square quantum well, shown in the inset of Fig. 8.2, is used to calculate the error produced by the REM. The initial wave packet is chosen to be the lowest eigenstate. Thus there should be no change in magnitude with time because this is a stationary state. The spatial resolution was chosen to be 1 Å. Here the rms error is the change in the magnitude of the sinusoidal wavefunction, after a time period of 0.01 fs, as a function of N. The error goes from 10^{-7} at $N = 1$ to the machine limit, 10^{-16}, at $N = 4$.

The Jacobi and Gauss-Seidel methods have the same right-hand side as the REM case for $N = 1$. Thus the improvement in accuracy is 10^{9} for $N \geq 4$. This demonstrates the potential of using REM to accurately solve for the TDSE. For different Hamiltonians, the results may slightly vary. But it should show the same trend of increasing accuracy with N.

8.5 Computation speed of REM using 1D and 2D Hamiltonians

8.5.1 One-dimensional Hamiltonian

A 100 Å single quantum well (SQW), with a well depth of 25 meV, is used to demonstrate the computation speed of REM. The SQW is spatially situated in the middle of a system that is 20100 Å wide. The inset of Fig. 8.3 shows a simplified view of the structure. The spatial resolution is 1 Å. Initially there is a Gaussian wave packet which is centered 3000 Å left of the SQW with a width of 550 Å. It moves towards the right with a center-energy of 24 meV. The electron effective mass is 0.067 m_0 inside and 0.092 m_0 outside the SQW. The two end-boundaries are hard walls, *i.e.*, the wavefunctions are

zeroes at the two end-points. Terminating the calculation before the wavepacket hits the boundaries minimizes the effects of the boundaries on the calculation.

We use Ben-Daniel and Duke Electronic Hamiltonian[8]

$$H_e\psi = -\frac{\hbar^2}{2}\frac{\partial}{\partial z}\left[\frac{1}{m^*(z)}\frac{\partial}{\partial z}\psi(z)\right] + V(z)\psi(z), \tag{8.15a}$$

which can be discretized as

$$H_e\psi = -\frac{\hbar^2}{\varepsilon^2}\left[\frac{\psi_{j-1}}{m_{j-1}+m_j} + \frac{\psi_{j-1}}{m_{j-1}+m_j} - \frac{\psi_j}{m_{j-1}+m_j} - \frac{\psi_j}{m_{j-1}+m_j}\right] + V_j\psi_j. \tag{8.15b}$$

This Hamiltonian forms symmetric matrices for both the forward-time and backward-time operators.

A convenient unit for computation speed is one Hamiltonian operation. It is theoretically possible to solve one spatial element per processor. Thus n processors can be used to solve for n elements of the Hamiltonian simultaneously. In Fig. 8.3, the stability region or the maximum time step for convergence for various N is shown in the shaded region. A linear line is shown at the half of the maximum time step. This half-maximum time step is used for finding computation speed in this paper. The number of computations (Hamiltonian operations or stages) needed for convergence over 1 fs are shown in Fig. 8.4 as function of N or Δt for REM and only Δt while for Jacobi. The important feature to note in Fig. 8.4 is that for REM the number of computations quickly decreases up to $N = 21$, corresponding to a time step of 0.025 fs. It remains relatively constant thereafter. This is in contrast to the Jacobi method where number of iterations increase very fast with Δt. Thus for a time step of 0.05 fs, computation speed for REM with $N = 40$ is faster than that of Jacobi by a factor of 7. This speed difference will

increase as N increases. The exact number of the speed enhancement may vary for other Hamiltonians but they will show the same trend of the speed enhancement as N increases. Thus, REM is very efficient at handling large time step.

8.5.2 Two-dimensional Hamiltonian

Single electron devices[9] in near future might be the counterparts of field-effect-transistors in today's computers. A simple structure is used to show a basic feature of these devices. This structure consists of two quantum boxes (QBs), each with a dimension of 100 by 100 Å. A barrier of 1 Å thickness and 1 eV height separates them. There is a 20 Å hole in the middle of the barrier. The inset of Fig. 8.5 shows a simplified view of the structure. The spatial mesh is a 1×1 Å^2 box. The boundaries of the system are infinitely high potential barriers for electron. Hence the electron wave function is zero at these boundaries. The electron that is initially prepared in the left box oscillates between the two boxes with a period of 111 fs.

The 2D electron Hamiltonian

$$H_e\psi = -\frac{\hbar^2}{2m}\left[\frac{\partial^2\psi}{\partial x^2}+\frac{\partial^2\psi}{\partial y^2}\right]+V\psi\,, \tag{8.16a}$$

is discretized as

$$H_e\psi = -\frac{\hbar^2}{8\varepsilon^2 m_{i,j}}\left[\psi_{i,j-1}+\psi_{i,j-1}+\psi_{i-1,j}+\psi_{i-1,j}\right]+\left[\frac{\hbar^2}{2\varepsilon^2 m_{i,j}}+V_{i,j}\right]\psi_{i,j}\,. \tag{8.16b}$$

Fig. 8.5 shows the stability region as well as the half-maximum time step that is used for calculating the speed of REM for the 2D Hamiltonian case. In Fig. 8.6 the number of computations needed for convergence are shown for REM and for Jacobi over

1 fs. They quickly decrease for the REM up to $N = 30$ that corresponds to a time step of 0.019 fs. and stays relatively constant afterwards. For a time step of 0.025 fs. a speed improvement by a factor of 9 for REM with $N = 40$ in comparison with Jacobi. It should be noted that it is desirable to have larger time steps and the REM is well suited for this.

8.6 Conclusion

The REM is a stationary method with convergence properties similar to nonstationary methods. Unlike Jacobi and Gauss-Seidel methods where the Hamiltonian must be broken into diagonal and non-diagonal parts. the REM allows us solve the TDSE with any Hamiltonian. The parallelism of the REM is related to number of terms in the expansion of propagation operator. rather than size of problem as in the split-operator technique. Thus it should easily scale for larger spatial and non-spatial dimensions. The accuracy and speed of the REM permit the use of larger time steps in calculations. Therefore. this method is ideally suited for solving the TDSE on parallel computers.

8.7 References

1. F. Tisseur and J. Dongarra. SIAM J. Sci. Comput. **20**. 2223 (1999).

2. A. Goldberg, H. M. Schey and J. L. Schwartz. Am. J. Phys. **35**. 177 (1967).

3. R. Barret. M. Berry. T. F. Chan. J. Demmel. J. Donato. J. Dongarra. V. Eijkhout. R. Pozzo. C. Romine and H. Van der Vorst. *Templates for the solution of Linear Systems: Building Blocks for Iterative Methods* (Society of Industrial and Applied Mathematics. Philadelphia. PA. 1994).

4. J. M. Ortega and R. M. Voigt. SIAM Rev. **27**. 149 (1985).

5. M. D. Feit. J. A. Fleik. Jr. and A. Steiger. J. Comput. Phys. **47**. 412 (1982).

6. A. Askar and A. S. Cakmak. J. Chem. Phys. **68**. 2794 (1978).

7. R. L. Liboff. *Introductory Quantum Mechanics* (Addison-Wesley Publishing Company. Reading. MA. 1992).

8. J. M. Mohaidat. K. Shum and R. R. Alfano. Phys. Rev. B **45**. 3822 (1992).

9. K. K. Likharev. Proc. IEEE **87**. 606 (1999).

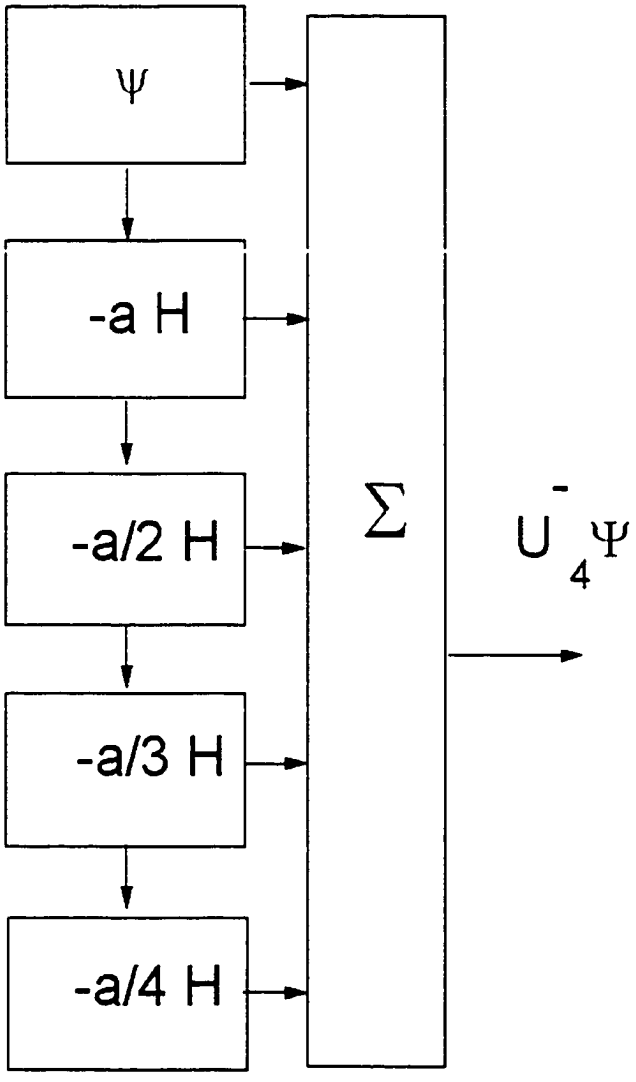

Fig. 8.1: Implementation of the operator U_4^-.

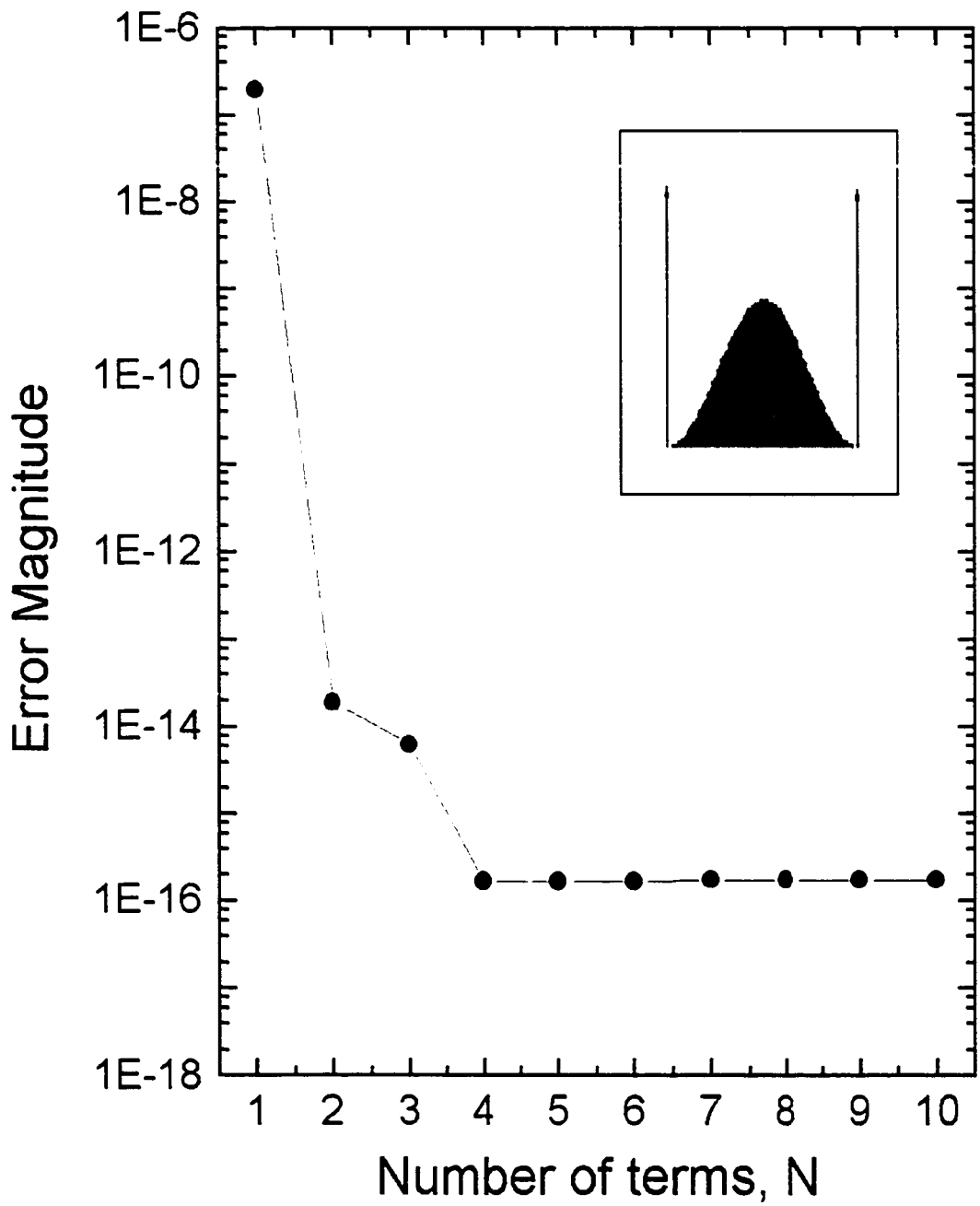

Fig. 8.2: Accuracy of REM as a function of the number of terms for the square quantum well structure. The inset shows the quantum structure.

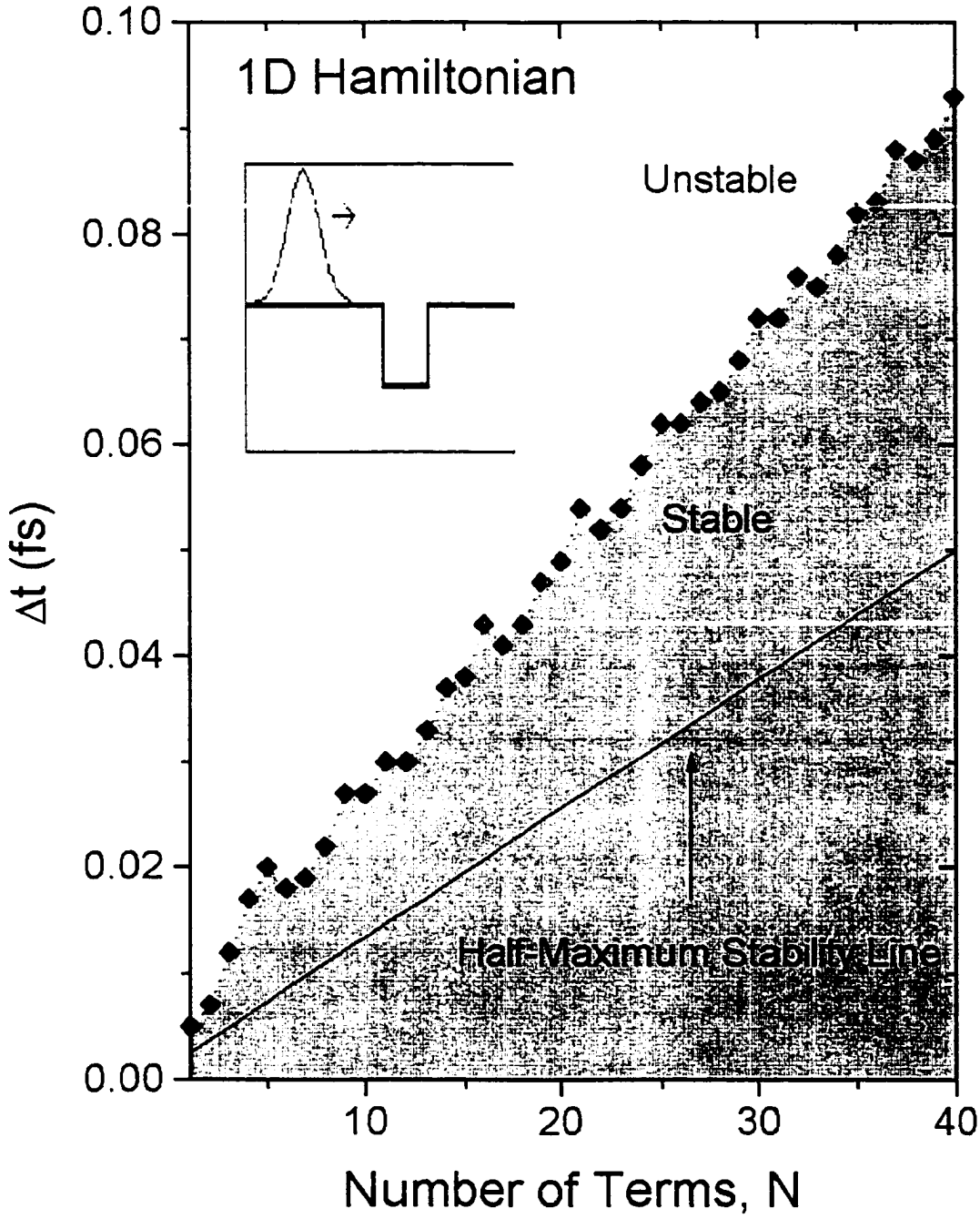

Fig. 8.3: Stability diagram of REM for a 1D SQW Hamiltonian. The stable region is shown in the shaded region. The half-maximum time step-size is also shown. The inset shows the quantum structure.

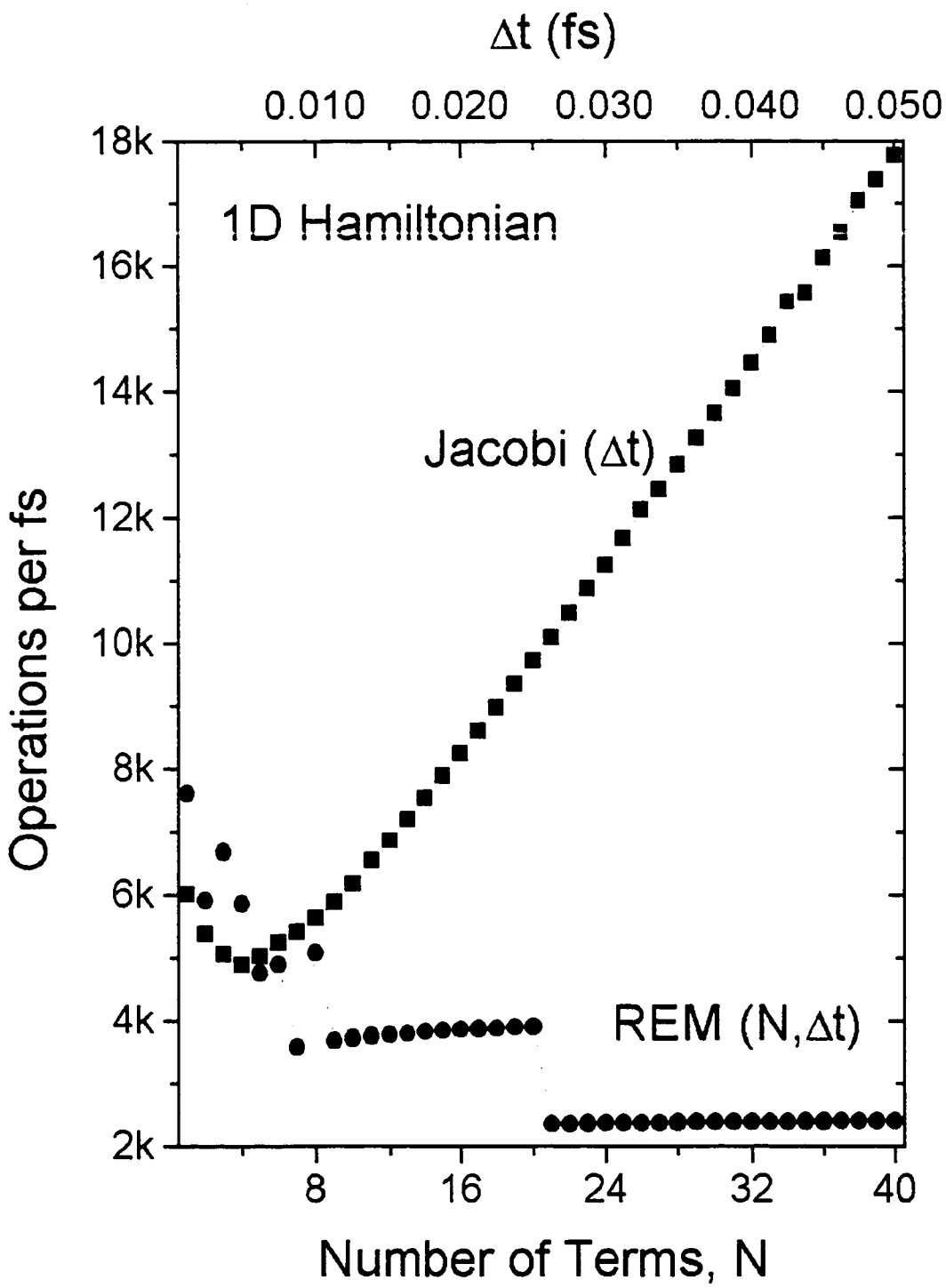

Fig. 8.4: Calculation overhead of REM as a function of N (circles) and Jacobi as a function of time step (squares) for a 1D SQW Hamiltonian.

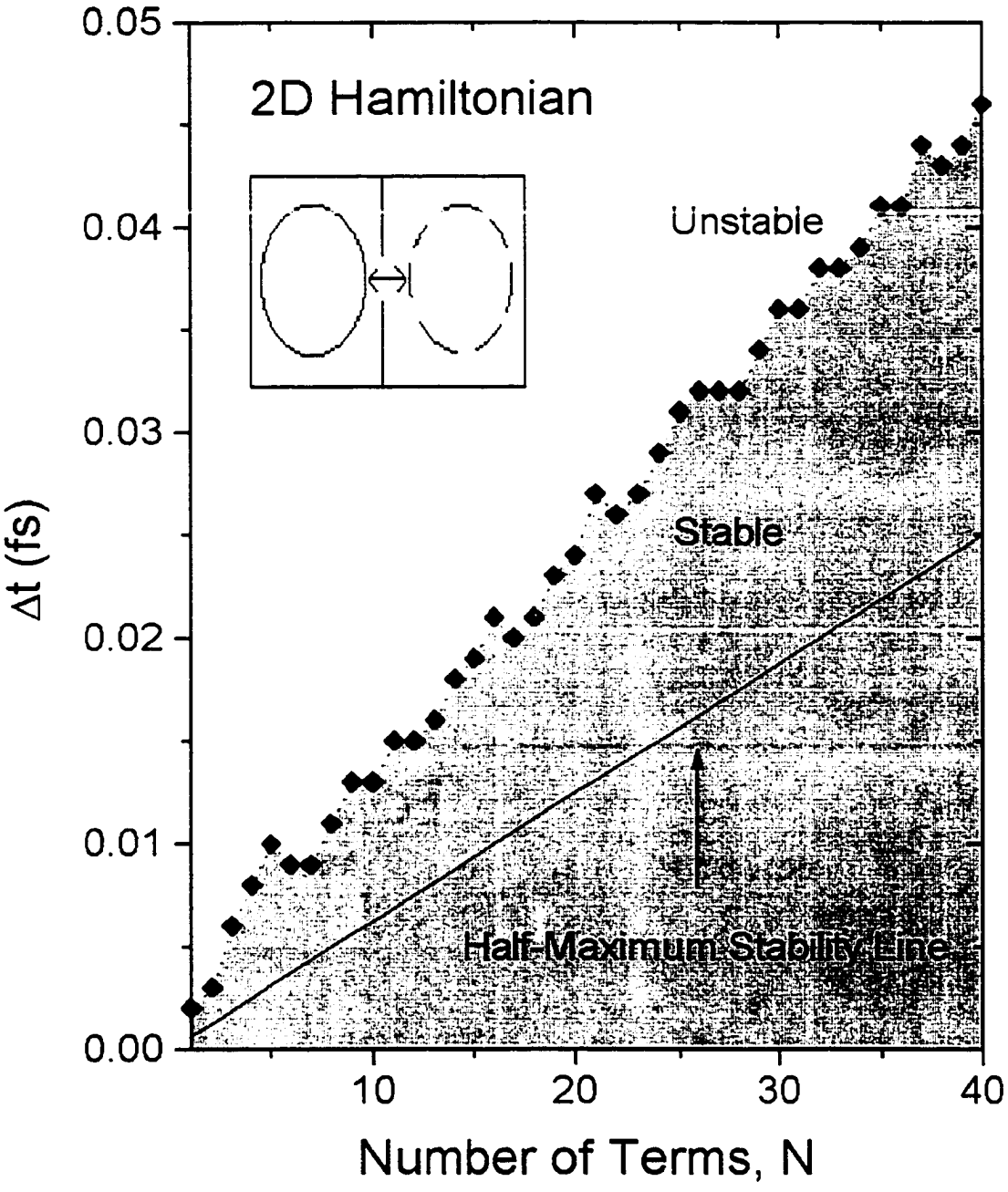

Fig. 8.5: Stability diagram of REM for a 2D QBs Hamiltonian. The stable region is shown in the shaded region. The half-maximum time step-size is also shown. The inset shows the quantum structure.

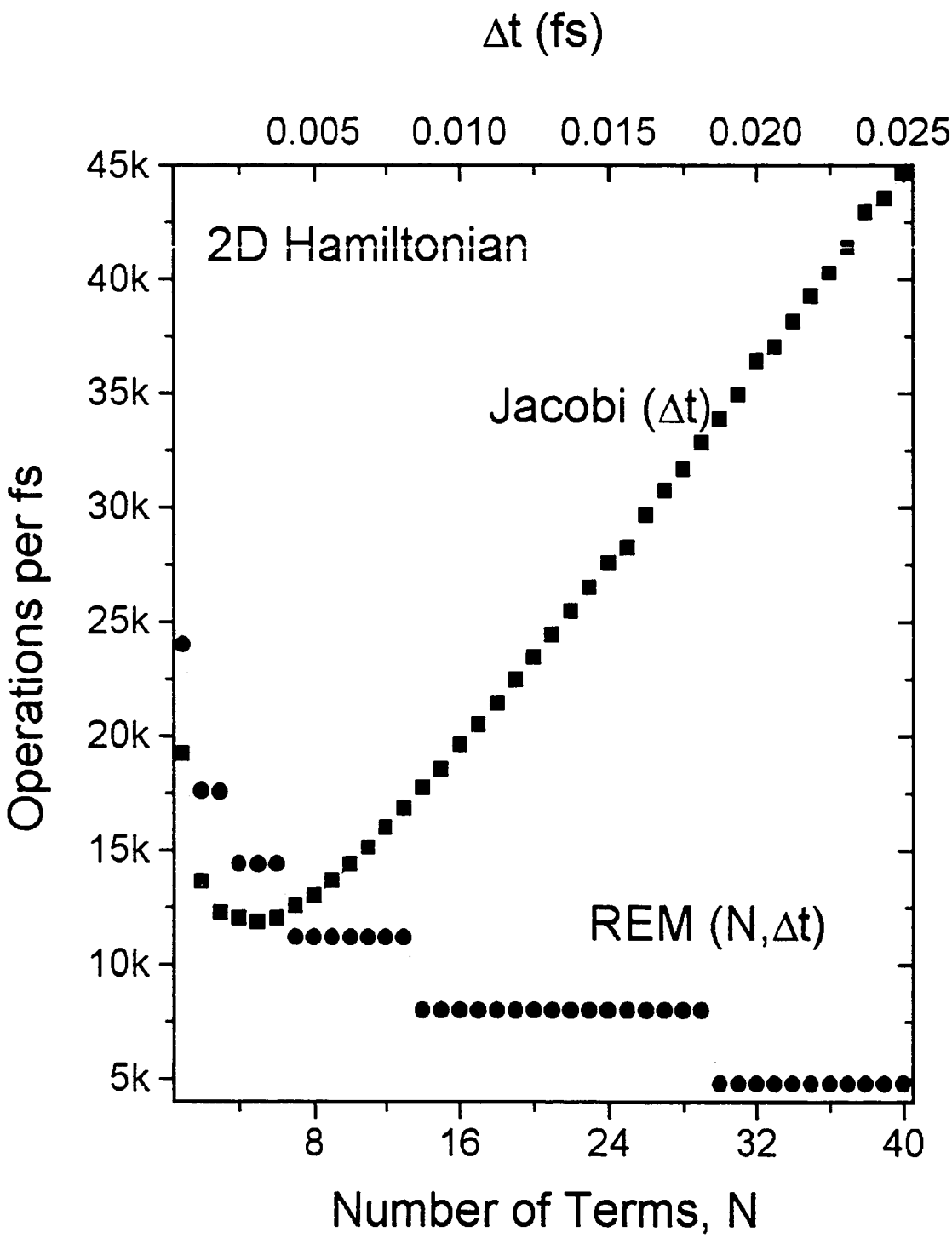

Fig. 8.6: Calculation overhead of REM as a function of N (circles) and Jacobi as a function of time step (squares) for a 2D QBs Hamiltonian.

SOD	$H\psi = H(t)\psi(t)$
Crank-Nicolson	$H\psi = \frac{H(t+\Delta t)\psi(t+\Delta t) + H(t-\Delta t)\psi(t-\Delta t)}{2}$
REM	$H\psi = \frac{H(t)\psi(t+\Delta t) + H(t)\psi(t-\Delta t)}{2}$

Table 8.1: The right hand side of the TDSE for different methods.

N	$U_N^{\dagger}U_N^{-}$
1	$1 \quad a^2 \cdot H^2$
2	$1 \quad \frac{1}{4} \cdot a^4 \cdot H^4$
3	$1 \quad \frac{1}{12} \cdot a^4 \cdot H^4 \quad \frac{1}{36} \cdot a^6 \cdot H^6$
4	$1 \quad \frac{1}{72} \cdot a^6 \cdot H^6 \quad \frac{1}{576} \cdot a^8 \cdot H^8$
5	$1 \quad \frac{1}{360} \cdot a^6 \cdot H^6 \quad \frac{1}{960} \cdot a^8 \cdot H^8 \quad \frac{1}{14400} \cdot a^{10} \cdot H^{10}$

Table 8.2: Analytic values of the unitary operator.

Inputs: N, Δt, H, ψ_0, *last*, *max*, *tol*, $\psi_{in} \leftarrow \psi_0$

for t = 1.....*last*

RHS $\leftarrow U_N^{\dagger} \psi_{in}$

$\psi \leftarrow$ RHS

for r = 1.....*max*

$e \leftarrow U_N^{\dagger} \psi -$ RHS

if ($\|e\|_2 <$ *tol*) **break**

$\psi \leftarrow \psi - U_N^{\dagger} e$

end

Save t, ψ

$\psi_{in} \leftarrow \psi$

end

Table 8.3: The REM algorithm.

CHAPTER 9

FUTURE WORK

9.1 Software for real time visualization of quantum projects

A professional program based on the real time visualization of quantum transport is in development and will be completed both as an executable file and as a java program available on the internet. The program (VQP) has been described in Chapter 4.

9.2 Electron-electron and electron-hole scattering

Electron-electron and electron-hole scattering will be included in the program by running two independent programs for each of the two particles. The potential that each particle experiences at a particular time will be calculated based on Coulomb interaction.

9.3 2D simulator based on REM

Recursive error method will be used to solve 2D quantum structures. A numerical package similar to that discussed in Chapter 4 for 1D problems will be written. It will be written for multiprocessor environments to utilize parallelism inherent in the method.

APPENDIX

A.1 The project file to view Bloch oscillations in the example of Chapter 4.

```
Project Title:          Bloch_Oscillation
Project Note:           This project will show Bloch oscillations in
superlattice.

space           1                                       Spatial Resolution (Ang)
time            1                                       Temporal Resolution (fs)
volt            0.15        1           0.15            External potential (eV)
region          75                                      Distinct regions

Problem: One Electron


Electron 1:     Traveling Right

z0          42004                               Wavepacket Center (Ang)
s0          150                                 Wavepacket Width (Ang)
E0          0           0.001       0           Wavepacket Energy (eV)

Default Values: (used in Setting New Quantum Structures)

Barrier Width (Ang):        17
Well Width (Ang):           97
Well Depth (eV):            0.243
Interaction Strength:       9
Barrier Mass (me):          0.092
Well Mass (me):             0.067
Boundary (Ang):             40000
Transport (Ang):            1
```

region	z		V(eV)		m
#	Ang	Start	Step	End	me
1	40000	0	0	0	0.067
2	40001	0	1	0	0.067
3	40018	0.243	1	0.243	0.092
4	40115	0	1	0	0.067
5	40132	0.243	1	0.243	0.092
6	40229	0	1	0	0.067
7	40246	0.243	1	0.243	0.092
8	40343	0	1	0	0.067
9	40360	0.243	1	0.243	0.092
10	40457	0	1	0	0.067
11	40474	0.243	1	0.243	0.092
12	40571	0	1	0	0.067
13	40588	0.243	1	0.243	0.092

14	40685	0	1	0	0.067
15	40702	0.243	1	0.243	0.092
16	40799	0	1	0	0.067
17	40816	0.243	1	0.243	0.092
18	40913	0	1	0	0.067
19	40930	0.243	1	0.243	0.092
20	41027	0	1	0	0.067
21	41044	0.243	1	0.243	0.092
22	41141	0	1	0	0.067
23	41158	0.243	1	0.243	0.092
24	41255	0	1	0	0.067
25	41272	0.243	1	0.243	0.092
26	41369	0	1	0	0.067
27	41386	0.243	1	0.243	0.092
28	41483	0	1	0	0.067
29	41500	0.243	1	0.243	0.092
30	41597	0	1	0	0.067
31	41614	0.243	1	0.243	0.092
32	41711	0	1	0	0.067
33	41728	0.243	1	0.243	0.092
34	41825	0	1	0	0.067
35	41842	0.243	1	0.243	0.092
36	41939	0	1	0	0.067
37	41956	0.243	1	0.243	0.092
38	42053	0	1	0	0.067
39	42070	0.243	1	0.243	0.092
40	42167	0	1	0	0.067
41	42184	0.243	1	0.243	0.092
42	42281	0	1	0	0.067
43	42298	0.243	1	0.243	0.092
44	42395	0	1	0	0.067
45	42412	0.243	1	0.243	0.092
46	42509	0	1	0	0.067
47	42526	0.243	1	0.243	0.092
48	42623	0	1	0	0.067
49	42640	0.243	1	0.243	0.092
50	42737	0	1	0	0.067
51	42754	0.243	1	0.243	0.092
52	42851	0	1	0	0.067
53	42868	0.243	1	0.243	0.092
54	42965	0	1	0	0.067
55	42982	0.243	1	0.243	0.092
56	43079	0	1	0	0.067
57	43096	0.243	1	0.243	0.092
58	43193	0	1	0	0.067
59	43210	0.243	1	0.243	0.092
60	43307	0	1	0	0.067
61	43324	0.243	1	0.243	0.092
62	43421	0	1	0	0.067
63	43438	0.243	1	0.243	0.092
64	43535	0	1	0	0.067
65	43552	0.243	1	0.243	0.092
66	43649	0	1	0	0.067
67	43666	0.243	1	0.243	0.092
68	43763	0	1	0	0.067
69	43780	0.243	1	0.243	0.092
70	43877	0	1	0	0.067

71	43894	0.243	1	0.243	0.092
72	43991	0	1	0	0.067
73	44008	0.243	1	0.243	0.092
74	44009	0	1	0	0.092
75	84009	0	0	0	0.092

Interaction: Phonon

Ep	0.0362	0.001	0.0362	Phonon Energy (eV)
Temp			300	Temperature(K)

Temporal: Continuous

region #	z Ang	Start	Step	Interaction Stop
1	40000	0	0	0
2	40001	0	1	0
3	40018	0	1	0
4	40115	9	1	9
5	40132	0	1	0
6	40229	9	1	9
7	40246	0	1	0
8	40343	9	1	9
9	40360	0	1	0
10	40457	9	1	9
11	40474	0	1	0
12	40571	9	1	9
13	40588	0	1	0
14	40685	9	1	9
15	40702	0	1	0
16	40799	9	1	9
17	40816	0	1	0
18	40913	9	1	9
19	40930	0	1	0
20	41027	9	1	9
21	41044	0	1	0
22	41141	9	1	9
23	41158	0	1	0
24	41255	9	1	9
25	41272	0	1	0
26	41369	9	1	9
27	41386	0	1	0
28	41483	9	1	9
29	41500	0	1	0
30	41597	9	1	9
31	41614	0	1	0
32	41711	9	1	9
33	41728	0	1	0
34	41825	9	1	9
35	41842	0	1	0
36	41939	9	1	9
37	41956	0	1	0
38	42053	9	1	9
39	42070	0	1	0

40	42167	9	1	9
41	42184	0	1	0
42	42281	9	1	9
43	42298	0	1	0
44	42395	9	1	9
45	42412	0	1	0
46	42509	9	1	9
47	42526	0	1	0
48	42623	9	1	9
49	42640	0	1	0
50	42737	9	1	9
51	42754	0	1	0
52	42851	9	1	9
53	42868	0	1	0
54	42965	9	1	9
55	42982	0	1	0
56	43079	9	1	9
57	43096	0	1	0
58	43193	9	1	9
59	43210	0	1	0
60	43307	9	1	9
61	43324	0	1	0
62	43421	9	1	9
63	43438	0	1	0
64	43535	9	1	9
65	43552	0	1	0
66	43649	9	1	9
67	43666	0	1	0
68	43763	9	1	9
69	43780	0	1	0
70	43877	9	1	9
71	43894	0	1	0
72	43991	9	1	9
73	44008	0	1	0
74	44009	0	1	0
75	84009	0	0	0

Linear Potential: No

BIBLIOGRAPHY

Askar, A. and A. S. Cakmak, J. Chem. Phys. **68**, 2794 (1978).

Barret, R., M. Berry, T. F. Chan, J. Demmel, J. Donato, J. Dongarra, V. Eijkhout, R. Pozzo, C. Romine and H. Van der Vorst, *Templates for the solution of Linear Systems: Building Blocks for Iterative Methods* (Society of Industrial and Applied Mathematics, Philadelphia, PA, 1994).

Born, M. and K. Huang, *Dynamical Theory of Crystal Lattices* (Oxford University Press, London, 1954).

Brum, J. A. and G. Bastard, Phys. Rev. B **33**, 1420 (1986).

Cai, W., P. Hu, T. F. Zheng, B. Yudanin and M. Lax, Phys. Rev. B **41**, 3513 (1990).

Callen, H. B., Phys. Rev. **76**, 1394 (1949).

Chamberlain, M. P. and M. Cardona, Semicond. Sci. Technol. **9**, 794 (1994).

Cheng, D. K., *Field and Wave Electromagnetics* (Addison Wesley Publishing Company, Reading, MA, 1983).

Couch II, L., *Digital and Analog Communication Systems*, 3rd Ed. (Macmillan Publising Company, New Yok, 1990).

Crow, G. C. and R. A. Abram, Semicond. Sci. Technol. **14**, 1 (1999).

Dignam, M., J. E. Sipe and J. Shah, Phys. Rev. B **49**, 10502 (1994).

Esaki, L. and R. Tsu, IBM J. Res. Develop. **14**, 61 (1970).

Esaki, L. and L. L. Chang, Phys. Rev. Lett. **33**, 495 (1974).

Feldmann, J., K. Leo, J. Shah, D. A. B. Miller, J. E. Cunningham, T. Meier, G. von Plessen, P. Thomas and S. Schmitt-Rink, Phys. Rev. B **46**, 7252 (1992).

Feit, M. D., J. A. Fleik, Jr. and A. Steiger, J. Comput. Phys. **47**, 412 (1982).

Ferry, D. K., *Semiconductors* (Macmillan Publishing Company, New York, 1991).

Fox, A. M., D. A. B. Miller, J. E. Cunningham, W.Y. Jan, C. Y. P. Chao and S. L. Chuang, Phys. Rev. B **46**, 15365 (1992).

Fröhlich, H., Proc. Roy. Soc. A **160**, 230 (1937).

Fröhlich, H., Proc. Roy. Soc. A **188**, 521 (1947).

Giles, C. R., T. Li, T. H. Wood, C. A. Burrus and D. A. B. Miller, Electron. Lett. **24**, 848 (1988).

Goldberg, A., H. M. Schey and J. L. Schwartz, Am. J. Phys. **35**, 177 (1967).

Haug, H. and L. Bányai, Eds., *Optical Switching in Low-Dimensional Systems* (Plenum Press, New York, 1988).

Kittel, C., *Introduction to Solid State Physics*, 6th Ed. (John Wiley & Sons, New York, 1986).

Lee, I. and C. Y. Fong, Phys. Rev. B **44**, 6270 (1991).

Leisching, P., T. Dekorsy, H. J. Bakker, H. Kurz and K. Köhler, Phys. Rev. B **51**, 18015 (1995).

Leisching, P., P. Haring Bolivar, W. Beck, Y. Dhaibi, F. Brüggemann, R. Schwedler, H. Kurz, K. Leo and K. Köhler, Phys. Rev. B **50**, 14389 (1994).

Leo, K., Semicond. Sci. Technol. **13**, 249 (1998).

Liboff, R. L., *Introductory Quantum Mechanics* (Addison-Wesley Publishing Company, Reading, MA, 1992).

Likharev, K. K., Proc. IEEE **87**, 606 (1999).

Maestri, Jon J. V., R. H. Landau and M. J. Páez, Am. J. Phys. **68**, 1113 (2000).

Mahan, G. D., *Many-Particle Physics* (Plenum Press, New York, 1981).

Mendez, E. E., F. Agulló-Rueda, and J. M. Hong, Phys. Rev. Lett. **60**, 2426 (1988).

Miller, D. A. B., Proc. of the IEEE, **88**, 728 (2000).

Miller, D. A. B., D. S. Chemla, T. C. Damen, A. C. Gossard, W. Wiegmann, T. H. Wood and C. A Burrus, Phys. Rev. B **32**, 1043 (1985).

Mohaidat, J. M., K. Shum and R. R. Alfano, Phys. Rev. B **45**, 3822 (1992).

Oberli, D. Y., G. Böhm and G. Weimann, Phys. Rev. B **47**, 7630 (1993).

Ortega, J. M. and R. M. Voigt, SIAM Rev. **27**, 149 (1985).

Plessen, G. von, T. Meier, J. Feldmann, E. O. Göbel, P. Thomas, K. W. Goossen, J. M. Kuo and R. F. Kopf, Phys. Rev. B **49**, 14058 (1994).

Register, L. F. and K. Hess, Appl. Phys. Lett. **71**, 1222 (1997).

Reynolds, J. P. and M. Luban, Phys. Rev. B **54**, 14301 (1996).

Ridley, B. K., J. Phys. C: Solid State Phys. **15**, 5899 (1982).

Schomburg, E., A. A. Ignatov, J. Grenzer, K. F. Renk, D. G. Pavel'ev, Yu. Koschurinov, B. Ja. Melzer, S. Ivanov, S. Schaposchnikov and P. S. Kop'ev, Appl. Phys. Lett. **68**, 1096 (1996).

Shum, K., J. Appl. Phys. **69**, 6484 (1991).

Sibille, A., J. F. Palmier and F. Mallot, Appl. Phys. Lett. **60**, 457 (1992).

Tisseur, F. and J. Dongarra, SIAM J. Sci. Comput. **20**, 2223 (1999).

Tsuchiya, T. and T. Ando, Phys. Rev. B **47**, 7420 (1996).

Waschke, C., H. G. Roskos, R. Schwedler, K. Leo, H. Kurz and K. Köhler, Phys. Rev. Lett. **70**, 3319 (1993).

Wenckbach, T., *Essentials of Semiconductor Physics* (John Wiley & Sons, New York, 1991).

Wendler, L., Phys. Stat. Sol. (b) **129**, 513 (1985)

Wendler, L. and R. Pechstedt, Phys. Stat. Sol. (b) **141**, 129 (1987).

Wendler, L. and R. Haupt, Phys. Stat. Sol. (b) **143**, 487 (1987).

Wingreen, N. S., K. W. Jacobsen and J. W. Wilkins, Phys. Rev. Lett. **61**, 1396 (1988).

Yariv, A., *An Introduction to Theory and Applications of Quantum Mechanics* (John Wiley & Sons, New York, 1982).

Yariv, A., *Quantum Electronics*, 2nd Ed. (John Wiley & Sons, New York, 1975).